

UC Santa Cruz

UC Santa Cruz Electronic Theses and Dissertations

Title

Lipoxygenase Investigations Lead to the Discovery of Potent Inhibitors and their Mechanism of Action

Permalink

<https://escholarship.org/uc/item/4bd9n3t9>

Author

Armstrong, Michelle Marie

Publication Date

2016

Peer reviewed|Thesis/dissertation

UNIVERSITY OF CALIFORNIA

SANTA CRUZ

**LIPOXYGENASE INVESTIGATIONS LEAD TO THE DISCOVERY
OF POTENT INHIBITORS AND THEIR MECHANISIM OF ACTION**

A dissertation submitted in partial satisfaction
of the requirement for the degree of

DOCTOR OF PHILOSOPHY

in

CHEMISTRY

by

Michelle Marie Armstrong

June 2016

The Dissertation of Michelle Marie
Armstrong is approved:

Professor Ólöf Einarsdóttir, Chair

Professor Theodore R. Holman

Professor William G. Scott

Tyrus Miller

Vice Provost and Dean of Graduate Studies

Copyright © by
Michelle M. Armstrong
2016

Table of Contents

List of Figures.....	iv
List of Tables.....	vi
List of Schemes.....	vii
Abstract.....	viii
Acknowledgements.....	xii
Chapter 1 Introduction.....	1
Chapter 2 Inhibitory and mechanistic investigations of oxo-lipids against lipoxygenase isozymes.....	30
Chapter 3 Discovery of three small molecule inhibitors targeting human epithelial 15-lipoxygenase-2.....	49
Chapter 4 A potent and selective inhibitor targeting human and murine 12/15- LOX.....	78
Chapter 5 Human 15-LOX-1 active site mutations alter inhibitor binding and decrease potency.....	108
Chapter 6 Kinetic and mechanistic investigation of the reaction between 15S- HpETE with h15-LOX-1 and an active mutant, F414I.....	139

List of Figures

Chapter 1

Figure 1.1.....	2
Figure 1.2.....	3
Figure 1.3.....	9
Figure 1.4.....	10
Figure 1.5.....	12
Figure 1.6.....	14
Figure 1.7.....	16
Figure 1.8.....	17
Figure 1.9.....	21
Figure 1.10.....	24

Chapter 2

Figure 2.1.....	43
Figure 2.2.....	46

Chapter 3

Figure 3.1.....	61
Figure 3.2.....	62
Figure 3.3.....	69
Figure 3.4.....	75

Chapter 4

Figure 4.1.....	82
Figure 4.2.....	89
Figure 4.3.....	91
Figure 4.4.....	92
Figure 4.5.....	101
Figure 4.6.....	103

Chapter 5

Figure 5.1.....113
Figure 5.2.....114
Figure 5.3.....122
Figure 5.4.....123
Figure 5.5.....135

Chapter 6

Figure 6.1.....154
Figure 6.2.....155
Figure 6.3.....156
Figure 6.4.....157
Figure 6.5.....158
Figure 6.6.....159
Figure 6.7.....160

List of Tables

Chapter 1

Table 1.1.....	6
----------------	---

Chapter 2

Table 2.1.....	41
----------------	----

Chapter 3

Table 3.1.....	63
Table 3.2.....	71
Table 3.3.....	74

Chapter 4

Table 4.1.....	96
Table 4.2.....	97
Table 4.3.....	98

Chapter 5

Table 5.1.....	124
Table 5.2.....	125
Table 5.3.....	130
Table 5.4.....	131
Table 5.5.....	132

Chapter 6

Table 6.1.....	161
Table 6.2.....	165

List of Schemes

Chapter 6	
Scheme 6.1.....	142

Abstract

Lipoxygenase investigations lead to the discovery of potent inhibitors and their mechanism of action

Michelle M. Armstrong

The research in this dissertation describes the discovery of potent and selective inhibitors of various human lipoxygenases (LOXs). The binding modes of specific inhibitors and substrates in the active site of human 15-lipoxygenase-1 (h15-LOX-1) were also investigated. Oxo-lipids, a large family of oxidized human lipoxygenase products, are involved in different inflammatory responses in the cell. Oxo-lipids contain electrophilic sites that can potentially form covalent bonds through a Michael addition mechanism with nucleophilic residues in protein active sites and increase inhibitor potency. Due to the resemblance of oxo-lipids to LOX substrates, the inhibitor potency of 4 different oxo-lipids; 5-oxo-6,8,11,14-(E,Z,Z,Z)-eicosatetraenoic acid (5-oxo-ETE), 15-oxo-5,8,11,13-(Z,Z,Z,E)-eicosatetraenoic acid (15-oxo-ETE), 12-oxo-5,8,10,14-(Z,Z,E,Z)-eicosatetraenoic acid (12-oxo-ETE), and 13-oxo-9,11-(Z,E)-octadecadienoic acid (13-oxo-ODE) were determined against a library of LOX isozymes; leukocyte 5-lipoxygenase (h5-LOX), human reticulocyte 15-lipoxygenase-1 (h15-LOX-1), human platelet 12-lipoxygenase (h12-LOX), human epithelial 15-lipoxygenase-2 (h15-LOX-2), soybean 15-lipoxygenase-1 (s15-LOX-1), and rabbit reticulocyte 15-LOX (r15-LOX). 15-oxo-ETE exhibited the highest potency against h12-LOX of all the oxo-lipids studied, with an $IC_{50} = 1 \pm 0.1 \mu M$ and was highly selective. Time-dependent studies did not demonstrate irreversible

inhibition with 15-oxo-ETE, however, this does not preclude the role of its Michael acceptor in increasing its potency. Steady-state inhibition kinetic experiments determined 15-oxo-ETE to be a mixed inhibitor against h12-LOX, with a K_{ic} value of $0.087 \pm 0.008 \mu\text{M}$. These data are the first observations that oxo-lipids can inhibit LOX isozymes and may be another mechanism in which LOX products regulate LOX activity.

Epithelial h15-LOX-2 is of clinical interest due to its link in the progression of macrophages to foam cells, which are present in atherosclerotic plaques. Coronary artery disease is the primary cause of deaths in men and women in America. The discovery of novel inhibitors that are selective and potent against h15-LOX-2 may aid in identifying this protein's role in heart disease. Two novel molecular scaffolds, (MLS000545091 and MLS000536924), were identified using High Throughput Screening (HTS) that are selective and potent against h15-LOX-2.

Human reticulocyte 15-Lipoxygenase-1 (h15-LOX-1 or h12/15-LOX) is a lipid-oxidizing enzyme that can directly oxidize lipid membranes in the absence of a phospholipase, leading to a direct attack on organelles, such as the mitochondria. This cytotoxic activity of h15-LOX-1 is up-regulated in neurons and endothelial cells after a stroke and thought to contribute to both neuronal cell death and blood-brain barrier leakage. Stroke is the fifth leading cause of death and the first leading cause of disability in America. The discovery of inhibitors that selectively target recombinant h15-LOX-1 *in vitro*, as well as possessing activity against the murine ortholog *ex vivo*, could potentially support a novel therapeutic strategy for the treatment of stroke.

A new family of inhibitors was identified in a High Throughput Screen that are selective and potent against recombinant h15-LOX-1 and cellular mouse 15-LOX (m15-LOX). MLS000099089 (compound **99089**), the parent molecule, exhibits an IC_{50} potency of $3.4 \pm 0.5 \mu\text{M}$ against h15-LOX-1 *in vitro* and an *ex vivo* IC_{50} potency of approximately $10 \mu\text{M}$ in a mouse neuronal cell line, HT-22. These data indicate that **99089** and related derivatives may serve as a starting point for the development of anti-stroke therapeutics due to their ability to selectively target h15-LOX-1 *in vitro* and m15-LOX *ex vivo*.

The discovery of h15-LOX-1 inhibitors could potentially be novel therapeutics in the treatment of stroke, however, little is known about the inhibitor/active site interaction due to the lack of a protein crystal structure. Site-directed mutagenesis and molecular modeling were utilized to gain a better structural understanding of inhibitor interactions with the active site of h15-LOX-1. Eight mutants (R402L, R404L, F414I, F414W, E356Q, Q547L, L407A, I417A) of h15-LOX-1 were generated to determine whether these active site residues interact with two structurally similar h15-LOX-1 inhibitors, a **ML094** derivative and **ML351**. IC_{50} values and steady-state inhibition kinetics were determined with the eight mutants and four of the mutants affected inhibitor potency relative to wild type h15-LOX-1 (F414I, F414W, E356Q and L407A). The data indicate that the **ML094** derivative and **ML351** bind to similar sites in the active site but have subtle differences in their binding modes.

Lipoxygenases are capable of catalyzing dioxygenation and dehydration reactions when reacting with conjugated mono-hydroperoxy fatty acids. Dioxygenation of mono-hydroperoxide fatty acids lead to di-hydroperoxide products while dehydration of mono-hydroperoxides followed by hydrolysis lead to di-hydroxide products. The fatty acid kinetics, product profile and mechanism of product formation were investigated between WT human 15-lipoxygenase-1 and 15S-HpETE in comparison to the reaction between an active site mutant, F414I, and 15S-HpETE. The substrate affinity and k_{cat} of 15S-HpETE turnover were comparable for both WT h15-LOX-1 and F414I. Alternatively, the substrate affinity and k_{cat} of AA turnover varied for WT h15-LOX-1 and F414I leading to a decreased catalytic efficiency of AA turnover by F414I relative to WT h15-LOX-1. The kinetic data suggests that the active site mutant, F414I, is less efficient at turning over AA relative to WT but comparable at turning over 15S-HpETE. 5S,15S-DiHpETE, 8S,15S-DiHETE and 14R,15S-DiHpETE were identified as the major products in the reaction for both WT 15-LOX-1 and F414I, possibly indicating that this active site mutation does not significantly affect the binding mode of 15S-HpETE in the active site. Comparison of the mass spectra of the reduced and unreduced reactions of 15S-HpETE and both enzymes reveal that 14R,15S-DiHpETE and 5S,15S-DiHETE are dioxygenation products while 8S,15S-DiHETE is the hydrolyzed dehydration product. In contrast to rabbit 15-LOX, h15-LOX-1 does not react with 15S-DiHETE with or without 13S-HpODE.

Acknowledgements

I would like to thank my advisor, Theodore R. Holman, for his leadership, mentorship, patience and guidance throughout my graduate work in the Holman lab. I have learned more than I ever imagined about myself, working with others and most importantly, lipoxygenases! I could not have progressed as far as I did without you Ted, so thank you for believing in me! Thank you to my committee chair, Ólöf Einarsdóttir for all of her help with my thesis as well as the encouragement she has given me throughout my graduate career. Ólöf is a phenomenal role model to many young women in the sciences. Thank you to William Scott for kindly agreeing to be a part of my thesis committee and always being supportive. I also owe a big thanks to Gene Switkes and Claude Bernasconi for all of their encouragement, advice and letters of support throughout the years. Having a community of supportive faculty has tremendously helped me navigate my way through graduate school.

I would like to thank all of the funding sources I received while working towards my PhD. Thank you to the Bridge to the Doctorate program (B2D) sponsored by the UC-NSF Louis Stokes Alliance for Minority Participation for funding my first two years of graduate school. I would like to thank Zia Isola, the associate program director for B2D, for all of her help and encouragement. I would like to thank the IMSD Program funded by National Institute of General Medical Sciences at NIH for one year of financial support. I would especially like to thank Yulianna Ortega for her guidance, advice and always believing in me from day one! Yuli, thank you for always being positive! You are an excellent role model to all of your students. I

would also like to thank Malika Bell for her guidance and support, she got me interested in research when I was an undergraduate which opened up many doors. I would also like to thank the Willis W. and Ethel M. Clark foundation out of Monterey for awarding me a \$10,000 fellowship to help fund my graduate studies. All of these funding sources have significantly helped reduce the financial burden of obtaining my PhD and have allowed me to focus on my research projects.

I want to thank my fellow graduate student cohorts; Tara DeBoer for always lending an ear, helping fine-tune presentations and positive energy; Chris Bailey, Rafael Palomino, Chelsea Gustafson, Kate Markham, Denise McGrath, Tyler Liban, Eefei Chen and everyone I've crossed paths with, thank you for sharing a laugh with me and making graduate school a fun place to be. I also want to thank my current fellow Holman lab cohort: Josh, Aby, Ansari, Cody, Caitlin and Steve as well as my past Holman lab cohort: Kenny, Victor, Netra, Brian, Eric, Shannon, Thomas and Gio. I would like to take a moment to remember Kenny Ikei; when I first started in the Holman lab Kenny was my go-to guy, always willing to help and explain anything and everything. Kenny made being in lab very enjoyable and a fun place to be. We miss you Kenny!

Last but not least, I would like to thank my family and friends for their unconditional love and tremendous support. First, I would like to thank my sisters, Rachel Kassabian and Kris Alba, without them I would not have gone to college to begin with. Thank you for always being there and thank you for pushing me to set high goals for myself. Without your encouragement, love and support I would not be

the independent and successful woman that I am today! I would also like to thank my mother-in-law, Patty Armstrong, who has been a tremendous supporter of my family and my goals. I would also like to thank my father-in-law, Terry Armstrong, who passed away over a year ago. Terry loved me unconditionally and was more of a father to me than my biological father. I couldn't have asked for better in-laws than Patty and Terry, thank you for welcoming me with open arms into your family and thank you for being the best grandparents to Jade, Liah and Kalyb! I want to thank my husband, Damien Armstrong, for everything he does for our family, for the enormous amount of love he has for me, for comforting me when things got stressful, for rearranging his schedule to accommodate mine, for encouraging me when I wanted to give up and for giving me three beautiful children. My husband is the best and I could not have made it through graduate school without his unconditional love and unending support! Thank you to my little munchkins, Jade, Liah and Kalyb for brightening up my life with their smiles and personalities. No matter how stressful my days got in graduate school, it was always nice to know that I had my wonderful family to go home to everyday! I also want to thank my extended family, friends and family in-laws; Melissa Herrick, Aaron Armstrong, Crystal Petrocelli, Mark Alba, Dan Kassabian, Kate & Jeremiah McCord, Ann Penfield, Mary & Chris Vedborg, Jonathan Penfield, Mary and Lou Henderson. I also want to say a big thanks to my best friend Elizabeth Mitchell (Auntie Liz), who I know I can always depend on and who has been there for me from day one!

Chapter 1

Introduction

1.1 Lipoxygenase

Lipoxygenases (LOXs) constitute a heterogeneous family of lipid-peroxidizing enzymes that catalyze the dioxygenation of free and esterified polyunsaturated fatty acids to their corresponding hydroperoxy derivatives.¹ In mammals, linoleic acid (C18:Δ2, n-6) and arachidonic acid (C20: Δ4, n-6) are the most abundant polyenoic fatty acid substrates for LOXs.² Most mammalian LOXs prefer free fatty acids as substrates over esterified lipids present in cellular membranes but the cellular concentration of free fatty acids are rather low.² The activity of cytosolic phospholipase A2³ is necessary to liberate fatty acids from cellular membranes consisting mainly of arachidonic acid (AA), eicosapentaenoic acid (EPA – C20:Δ5, n-3) and docosahexaenoic acid (DHA - C22:Δ6, n-3). The primary products of the LOX pathway are subsequently converted to a large array of bioactive lipid mediators, which include leukotrienes,⁴ lipoxins,⁵ hepoxilins,⁶ eoxins,⁷ resolvins,⁸ protectins⁹ and others originating from AA, EPA and DHA (**Figures 1.1 and 1.2**).

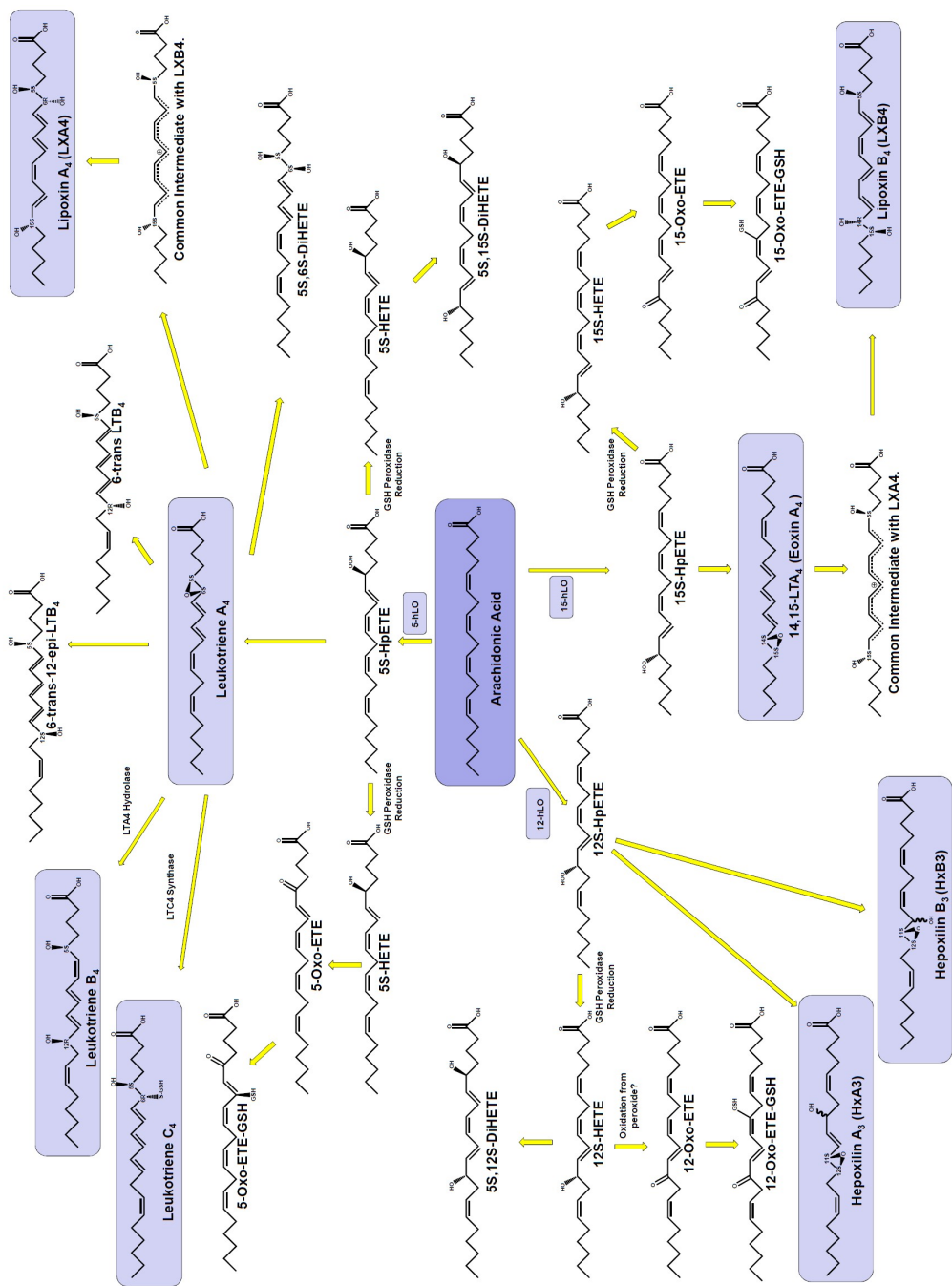


Figure 1.1. AA pathways generating lipoxins, eoxins, hepoxilins and leukotrienes.

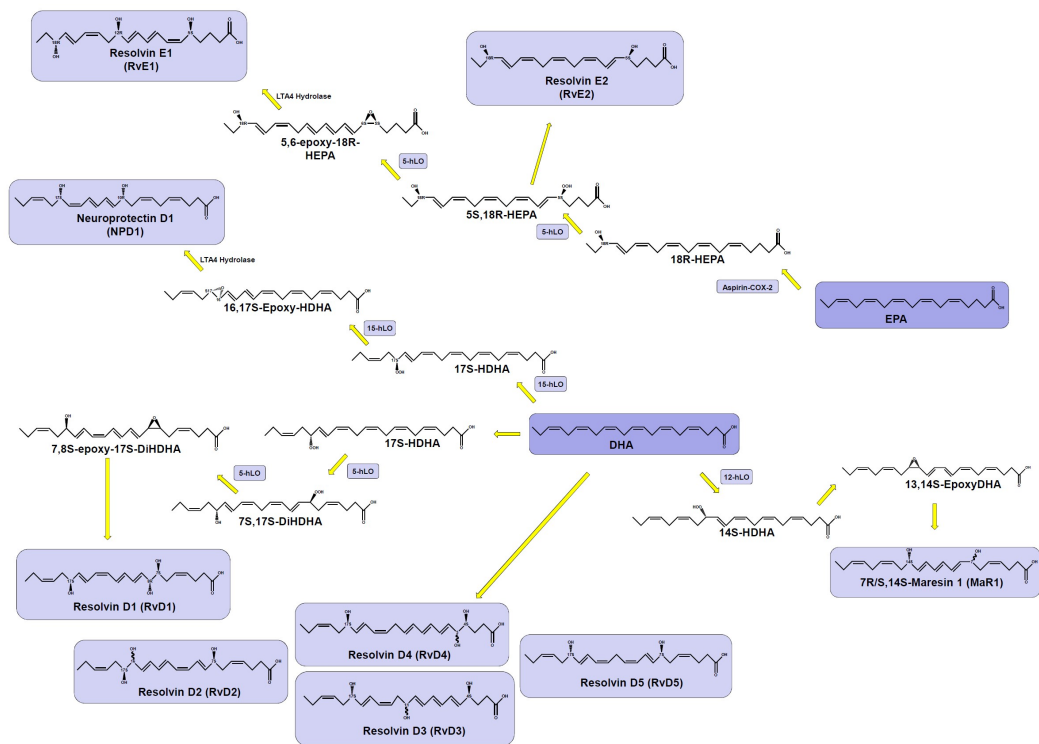


Figure 1.2. EPA and DHA pathways generating resolvins and protectins.

1.2 Lipoxygenases in the Human Genome

The human genome contains six functional LOX genes (ALOX3, ALOX12B, ALOX5, ALOX12, ALOX 15B, ALOX15), which encode for six distinct LOX-isoforms¹⁰ (**Table 1.1**). The ALOX3¹¹ and ALOX12B¹² genes encode for two different epidermis type LOX enzymes, eLOX-3 and h12R-LOX, respectively, that are co-expressed in the skin. eLOX-3 is a unique lipoxygenase in that it metabolizes fatty acid hydroperoxides via a hydroperoxide isomerase activity, generating mostly hepoxilins and a small amount of oxo-lipids. The preferred substrate of eLOX-3 is 12R-HpETE, the primary product of h12R-LOX and AA. These two isoforms are involved in the same pathway and have been implicated in epidermal differentiation as well as epidermal water barrier function. The ALOX5¹³ gene encodes for a 5-lipoxygenating enzyme (h5-LOX) found in leukocytes as well as macrophages and plays an extensive role in leukotriene biosynthesis. The primary product of h5-LOX and AA is 5S-HpETE, which results from a C7 hydrogen atom abstraction. This isozyme also generates a variety of side products. The ALOX12¹⁴ gene encodes for a 12S-lipoxygenating enzyme (h12S-LOX) that is highly expressed in blood platelets and implicated as a key player in regulating platelet function and thrombosis. The human 12S-LOX reacts with AA to form 12S-HpETE by abstraction of the C10 hydrogen atom. The ALOX15B¹⁵ gene encodes for a 15-lipoxygenating enzyme (h15-LOX-2) found to be abundant in epithelial cells and linked to the pathogenesis of atherosclerosis. Human 15-LOX-2 abstracts the C13 hydrogen atom on AA, generating 15S-HpETE. Human 12/15-LOX (h12/15-LOX and/or h15-LOX-1),

encoded by the ALOX15 gene,¹⁶ is expressed at high levels in eosinophils, bronchoalveolar epithelial cells as well as interleukin 4-treated monocytes. Human 12/15-LOX is unique in that it can abstract C10, generating 12S-HpETE, as well as C13 to produce 15S-HpETE. A large body of evidence suggests that h12/15-LOX is involved in causing brain injury after a stroke.

Human Gene	Enzyme Name	Major Expression Site(s)	References
ALOX15	12/15-LOX	Eosinophils, bronchial epithelium	16
ALOX15B	15-LOX-2	Hair roots, skin, prostate	15
ALOX12	12S-LOX	Thrombocytes, skin	14
ALOX12B	12R-LOX	Skin	12
ALOXE3	eLOX-3	Skin	11
ALOX5	5-LOX	Leukocytes, macrophages	13

Table 1.1. Human genes with nomenclature for each isozyme and the site(s) of their major expression.

1.3 Structure

Mammalian LOXs are made up of a single polypeptide chain that folds into a two-domain structure, a small N-terminal domain (β -barrel domain) and a C-terminal catalytic domain, which contains the catalytic non-heme iron located in the putative substrate-binding channel. The N- and C-terminal domains are covalently interconnected by a randomly-coiled oligopeptide. For mammalian LOXs, complete crystal structures are available for rabbit 15-LOX,^{17,18} which is utilized as a model for the human ortholog (**Figure 1.3**), a stabilized version of the human 5-LOX,¹⁹ human 15-LOX-2,²⁰ and for the catalytic domain of porcine 15-LOX.²¹

The β -barrel domain consists primarily of anti-parallel β -strands. For soybean 15-LOX-1²² and rabbit 15-LOX,²³ the β -barrel domain makes up the first 146 and 110 amino acid residues, respectively. Although the β -barrel domain of soybean 15-LOX-1 is significantly larger than that of the mammalian enzymes, their overall structures are similar. Due to its structural similarity to the β -barrel domain of human lipases,²⁴ the N-terminal domains of plant and mammalian LOXs have been implicated in membrane binding.²⁵ Site-directed mutagenesis of surface-exposed tryptophans in the N-terminal domain impairs membrane binding of the human 5-LOX,²⁶ while for the rabbit 15-LOX²⁷ and soybean 15-LOX-1,²⁸ truncation of the β -barrel domain augments membrane binding. Besides membrane binding, the N-terminal β -barrel domain may play a role in regulating enzymatic activity. A truncated soybean 15-LOX-1, lacking the N-terminal domain (mini-LOX), was found to be catalytically

active with improved catalytic efficiency for LA turnover.²⁸ Additionally, the non-heme iron can be reversibly removed from the active site of the mini-LOX unlike the complete enzyme.²⁸ A similar truncation in rabbit 15-LOX resulted in a reduction of catalytic efficiency with AA turnover as well as rapid suicidal inactivation.²⁷ These data suggest that the N-terminal β -barrel domain in s15-LOX-1 and r15-LOX is not essential for catalytic activity but may play a role in the regulation of substrate turnover.^{27,28}

The catalytic domain of all LOX-isoforms consists primarily of α -helices. The essential catalytically active non-heme iron of all LOX-isoforms is coordinated by five amino acid side chains and a hydroxide (or water) in an octahedral geometry.²² In soybean 15-LOX-1, the iron ligands are three His, one Asn and the C-terminal Ile. Detailed analysis of the crystal structure and X-ray coordinates indicate the presence of an extensive hydrogen bonding network that connects the iron-ligating Asn via two second sphere residues (Gln495, Gln697) to another equatorial iron ligand (His499).²⁹ In the rabbit 15-LOX, the iron is coordinated by four His and the C-terminal Ile. A second sphere hydrogen-bonding network is also present in r15-LOX, in which Glu357 and Gln548 participate (**Figure 1.4**).²³

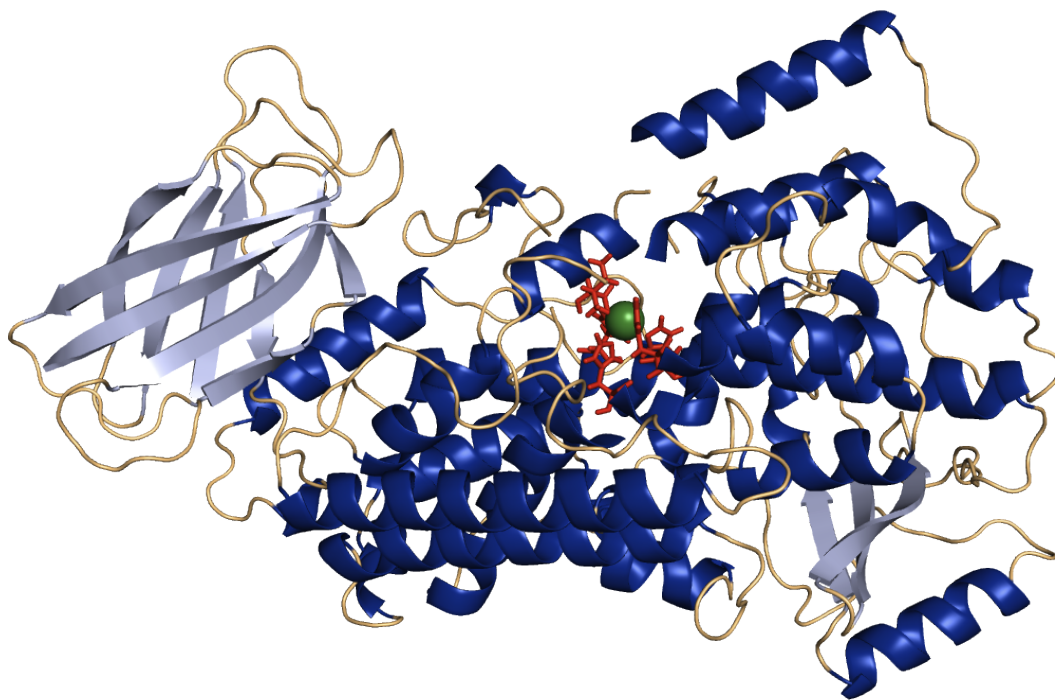


Figure 1.3. Structure of r15-LOX with N-terminal β -barrel domain and C-terminal α -helical domain. Iron ligands are shown in red and the iron metal is shown in green.

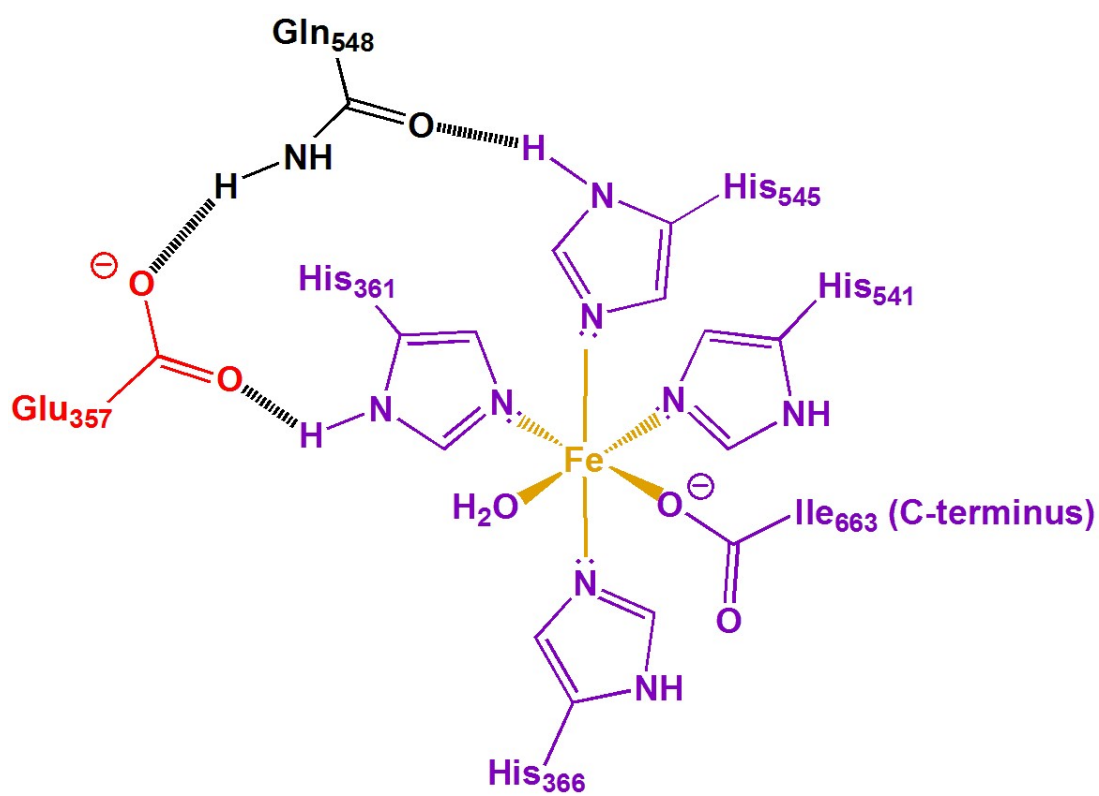


Figure 1.4. Hydrogen-bonding network in r15-LOX.

The substrate-binding pocket is a hydrophobic cavity accessible from the protein surface. The soybean 15-LOX-1 contains two major cavities, a fatty acid substrate-binding pocket and a proposed oxygen channel, which intersect near the non-heme iron.³⁰ The substrate-binding pocket is intersected by the oxygen channel between Ile553 and Trp500. Site-directed mutagenesis studies suggest that Ile553 functions to control oxygen diffusion into the substrate-binding channel while another study suggests it ensures proper fatty acid alignment.³⁰ Structural data for rabbit 15-LOX also reveal two major cavities. During substrate binding, Leu597 retracts allowing the methyl end of the substrate to slide deep into the binding pocket, interacting with residues Ile418, Phe353 and Ile593.²² The putative oxygen channel intersects the substrate-binding pocket from behind Leu367, a residue thought to control oxygenation in r15-LOX (**Figure 1.5**).²²

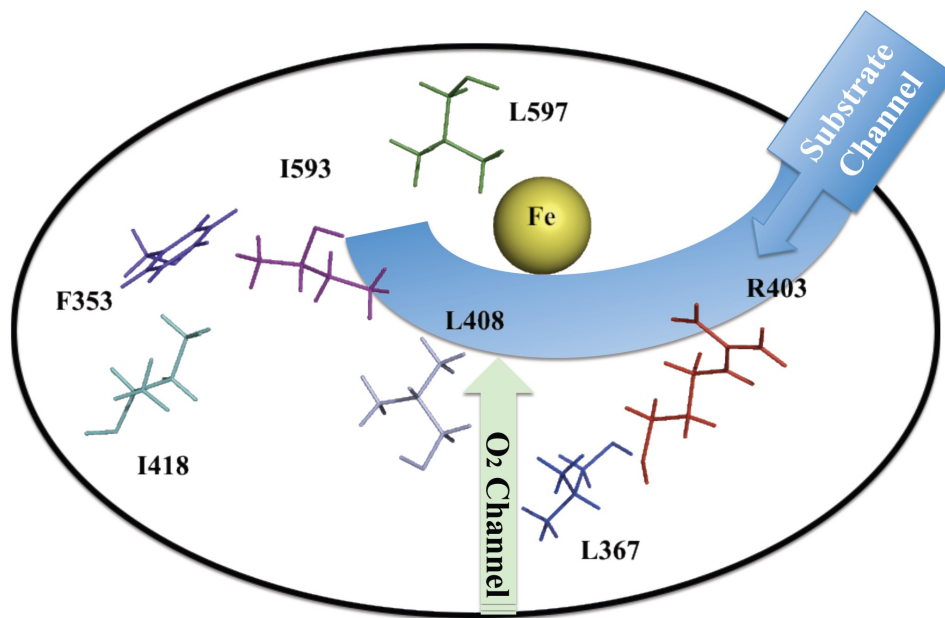


Figure 1.5. Diagram of r15-LOX active site depicting the fatty-acid substrate channel and oxygen channel.

1.4 Catalytic Cycle of LOXs

The catalytic cycle of the LOX reaction (**Figure 1.6**) involves four consecutive elementary reactions: i) stereoselective hydrogen atom abstraction from a doubly allylic methylene, generating a carbon centered fatty acid radical, ii) rearrangement of the fatty acid radical, iii) insertion of molecular oxygen forming an oxygen-centered peroxy radical, and iv) radical reduction generating a conjugated hydroperoxy fatty acid.³¹ When isolated from native or recombinant source, LOXs are present as catalytically inactive ferrous enzyme. The enzyme must first be oxidized to the catalytically active ferric form with one or more equivalents of hydroperoxide product. Studies suggest that the hydrogen abstraction is a proton-coupled electron transfer (PCET) reaction, which involves hydrogen tunneling and is the rate-limiting step of the catalytic cycle.^{31,32,33} Oxygenation is characterized by an antarafacial relationship between the hydrogen abstraction and the reaction with molecular oxygen.³⁴ Kinetic and structural data suggest that O₂ enters via a discrete channel that intersects the fatty acid substrate pocket and allows O₂ to partition from bulk solvent to a specific region of the protein.³⁴ The prebound O₂ undergoes further diffusion past a constriction in the channel, facilitated by protein motions permitting O₂ to pass into the substrate-binding pocket. This confinement of dioxygen allows for the stereospecific formation of a conjugated hydroperoxide product. In the cell, this hydroperoxy fatty acid is quickly reduced to a hydroxy fatty acid by glutathione peroxidases.

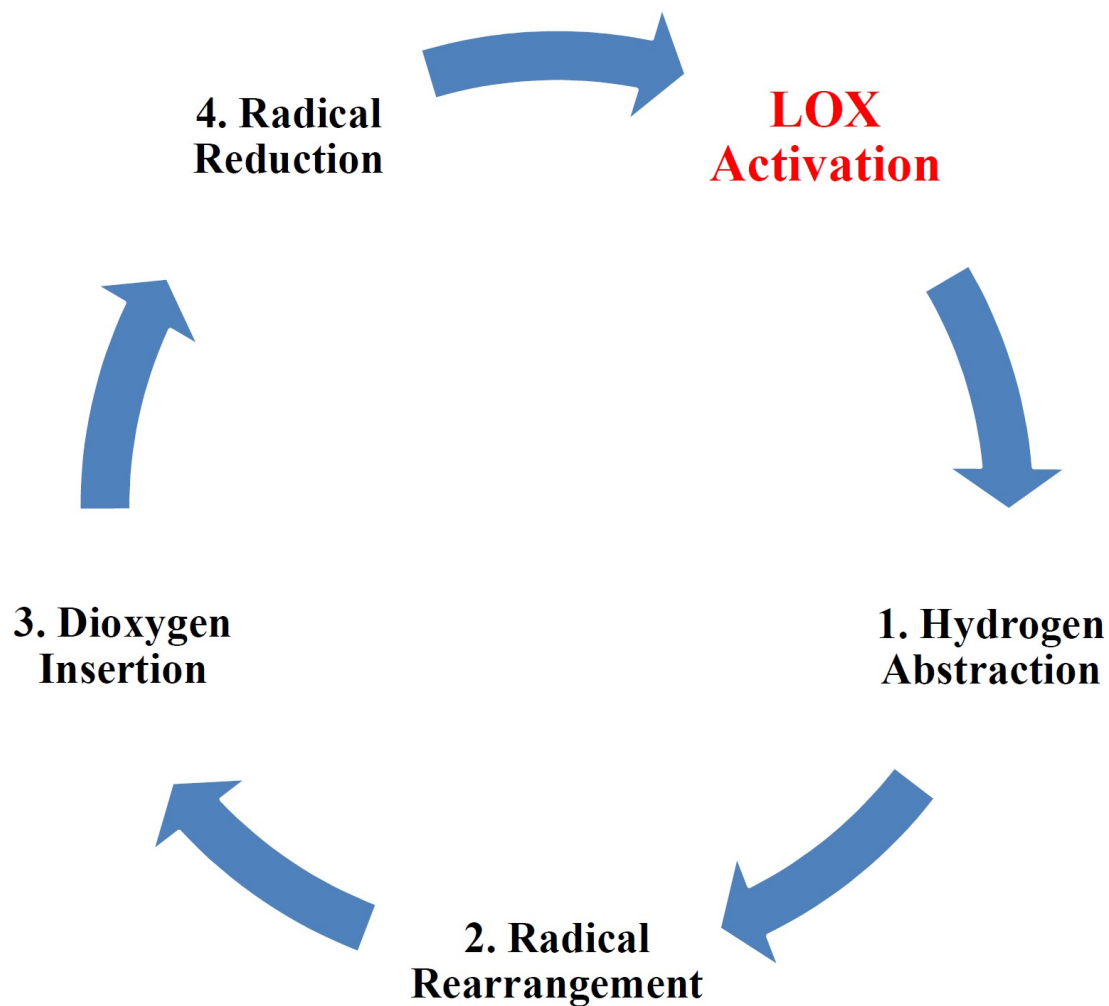


Figure 1.6. General scheme of the LOX catalytic cycle.

1.5 Multiple Catalytic Activities

Various LOX-isoforms exhibit multiple catalytic activities. The primary oxygenation products of LOXs are conjugated hydroperoxide fatty acids that absorb at 234 nm which can then serve as substrates to generate secondary lipid products that absorb at 245 and 270 nm.² If the hydroperoxide fatty acid is the substrate, the catalytic reaction can proceed via an oxygenation (**Figure 1.7**) or an epoxidation mechanism (**Figure 1.8**).² In contrast, when a hydroxide fatty acid is used as the substrate the only mechanism possible is oxygenation. The oxygenation of hydroperoxides/hydroxides is similar to that of non-oxygenated polyenoic unsaturated fatty acids like AA but is distinct in that the final products are dihydroperoxide fatty acids instead of monohydroperoxide fatty acids. The epoxidation of hydroperoxide fatty acids involves homolytic cleavage of the hydroperoxy oxygen-oxygen bond, resulting in the formation of epoxide that, in turn, gets hydrolyzed by water to generate dihydroxy fatty acids.²

Dioxygenation (Hydroperoxidation Activity)

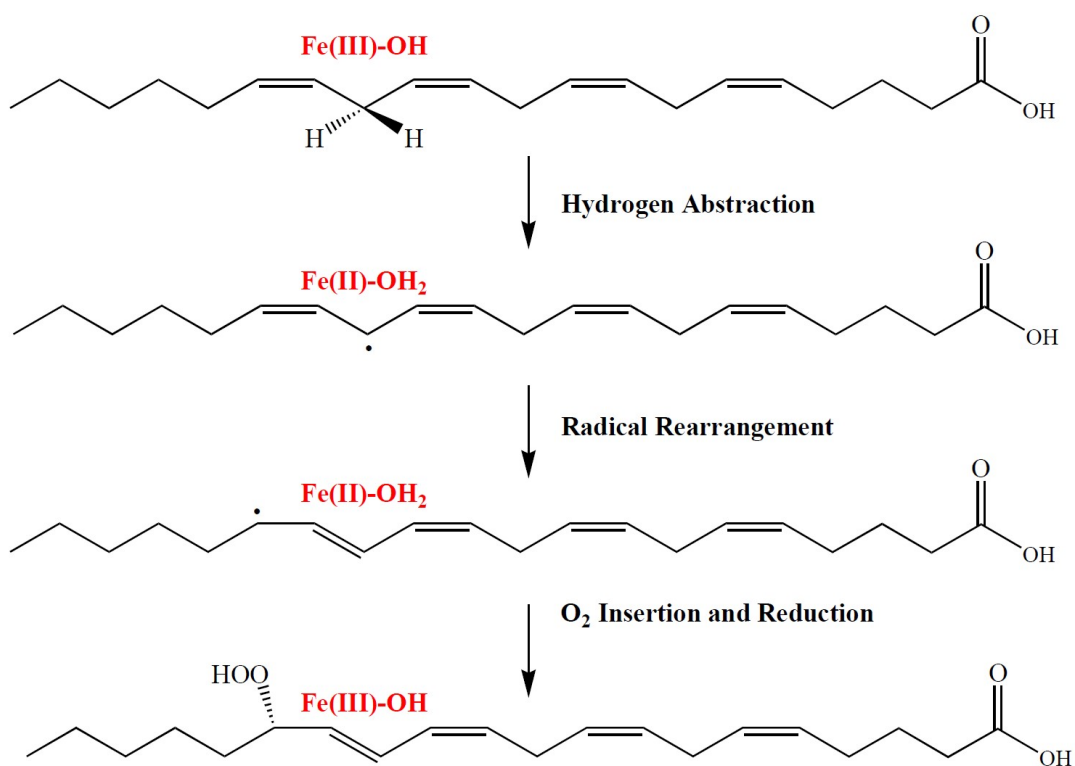


Figure 1.7. Dioxygenation activity (hydroperoxidation) of LOXs resulting in the formation of conjugated hydroperoxide fatty acids.

Epoxidation (Leukotriene Synthase Activity)

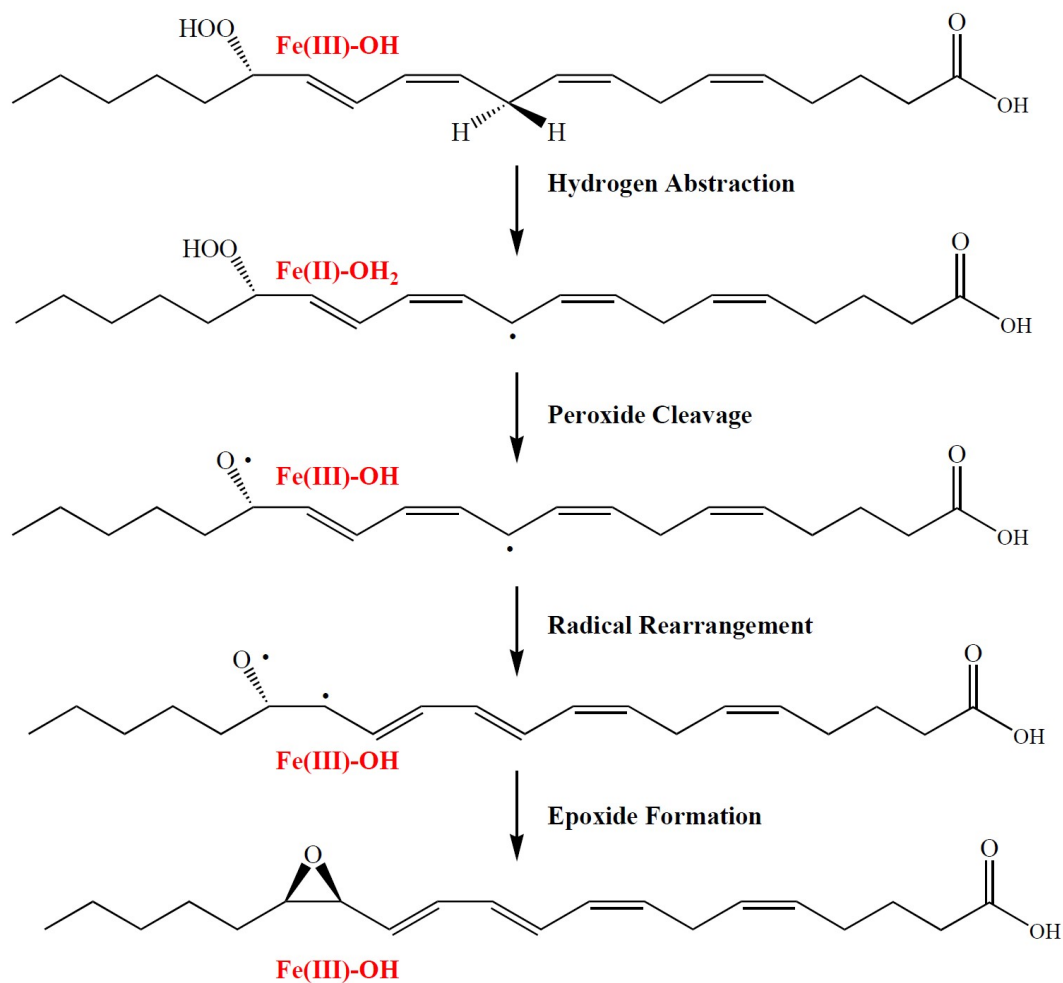


Figure 1.8. Epoxidation of hydroperoxy fatty acids by LOXs, also known as the leukotriene synthase activity of LOXs.

1.6 Substrate Alignment and Positional Specificity

The reaction specificity of LOXs with polyunsaturated fatty acids is the basis of the conventional LOX nomenclature, with arachidonic acid used as the model substrate. Although the molecular basis for the reaction specificity of different LOX-isoforms has been explored in the past, there is no unifying concept applicable for all LOX-isoforms. Poly-unsaturated fatty acids are extremely flexible molecules with a large number of possible conformations, making it difficult to predict which conformation they adopt when bound at the active site. Experiments using synthetic fatty acid isomers suggest that for s15-LOX-1³⁵ and r15-LOX,³⁶ the distance of the bisallylic methylene is of major importance. Based on experimental data with s15-LOX-1, a topological model for the alignment of fatty acids at the active site was developed, in which the fatty acids enter the hydrophobic substrate-binding channel with the methyl end first (tail-first model) so that the proS-hydrogen at C13 of arachidonic acid is localized in close proximity to the hydrogen acceptor (non-heme iron-bound hydroxyl).³⁷ This alignment of the fatty acid substrate has been well accepted in the LOX scientific community but cannot explain the products observed in many LOX reactions.

Studies show the positional specificity of lipoxygenases is not an invariant enzyme characteristic but instead may depend on the alignment of the substrate at the active site. Site-directed mutagenesis studies of recombinant human 12/15-LOX identified a three-point interaction between the enzyme and substrate polyenoic fatty

acid: i) the physical contact of amino acids Ile417, Met418 and Phe352 with the methyl terminus of the substrate molecule, ii) formation of a salt bridge between Arg402 and the negatively charged carboxylate group of the fatty acid, and iii) a π - π electron interaction of Phe414 with double bonds on AA.³⁸ There are two possible binding alignments of a particular substrate in the active site of LOXs: i) tail-first binding (as previously mentioned) and ii) head-first binding. Tail-first binding aligns the substrate fatty acid in such a way that the methyl end of the substrate protrudes into the inner cavity of the binding pocket, allowing for a hydrophobic interaction between the methyl terminus and Leu417, Met418 and Phe352 as well as an ionic interaction between Arg402 and the carboxylate of the fatty acid substrate.³⁸ Head-first binding aligns the fatty acid substrate with the carboxylate buried in the hydrophobic inner cavity of the binding pocket. This head-first substrate orientation has been heavily debated in the past due to the requirement of burying a positively charged residue in a hydrophobic environment.³⁹ The head-first binding seems energetically unfavorable but studies with soybean 15-LOX-1 and 15S-HpETE revealed products that could only be possible if the substrate was oriented head-first.

The soybean enzyme converts 15S-HpETE to a mixture of 8S,15S-DiHpETE and 5S,15S-DiHpETE.⁴⁰ This stereochemical outcome differs from that of arachidonic acid oxygenation. Soybean 15-LOX-1, when reacting with AA, produces only 15S-HpETE. Assuming a tail-first binding, s15-LOX-1 abstracts the C13 hydrogen from AA to generate 15S-HpETE (**Figure 1.9a**), which is typical activity of 15-LOXs. Assuming an arachidonic acid-like alignment of 15S-HpETE at the active

site (**Figure 1.9b**), 5S-lipoxygenation (5S,15S-DiHpETE formation), which involves hydrogen abstraction from C7, is difficult to understand. However, if a head-first substrate orientation (**Figure 1.9c**) is assumed, the stereochemical outcome of 15S-HpETE oxygenation can be explained.⁴¹ A study involving rabbit 15-LOX and 15S-HETE supports the head-first substrate binding.⁴¹ According to the published data available, head-first substrate binding is equally as likely to occur as tail-first substrate binding, depending on the LOX isoform, the nature of the substrate as well as the reaction conditions. At present, the literature lacks detailed kinetic and structural data of the reaction between recombinant human 12/15-LOX and 15S-HpETE/15S-HETE.

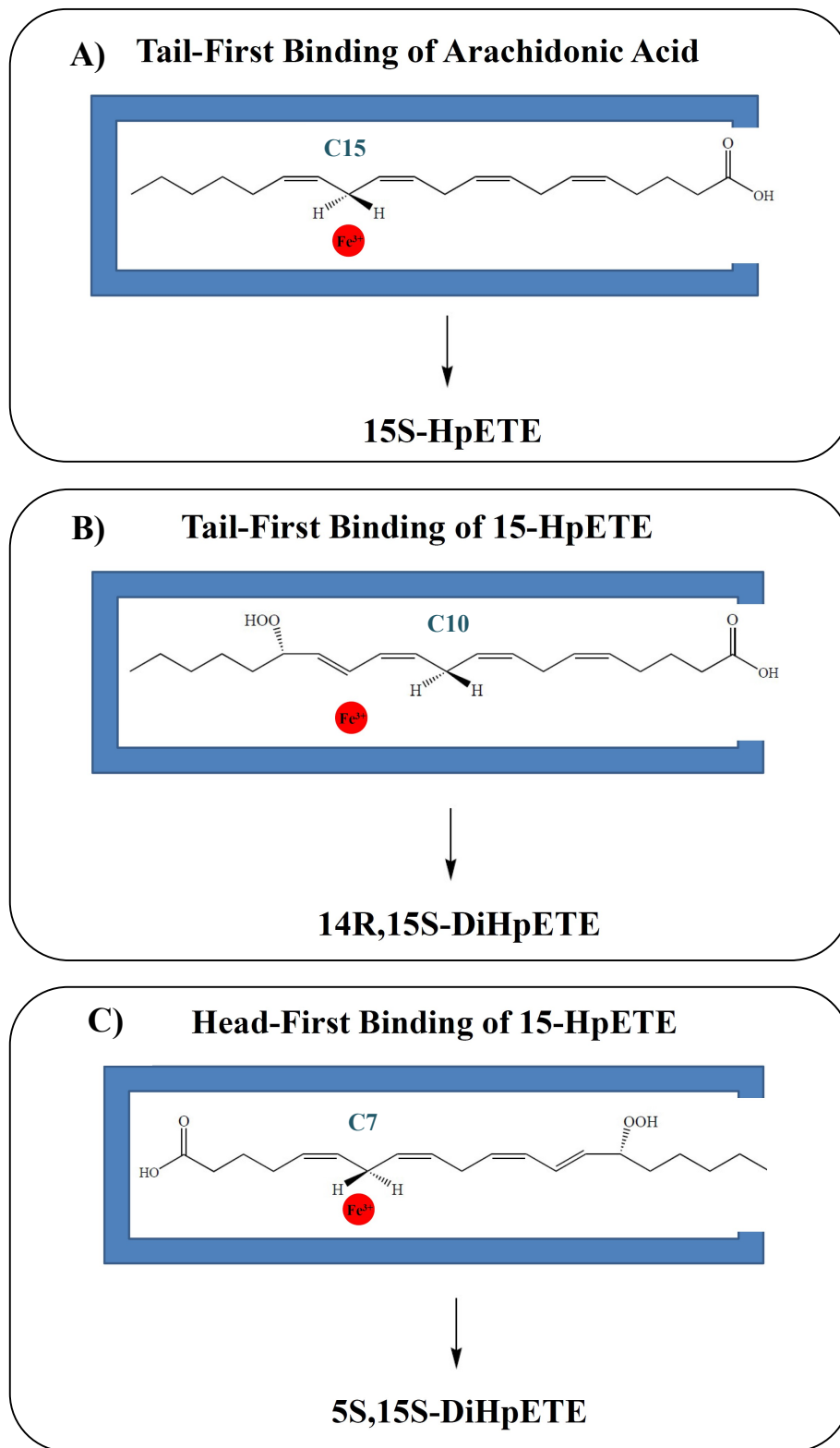


Figure 1.9. Tail-first (A,B) and head-first (C) binding of LOX substrates.

1.7 15-LOX Involvement in Stroke

The strongest evidence for any LOX isoform causing injury to the central nervous system exists in stroke.⁴² Under stroke conditions, an increased activity of cytosolic phospholipase A2 is observed, liberating arachidonic acid and thus activating the h12/15-LOX pathway.⁴² In addition, intracellular levels of calcium rise during a stroke, which favors membrane binding and augment, the catalytic activity of h12/15-LOX. The protein levels of h12/15-LOX specifically increase in the penumbra region, part of the brain that is highly vulnerable to ischemia-induced cell death, which surrounds the core infarct.⁴² The factors leading to the transcriptional up-regulation of h12/15-LOX expression in the ischemic brain have not been identified, but may include members of the STAT family of transcriptional activators, which regulate expression of the ALOX15 gene in other cell types.⁴² Increased 15-LOX in the ischemic cortex is accompanied by increased pro-apoptotic AIF, in both human stroke patients as well as mouse stroke models.⁴² A study found 15-LOX to co-localize with MDA2, an antibody that recognizes malondialdehyde-modified lysine residues, suggesting increased lipid peroxidation in the penumbra area.⁴² These findings implicate 15-LOX as being part of a major cell death pathway that is activated in the ischemic regions.⁴²

Increased levels of 15-LOX in the ischemic peri-infarct area suggested that blocking its activity might be protective. In mice, inactivation of the *alox15* gene protected them against stroke, reduced leakage of the blood-brain barrier and

minimized edema formation.⁴² Other studies replicated these protective effects by pre-treatment of the mice with LOX inhibitors.⁴² Most studies of 15-LOX in stroke have been carried out in by inducing an experimental stroke in mice by transiently occluding the middle cerebral artery with a filament (MCAO) leading initially to a striatal infarct, then expanding into the cortex with time.⁴² The cortical region, adjacent to the core infarct, dies and is a great representation of the penumbra region in human stroke patients.⁴²

1.8 Lipoxygenase Inhibitors As Potential Drugs

Finding inhibitors that target LOXs is of clinical interest due to their implication in the pathogenesis of important human diseases such as stroke. Lipoxygenase inhibitors can be classified into five different groups based on their inhibitory mechanism; redox inhibitors, allosteric inhibitors, iron chelators, active site probes and suicide substrates (**Figure 1.10**).⁴³ Redox inhibitors affect the oxidation state of the non-heme iron essential for catalytic activity.⁴³ Iron chelators bind directly to the iron, displacing active site ligands necessary for LOX activity.⁴³ Active site probes compete with fatty-acid substrates in the substrate binding pocket.⁴⁴ Suicide substrates lead to irreversible inactivation of the enzyme by forming a covalent bond with active site residues.⁴³ Allosteric inhibitors bind to a secondary site, which results in a conformational change preventing substrate turnover.⁴³

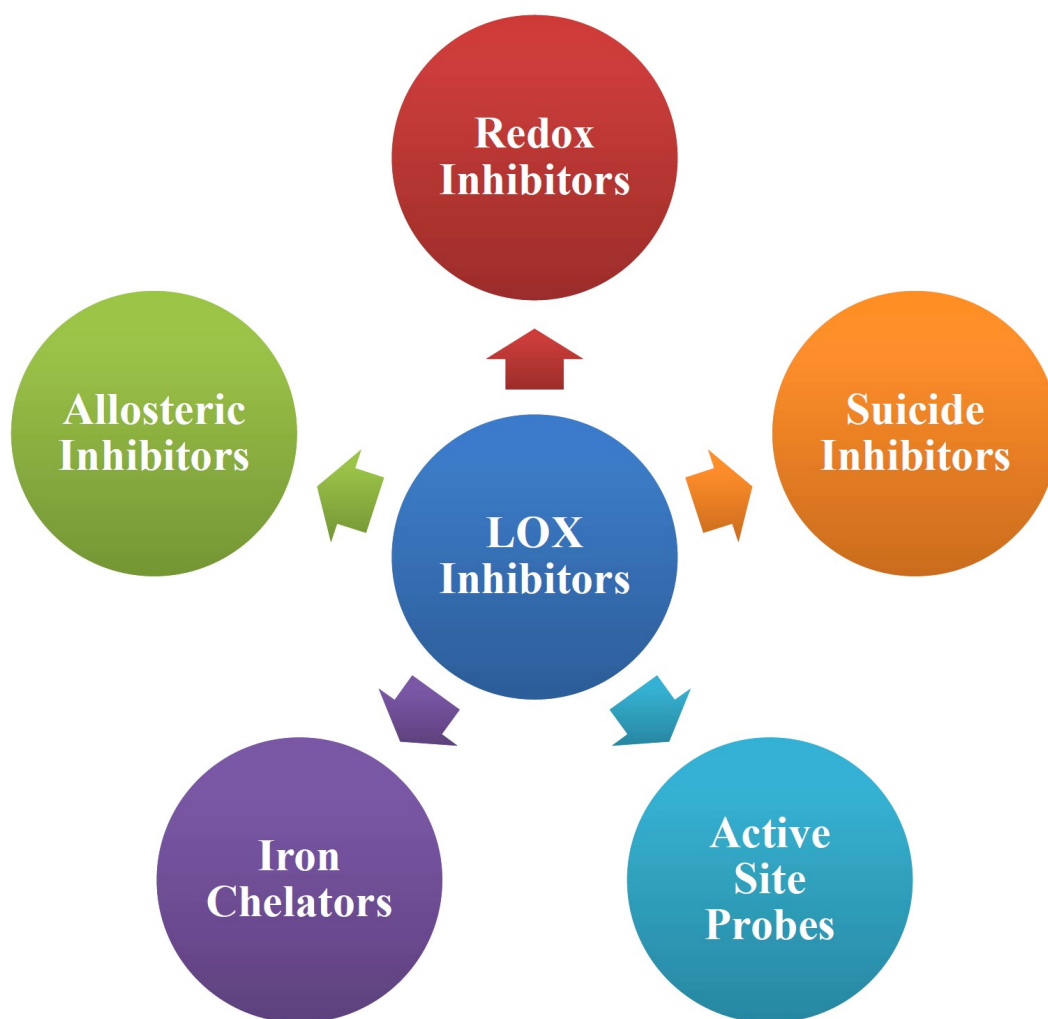


Figure 1.10. Different modes of inhibition of LOX inhibitors.

Although many pharmaceutical companies have pursued the development of LOX inhibitors, only one inhibitor has made it to the general public. Zileuton (ZYFLO) has been approved as an anti-asthmatic drug that inhibits h5-LOX leukotriene formation.⁴⁴ Many promising LOX-inhibiting compounds other than zileuton have been discovered but their therapeutic potentials have proved to be disappointing because of three important challenges: isoform specificity, species-specific activity and off-target effects.⁴³ In the human genome there are six functional LOX isoforms while in the murine genome there are seven. Finding an inhibitor that targets only one isoform has proved to be highly challenging but necessary to circumvent unwanted side effects.⁴³ To further the development of an inhibitor as a potential drug, a small animal model is necessary in addition to *in-vitro* studies. One such animal model employed in LOX inhibitor studies is the murine model.⁴² Unfortunately, some murine LOX isoforms have different catalytic activities compared to the human ortholog, which may impact the inhibitor potency. For example, the murine *alox15* gene encodes for a 12-lipoxygenating enzyme while the human *ALOX15* gene encodes for a 15-lipoxygenating enzyme.⁴³ One of the biggest challenges in LOX research in the past decade has been the lack of potent isoform-specific inhibitors that can be employed in animal disease models or in experimental clinical studies in humans.⁴³ In addition, the different functional characteristics of LOX orthologs in different mammalian species further complicates the situation. An experimental screening program for isoform-specific LOX inhibitors employing high

throughput systems that are based on purified recombinant human LOX isoforms would help address these problems.

The Holman lab has developed an inhibitor screening system in collaboration with the van Leyen lab (Harvard) and the National Institutes of Health (NIH) to find potential inhibitors against h12/15-LOX utilizing a sequence of *in-vitro*, *ex-vivo* and *in-vivo* tests. Initial hits against the recombinant human lipoxygenase are identified via a high-throughput screen and are then tested for activity in a neuronal HT22 murine cell line. Cell-active inhibitors are then screened *in-vitro* for selectivity against other lipoxygenases (h5-LOX, h12-LOX, h15-LOX-2 and COX-2). The radical scavenging activity of each inhibitor is determined in a pseudo-peroxidase experiment to eliminate molecules with an antioxidant mechanism. Finally, the structure-activity relationships are evaluated to determine if their potencies can be improved.

1.9 Scope of Dissertation

This dissertation focuses on several aspects of the lipoxygenase enzyme: determining the active site residues involved during inhibitor binding, the discovery of potent and selective inhibitors against h12-LOX, h12/15-LOX and h15-LOX-2, and the elucidation of the product profile and mechanism of the reaction between h12/15-LOX and 15-HpETE/15-HETE. Chapter 2 provides evidence that oxo-lipids, a family of oxidized human lipoxygenase products, exhibit potency against h12/15-LOX and h12-LOX, which may represent another mechanism by which LOX

products regulate LOX activity. Chapter 3 discusses the discovery of three small molecule inhibitors that exhibit potency and selectivity against h15-LOX-2, which may aid in understanding the specific role of this isozyme in atherosclerosis. Chapter 4 introduces a family of novel inhibitors that selectively target h12/15-LOX *in-vitro* and murine 12/15-LOX *ex-vivo*. Chapter 5 investigates the active-site residues that are involved in the binding of two previously published h12/15-LOX inhibitors, ML351 and an ML094 derivative, by generating eight active-site mutations of h12/15-LOX. The last chapter of this dissertation, Chapter 6, examines the steady-state kinetics, product profile and reaction mechanism of h12/15-LOX with 15-HpETE, 15-HETE and AA.

1.10 References

1. Brash, A.R. *J. Biol. Chem.* **1999**, 274, 23679.
2. Ivanov, I.; Kuhn, H.; Haydeck, D. *Gene*. **2015**, 573, 1.
3. Mancini, A.D.; Di Battista, J.A. *Inflamm. Res.* **2011**, 60, 1083.
4. Savari, S.; et. al. *World J. Gastroenterol.* **2014**, 20, 968.
5. Romano, M. *Scientific World Journal*. **2010**, 10, 1048.
6. Pace-Asciak, C.R. *Br. J. Pharmacol.* **2009**, 158, 972.
7. Sachs-Olsen, C.; et. al. *J. Allergy Clin. Immunol.* **2010**, 126, 859.
8. Yoo, S.; Lim, J.Y.; Hwang, S.W. *Curr. Neuropharmacol.* **2013**, 11, 664.
9. Serhan, C.N.; Petasis, N.A. *Chem. Rev.* **2011**, 111, 5922.
10. Funk, C.D.; et. al. *Prostaglandins Other Lipid Mediat.* **2002**, 68-69, 303.
11. Kinzigt, A.; Heidt, M.; et. al. *Genomics*. **1999**, 58, 158.
12. Boeglin, W.E.; Brash, A.R. *Proc. Natl. Acad. Sci. U.S.A.* **1998**, 95, 6744.
13. Haeggstrom, J.Z.; Funk, C.D. *Chem. Rev.* **2011**, 111, 5866.
14. Funk, C.D.; Fitzgerald, G.A. *Proc. Natl. Acad. Sci. U.S.A.* **1990**, 87, 5638.
15. Brash, A.R.; Boeglin, W.E. *Proc. Natl. Acad. Sci. U.S.A.* **1997**, 94, 6148.
16. Sigal, E.; et. al. *Biochem. Biophys. Res. Commun.* **1988**, 150, 376.
17. Gillmor, A.; et. al. *Nat. Struct. Biol.* **1997**, 4, 1003.
18. Choi, J.; Chon, J.K.; Kim, S.; Shin, W. *Proteins*. **2008**, 70, 1023.
19. Gilbert, N.C.; et. al. *Science*. **2011**, 331, 217.
20. Kobe, M.J.; et. al. *J. Biol. Chem.* **2014**, 289, 8562.
21. Xu, S.; Mueser, T.C.; Marnett, L.J.; Funk Jr., M.O. *Structure*. **2012**, 20, 1490.
22. Ivanov, I.; et. al. *Arch. Biochem. Biophys.* **2010**, 503, 161.

23. Gillmor, S.A.; et. al. *Nat. Struct. Biol.* **1997**, 4, 1003.
24. Winkler, F.K.; D'Arcy, A.; Hunziker, W. *Nature.* **1990**, 343, 771.
25. May, C.; Hohne, M.; et. al. *Eur. J. Biochem.* **2000**, 267, 1100.
26. Oldham, M.L.; Brash, A.R.; Newcomer, M.E. *J. Biol. Chem.* **2005**, 280, 39545.
27. Walther, M.; Wiesner, R.; Kuhn, H. *J. Biol. Chem.* **2004**. 279, 3717.
28. Maccarrone, M.; Salucci, M.L. *Biochemistry.* **2001**, 40, 6819.
29. Schenk, G.; Neidig, M.I.; Zhou, J.; Holman, T.R. *Biochemistry.* **2003**, 42, 7294.
30. Boyington, J.C.; Gaffney, B.J.; Amzel, L.M. *Biochem. Soc. Trans.* **1993**, 21, 744.
31. Glickman, M.H.; Klinman, J.P. *Biochemistry.* **1995**, 34, 14077.
32. Rickert, K.W.; Klinman, J.P. *Biochemistry.* **1999**, 38, 12218.
33. Lehnert, N.; Solomon, E.I. *J. Biol. Inorg. Chem.* **2003**, 8, 294.
34. Knapp, M.J.; Klinman, J.P. *Biochemistry.* **2003**. 42, 11466.
35. Hamberg, M.; Samuelsson, B. *J. Biol. Chem.* **1967**. 242, 5329.
36. Kuhn, H.; Sprecher, H.; Brash, A.R. *J. Biol. Chem.* **1990**. 265, 16300.
37. Kuhn, H.; et. al. *Adv. Enzymol. Relat. Areas Mol. Biol.* **1986**. 58, 273.
38. Gan, Q.F.; Browner, M.; Sloane, D.L.; Sigal, E. *J. Biol. Chem.* **1996**. 41, 25412.
39. Browner, M.; Gillmor, S.A., Fletterick, R. *Nat. Struct. Biol.* **1998**. 5, 179.
40. Cornelis, P.A.; et. al. *Biochim. Biophys. Acta.* **1981**. 663, 177.
41. Schwarz, K.; Anton, M.; Kuhn, H. *Biochemistry.* **1998**. 37, 15327.
42. van Leyen, K. *CNS Neurol. Disord. Drug. Targets.* **2013**. 12, 191.
43. Kuhn, H.; Banthiya, S.; van Leyen, K. *Biochim. Biophys. Acta.* **2015**. 1851, 308.
44. Berger, W.; De Chandt, M.T.; Cairns, C.B. *Int. J. Clin. Pract.* **2007**. 61, 663.

Chapter 2

INHIBITORY AND MECHANISTIC INVESTIGATIONS OF OXO-LIPIDS AGAINST LIPOXYGENASE ISOZYMES

2.1 Introduction

Human lipoxygenases (hLOX) generate hydroperoxyeicosatetraenoic acids (HpETEs) and hydroperoxyoctadecadienoic acid (HpODEs) as their primary products from polyunsaturated fatty acids such as arachidonic acid (AA)¹ and linoleic acid (LA)², respectively. These hydroperoxide products are in turn reduced by cellular glutathione peroxidase to the secondary alcohol product, hydroxyeicosatetraenoic acid (HETE) and hydroxyoctadecadienoic acid (HODE) respectively.^{3,4} The electrophilic oxo-lipids such as 5-oxo-EETE, 15-oxo-EETE, 12-oxo-EETE, and 13-oxo-ODE are derived either from HpETE and HpODE, such as in the macrophage⁵ or from the corresponding HETE and HODE, by a dehydrogenase-mediated oxidation.^{6,7} These oxo-lipids are of great interest because they are important biological molecules, whose interaction with LOX isozymes has not been fully explored.

The role of various oxo-lipids in biology is significant and expanding. 5-oxo-6,8,11,14-(E,Z,Z,Z)-eicosatetraenoic acid (5-oxo-EETE) is a multi-functional oxo-lipid that has been found to stimulate proliferation in cancer cell lines through a specific G_{αi}-coupled receptor.⁸⁻¹⁰ 5-oxo-EETE also plays an important role in the asthmatic inflammatory response,¹¹ gastrointestinal diseases¹² and activation of peroxisome proliferator-activated receptor γ (PPAR γ) transcriptional activity.¹³ Another oxo-lipid which plays a role in the cell is 12-oxo-5,8,10,14-(Z,Z,E,Z)-eicosatetraenoic acid (12-oxo-EETE). Powell et al.^{14,15} observed that 12-oxo-EETE had effects on cytosolic calcium levels at concentrations of 10 μ M, but Naccache et al.¹⁶ reported calcium effects as low as 10 nM. The third oxo-lipid generated from AA is 15-oxo-5,8,11,13-

(Z,Z,Z,E)-eicosatetraenoic acid (15-oxo-ETE). For this oxo-lipid, an esterified, 15-oxo-ETE phospholipid has been detected in patients with cystic fibrosis (CF)¹³ and shown to activate transcriptional activity in PPAR γ .¹² Activation of PPAR γ expression in CF mice ameliorates disease severity, suggesting that 15-oxo-ETE might potentially act to lower inflammation in CF.¹³ Finally, there is an oxo-lipid generated from LA, 13-oxo-9,11-(Z,E)-octadecadienoic acid (13-oxo-ODE), which was found to be an endogenous ligand to PPAR γ in intestinal epithelial cells (IEC). 13-oxo-ODE mediated the activation of PPAR γ to reduce mucosal damage and down-regulate inflammation in several mouse models of intestinal colitis,¹⁷ implicating it as a possible therapeutic target for the treatment of inflammatory bowel disease.¹⁷

Chemically, the oxo-lipids, like 5-oxo-ETE, 15-oxo-ETE, 12-oxo-ETE and 13-oxo-ODE, are unique in that they contain an α , β unsaturated carbonyl that can readily react with nucleophiles, such as proteins and glutathione (GSH), via Michael addition reaction, resulting in covalent modifications. The reversible conjugation of 13-oxo-ODE by GSH^{18,19} has been shown to occur by both enzymatic and non-enzymatic pathways, with the conjugate being exported from the cell via an energy-dependent process.²⁰ Similar synthetic molecules that form covalent linkages to their targets have been considered as therapeutics, but have traditionally been disfavored due to concerns for their off-target reactivity, either through direct tissue damage or through haptization of proteins, which could elicit an immune response.²¹ However, as selectivity and drug resistance remain a serious issue for reversible inhibitors, a resurgence of interest in this class of therapeutics has emerged. For

example, Taunton and co-workers,²² developed a fluoromethylketone-substituted ligand (fmk), which irreversibly inactivates p90 ribosomal protein S6 kinase (RSK1/2) in human cells at nanomolar concentrations by modifying an active site cysteine, without inhibiting over 130 other kinases.²² A similar covalent inhibitor, JNK-IN-8, was discovered as a specific, irreversible intracellular inhibitor against the mitogen-activated kinase JNK.²³ JNK-IN-8 inhibits phosphorylation of c-Jun, a direct substrate of JNK, by covalent modification of a conserved cysteine residue in the ATP-binding motif.²³ Both of these studies argue against the widely held view that electrophilic inhibitors are inherently nonselective²² and therefore it is possible that the oxo-lipids target non-conserved, non-catalytic cysteines in many proteins in the cell, such as lipoxygenase.

Due to the fact that oxo-lipids have interesting biological properties, that they are potential covalent modifiers and that they have similar structures to LOX substrates, we hypothesized that oxo-lipids could potentially inhibit LOX isozymes at concentrations that are biologically relevant. This hypothesis is reinforced by the fact that certain LOX isozymes have non-catalytic cysteines in their active sites,²⁴ which could serve as nucleophiles to oxo-lipids. In the current work, we present inhibitory data of a variety of oxo-lipids (5-oxo-ETE, 15-oxo-ETE, 12-oxo-ETE, and 13-oxo-ODE) against LOX isozymes (h5-LOX, h15-LOX-1, human platelet 12-lipoxygenase (h12-LOX), human epithelial 15-lipoxygenase-2 (h15-LOX-2), soybean 15-lipoxygenase-1 (s15-LOX-1), and rabbit reticulocyte 15-LOX (r15-LOX)) and demonstrate that certain oxo-lipids are LOX inhibitors.

2.2. Materials and Methods

2.2.1 Materials. All commercial fatty acids (Sigma-Aldrich Chemical Company) were re-purified using a Higgins HAlsil Semi-Preparative (5 mM, 250 x 10 mm) C-18 column. Solution A was 99.9% MeOH and 0.1% acetic acid; solution B was 99.9% H₂O and 0.1% acetic acid. An isocratic elution of 85% A: 15% B was used to purify all fatty acids, which were stored at -80°C for a maximum of 6 months. HPLC grade solvents were used for both semi-preparative HPLC purification and analytical HPLC analysis of LOX products. Large scale product purification was achieved by using a C18HAlsil 250 x 10 mm semi-preparative column, whereas a C18HAlsil 250 x 4.6 mm analytical column was used for product separation in tandem with MS/MS analysis. Both columns were purchased from Higgins Analytical (Mountain View, CA). All other chemicals were reagent grade or better and were used without further purification.

2.2.2 Protein Expression. All the LOX isozymes used in this publication were expressed and purified as previously published (h5-LOX,²⁸ h12-LOX,²⁵ h15-LOX-1²⁵ and s15-LOX-1²⁶, h15-LOX-2²⁷ and r15-LOX²⁹).

2.2.3 General Procedure for the Synthesis of Oxo-Lipids. The synthesis of all oxo-lipids consists of two steps, the first step is enzymatic while the second step is synthetic. In the synthesis of 13-oxo-ODE, s15-LOX-1 is reacted with linoleic acid (LA) in 100 mL of 100 mM Borate (pH 9.2) generating 13-HpODE. 15-oxo-ETE is generated by reaction between h15-LOX-2 and 40 μ M arachidonic acid (AA) in 100

mL of 25 mM HEPES (pH 7.5), generating 15-HpETE. 12-oxo-ETE is generated by reaction between h12-LOX and 40 μ M AA in 100 mL 25 mM HEPES (pH 8.0), generating 12-HpETE. 5-oxo-ETE is generated by reaction between 5-LOX and 40 μ M AA in 100 mL 25 mM HEPES (pH 7.3), 0.3 mM CaCl₂, 0.1 mM EDTA, 0.2 mM ATP, generating 5-HpETE. The reactions are quenched with 1-2% acetic acid and extracted using dichloromethane (DCM). The formation of 13-HpODE, 15-HpETE, 12-HpETE and 5-HpETE are monitored at 234 nm with a Perkin Elmer Lambda 40 UV/Vis spectrophotometer. The second step is an overnight synthetic reaction in which the hydroperoxy products are reacted with acetic anhydride and pyridine at 4°C in a 1:1 ratio to generate 13-oxo-ODE, 15-oxo-ETE, 12-oxo-ETE and 5-oxo-ETE respectively. The reactions are quenched with cold Milli-Q water for 2 hours. The oxo-lipids are purified via high performance liquid chromatography (HPLC) using a Higgins HAsiL Semi-Preparative C-18 column. Solution A was 99.9% ACN and 0.1% acetic acid; solution B was 99.9% H₂O and 0.1% acetic acid. An isocratic elution of 55% A: 45% B was used to purify each oxo-compound. The retention times for each oxo-lipid at 280 nm are as follows: 13-oxo-ODE (30 min), 15-oxo-ETE (33 min), 12-oxo-ETE (90 min) and 5-oxo-ETE (70 min). Analytical analysis was performed by liquid chromatography-mass spectrometry (LC-MS/MS). Solution A was 99.9% H₂O and 0.1% formic acid; solution B was 99.9% ACN and 0.1% formic acid. Oxo-lipids were injected onto a Phenomenex Synergi (4 μ M, 150 mm x 4.6 mm) C-18 column attached to a Thermo LTQ LC-MS/MS. The elution protocol consisted of 200 μ L/min, with an isocratic mobile phase of 45% solution A and 55% solution B.

Negative ion MS/MS was utilized (collision energy of 35 eV) to determine the fragmentation patterns of all the oxo-lipids. 13-oxo-ODE, parent $m/z = 293$, fragments $m/z = 113, 249, 293$; 15-oxo-ETE, parent $m/z = 317$, fragments $m/z = 113, 273, 299$; 12-oxo-ETE, parent $m/z = 317$, fragments $m/z = 153, 179, 273$; 5-oxo-ETE, parent $m/z = 317$, fragments $m/z = 129, 203, 273$.

The concentrations of the purified oxo-lipids are quantified using a Perkin Elmer Lambda 40 UV/Vis spectrophotometer based on the ϵ_{280} value of 13-oxo-ODE's ($28,000 \text{ M}^{-1}\text{cm}^{-1}$). The extinction coefficient for 13-oxo-ODE was determined by weighing the compound on an analytical balance, dissolving it with a known mass of HPLC grade methanol and measuring the absorbance (280 nm) for various concentrations of 13-oxo-ODE (Perkin-Elmer Lambda 40 UV/Vis spectrophotometer). A standard curve plot was used to extract the extinction coefficient for 13-oxo-ODE at 280 nm.

2.2.4 Lipoxygenase UV-Vis-based IC_{50} Assay. The initial one-point inhibition percentages were determined by following the formation of the conjugated diene product at 234 nm ($\epsilon = 25,000 \text{ M}^{-1}\text{cm}^{-1}$) with a Perkin-Elmer Lambda 40 UV/Vis spectrophotometer at one inhibitor concentration. The full IC_{50} experiments were done with at least five different inhibitor concentrations. All reactions were 2 mL in volume and constantly stirred using a magnetic stir bar at room temperature (23°C) with the appropriate amount of LOX isozyme (h5-LOX ($\sim 200 \text{ nM}$); h12-LOX ($\sim 100 \text{ nM}$); h15-LOX-1 ($\sim 60 \text{ nM}$); r15-LOX ($\sim 50 \text{ nM}$); h15-LOX-2 ($\sim 200 \text{ nM}$);

s15-LOX-1 (~ 2 nM)). The protein concentrations are the total protein concentration, however active protein concentration will be significantly less due to incomplete metallation. Incomplete metallation of the enzymes will not affect inhibitor potency, due to the relative nature of the IC₅₀ calculation. Reactions with h12-LOX were carried out in 25 mM HEPES (pH 8.0) 0.01% Triton X-100 and 10 μM AA. Reactions with the crude, ammonium sulfate precipitated h5-LOX were carried out in 25 mM HEPES (pH 7.3), 0.3 mM CaCl₂, 0.1 mM EDTA, 0.2 mM ATP, 0.01% Triton X100 and 10 μM AA. Reactions with h15-LOX-1, r15-LOX and h15-LOX-2 were carried out in 25 mM HEPES buffer (pH 7.5), 0.01% Triton X-100 and 10 μM AA. Reactions with s15-LOX-1 were carried out in 100 mM Borate (pH 9.2) 0.01% Triton X-100 and 10 μM AA. The concentration of AA was quantitated by allowing the enzymatic reaction to proceed to completion. IC₅₀ values were obtained by determining the enzymatic rate at various inhibitor concentrations and plotted against inhibitor concentration, followed by a hyperbolic saturation curve fit. The data used for the saturation curves were performed in duplicate or triplicate, depending on the quality of the data.

2.2.5 Incubation Activity Assay with Oxo-lipids and LOX. h15-LOX-1 and s15-LOX-1 rates and buffer conditions were utilized as described above, with the following modifications. A specific volume and concentration of h15-LOX-1 (or s15-LOX-1) was added to either the 12-oxo-ETE or 13-oxo-ODE oil (no solvent) and incubated on ice to ensure that the isozymes did not lose activity. It should be emphasized that the oxo-lipid was added as the oil, so as not to introduce solvent,

which could inhibit the LOX isozyme. Aliquots of approximately 20 μL of the incubated mixture were then added at designated time periods (intervals of 2 minutes, upwards to 30 minutes total) to a constantly stirring 2 mL cuvette, containing 10 μM AA. The control to this reaction was the same as above, but with no oxo-lipid oil added. This procedure was repeated for at least five different concentrations of 12-oxo-ETE or 13-oxo-ODE. The \ln (% Activity) was plotted versus time (s) to generate a slope = k_a . A second plot of k_a against $[\text{I}]_{\text{incubation}}$ allowed us to obtain K_i and k_2 .

2.2.6 Steady-State Inhibition Kinetics. h12-LOX rates were determined by monitoring the formation of the conjugated product, 12-HpETE, at 234 nm ($\epsilon = 25,000 \text{ M}^{-1}\text{cm}^{-1}$) with a Perkin Elmer Lambda 40 UV/Vis spectrophotometer. Reactions were initiated by adding h12-LOX to a constantly stirring 2 mL cuvette containing 0.4 μM – 10 μM AA in 25 mM HEPES buffer (pH 8.0), in the presence of 0.01% Triton X-100. The substrate concentration was quantitated by allowing the enzymatic reaction to proceed to completion. Kinetic data were obtained by recording initial enzymatic rates, at varied inhibitor concentrations (15-oxo-ETE), and subsequently fitted to the Henri-Michaelis-Menten equation, using KaleidaGraph (Synergy) to determine the microscopic rate constants, V_{max} ($\mu\text{mol}/\text{min}/\text{mg}$) and V_{max}/K_m ($\mu\text{mol}/\text{min}/\text{mg}/\mu\text{M}$). These rate constants were subsequently re-plotted $1/V_{\text{max}}$ and K_m/V_{max} versus inhibitor concentration, to yield K_{iu} and K_{ic} which are defined as the equilibrium constant of dissociation from the secondary and catalytic sites respectively.

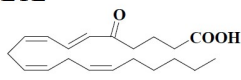
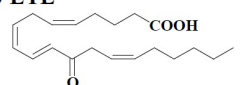
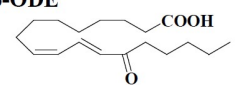
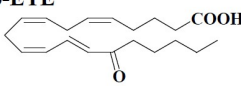
2.2.7 Determination of Oxo-lipids' Substrate Activity for LOX. The oxo-lipids were reacted with LOX to determine if they act as substrates due to their resemblance to LOX substrates. Two different experimental conditions were investigated. The first were the UV-Vis-based IC₅₀ assay conditions (see section 2.2.4), while the second were the incubation activity assay conditions (see section 2.2.5). For the IC₅₀ assay conditions, the following oxo-lipid and LOX combinations were followed by UV-Vis: h15-LOX-1, h12-LOX, and h5-LOX were each reacted with 10 μ M 5-oxo-ETE; h5-LOX and h15-LOX-1 were reacted with 10 μ M 12-oxo-ETE; and h12-LOX was reacted with 10 μ M 15-oxo-ETE. All reactions were in 2 mL of the enzyme's specific buffer and no change of absorbance at 234 nm or 280 nm was observed for any of the reactions. One pair, h12-LOX and 10 μ M 15-oxo-ETE, was also quenched with 2% acetic acid, extracted with DCM and shown under LC-MS that no oxidation product was formed, confirming that 15-oxo-ETE is not a substrate to h12-LOX under the IC₅₀ conditions. However, the pair that did result in a change of absorbance at 234 nm was h5-LOX with 10 μ M 15-oxo-ETE. This reaction was also quenched with 2% acetic acid, extracted with DCM and shown with LC-MS that multiple oxidation products were formed. Therefore, no inhibition data was gathered for this pair.

In the second set of conditions (incubation conditions), h12-LOX and h15-LOX-1 were each incubated with 10 μ M 15-oxo-ETE for 15 minutes. Each reaction was diluted with 2 mL of the corresponding enzyme buffer, quenched with 2% acetic acid, extracted with DCM, evaporated to dryness and brought up in 50 μ L of

methanol. HPLC (205 nm, 234 nm, 280 nm) and LC-MS analysis did not show significant degradation, confirming that 15-oxo-ETE is not a substrate for either h12-LOX or h15-LOX-1, under the time-dependence incubation conditions.

2.3 Results and Discussion

2.3.1 Evaluation of Oxo-Lipids As Inhibitors of LOXs. To determine the inhibitory potency and selectivity of 5-oxo-ETE, 12-oxo-ETE, 13-oxo-ODE and 15-oxo-ETE, each oxo-lipid was screened as an inhibitor against h5-LOX, h12-LOX, h15-LOX-1, h15-LOX-2, r15-LOX and s15-LOX-1 (**Table 2.1**). To summarize **Table 2.1**, 15-oxo-ETE exhibited the highest potency against h12-LOX, with an IC_{50} value of $1.0 \pm 0.1 \mu\text{M}$ and was also found to be the most selective oxo-lipid, with low potency against the other LOX isozymes (IC_{50} values greater than $25 \mu\text{M}$). 12-oxo-ETE inhibited both h12-LOX and h15-LOX-1, but with an almost three-fold difference, revealing a higher potency against h15-LOX-1 ($IC_{50} = 3.0 \pm 0.1 \mu\text{M}$) than h12-LOX ($IC_{50} = 8.0 \pm 1 \mu\text{M}$). On the contrary, 5-oxo-ETE did not inhibit any of the LOXs significantly, with only a slight activity against h12-LOX ($IC_{50} = 15 \pm 2 \mu\text{M}$). The oxo-lipid found to be the least potent against all the LOXs studied was 13-oxo-ODE with IC_{50} values greater than $100 \mu\text{M}$ for all LOXs.

Table 1. Inhibition potencies of various oxo-lipids against LOX isozymes ^a						
	h5-LOX	h12-LOX	h15-LOX-1	h15-LOX-2	r15-LOX	s15-LOX-1
5-oxo-EETE 	- ^b	15 ± 2	>25 ^c	>100	>25	>100
12-oxo-EETE 	>50	8.0 ± 1	3.0 ± 0.1	>100	>50	>100
13-oxo-ODE 	>100	>100	>100	>100	>100	>100
15-oxo-EETE 	>100	1 ± 0.1	>25	>100	>50	>100

^a All IC₅₀ values (μM) were conducted with 10 μM AA, 0.01% Triton X-100 and LOX isozyme specific buffers (see section 2). Each experiment was done in triplicate, with the average and SD presented.

^b Exhibited substrate activity.

^c The IC₅₀ value of weak inhibitors were approximated from one point inhibitor screens (in triplicate), at 25 μM inhibitor. Inhibitors with less than 5% inhibition at 25 μM were designated >100 μM. Inhibitors with less than 25% inhibition but greater than 5% inhibition were designated >50 μM, and inhibitors with less than 50% inhibition but greater than 25% inhibition were designated >25 μM. Inhibitors with greater than 50% inhibition at 25 μM were studied further and full IC₅₀ values determined.

Table 2.1. Inhibitor potencies of oxo-lipids against LOX isozymes.

2.3.2 Probing the Mechanism of Inhibition Via Time Dependence

Experiments. To further examine the mode of inhibitory action of oxo-lipids against LOX, time incubation experiments were performed. Due to these oxo-lipids' capability of behaving as general Michael acceptors, it was thought that these molecules could react with a nucleophilic residue in the active site, inactivating the enzyme. Such an action between a target-specific covalent inhibitor and an enzyme can be described by the general mechanism in **Figure 2.1**.²¹

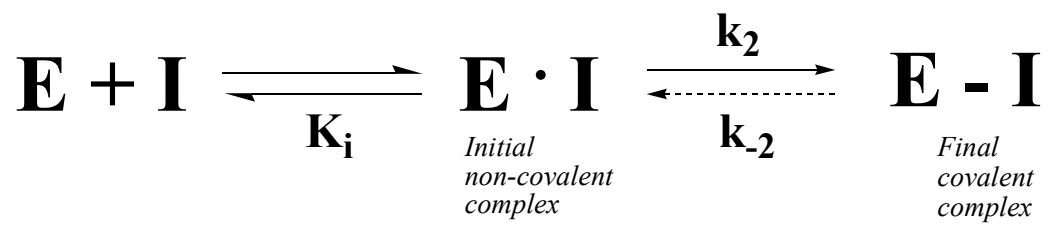


Figure 2.1. General mechanism of a covalent inhibitor.

The first event is the non-covalent binding of the oxo-lipid to the LOX active site, placing it close to an active site nucleophilic residue. At which point the nucleophilic residue attacks the Michael acceptor of the oxo-lipid. If these oxo-lipids behave as pure irreversible covalent inhibitors then k_{-2} will be essentially zero. Inhibitors that behave in this manner can be described by their equilibrium inhibitor constant (K_i) and their rate of covalent modification (k_2).²¹ To test if such a mechanism occurred with LOX inhibition, an oxo-lipid was incubated with a LOX isozyme where the concentration of the inhibitor was kept constant, while the incubation time was varied. The extent of inhibition was measured at several time points, and the observed rate of inhibition, k_a , extracted from the slope of a plot of the \ln (% Activity) versus time (data not shown). These graphs were repeated at various oxo-lipid concentrations and the k_a values were re-plotted against the concentration of oxo-lipids and then fitted to the hyperbolic equation, $k_{obs}=k_2[I]/(K_i+[I])$, which yields K_i and k_2 . For 12-oxo-ETE and h15-LOX-1, the data revealed a fit to the hyperbolic equation above, with a K_i of $36.8 \pm 13.2 \mu\text{M}$ and a k_2 of $0.0019 \pm 0.00032 \text{ s}^{-1}$. These data indicate that 12-oxo-ETE is a poor irreversible inhibitor to h15-LOX-1. This experiment was also performed with h15-LOX-1 versus 15-oxo-ETE and s15-LOX-1 versus 13-oxo-ODE, both of which had similarly large K_i values and long k_2 rates. Therefore, it appears that the irreversible Michael addition mechanism is not a biologically relevant mode of action by which these oxo-lipids inhibit LOX.

2.3.3 Steady State Inhibition Kinetics. The mode of inhibition of 15-oxo-ETE against h12-LOX was probed further with steady-state inhibition kinetics. The

formation of 12-HpETE was monitored as a function of substrate and inhibitor concentration in the presence of 0.01% Triton-X-100. A Dixon plot (**Figure 2.2A**) and replot (**Figure 2.2B**) of the kinetic data yielded a K_{ic} of $0.087 \pm 0.008 \mu\text{M}$ and a K_{iu} of $2.10 \pm 0.8 \mu\text{M}$, which are defined as the equilibrium constants of dissociation from the enzyme and enzyme substrate complex, respectively. These data are consistent with mixed inhibition, which is typical of LOX inhibitors.³⁰

2.4 Conclusion. In summary, the data reveals that 15-oxo-ETE exhibited the highest potency and selectivity against h12-LOX with an $\text{IC}_{50} = 1 \pm 0.1 \mu\text{M}$. 12-oxo-ETE had comparable potency against h15-LOX-1 ($\text{IC}_{50} = 3.0 \pm 0.1 \mu\text{M}$) but was not selective and inhibited h12-LOX with an $\text{IC}_{50} = 8.0 \pm 1 \mu\text{M}$. The steady state inhibition kinetics revealed a very low K_{ic} of $0.087 \pm 0.008 \mu\text{M}$ for 15-oxo-ETE against h12-LOX, which may be at a level that is biologically relevant. The time dependence incubation studies did not demonstrate irreversible inhibition of LOX isozymes by oxo-lipids, however, the large concentration needed and long time required precluded any biological relevance. To our knowledge, this is the first time that an oxo-lipid has been shown to inhibit LOX and could indicate selective regulation of h12-LOX by h15-LOX activity, through 15-oxo-ETE inactivation. Future work is planned to determine if oxo-lipids regulate LOX activity in the cell.

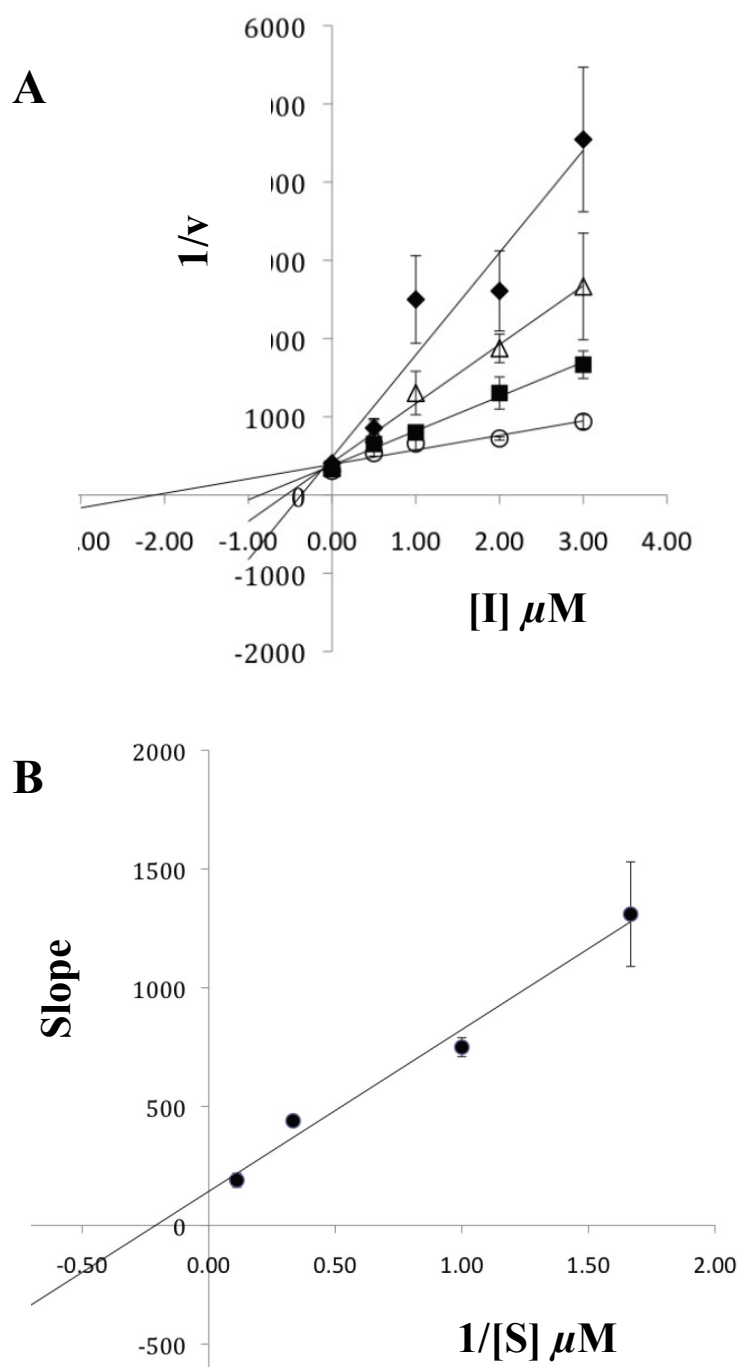


Figure 2.2. (A) The Dixon plot of the primary data from the steady-state inhibition kinetic experiments of h12-LOX and 15-oxo-EET. The substrate concentrations are 0.6 μM (closed diamonds), 1 μM (open triangles), 3 μM (closed squares) and 9 μM (open circles). (B) The Dixon replot of slope versus [Inhibitor] yielded K_{ic} of $0.087 \pm 0.008 \mu\text{M}$ and a K_{iu} of $2.1 \pm 0.8 \mu\text{M}$. All experiments were done in triplicate with averages and SD presented.

2.5 References

1. Needleman, P.; Turk, J.; Jakschik, B.A.; et. al. *Annu. Rev. Biochem.* **1986**, 55, 69.
2. Hamberg, M.; Samuelsson, B. *J. Biol. Chem.* **1967**, 212, 5329.
3. Borgeat, P. *Can. J. Physiol Pharmacol.* **1989**, 67, 936.
4. Murphy, R.C.; Zarini, S. *Prostaglandins Other Lipid Mediat.* **2002**, 68-69, 471.
5. Zarini, S.; Murphy, R.C. *J. Biol. Chem.* **2003**, 278, 11190.
6. Powell, W.S.; Gravelle, F.; Gravel, S. *J. Biol. Chem.* **1992**, 267, 19233.
7. Bergholte, J.M.; Soberman, R.J.; et. al. *Arch. Biochem. Biophys.* **1987**, 257, 444.
8. Powell, W.S.; MacLeod, R.J.; Gravel, S.; Gravelle, F. *J. Immunol.* **1996**, 156, 336.
9. Powell, W.S.; Gravel, S.; MacLeod, R.J.; Mills, E. *J. Biol. Chem.* **1993**, 268, 9280.
10. Hosoi, T.; Koguchi, Y.; Sugikawa, E.; et. al. *J. Biol. Chem.* **2002**, 277, 31459.
11. Sturm, G.J.; Schuligoi, R.; Amann, R. *J. Allergy Clin. Immunol.* **2005**, 116, 1014.
12. Huang, J.T.; Welch, J.S.; Ricote, M.; et. al. *Nature.* **1999**, 400, 378.
13. Hammond, V.J.; Morgan, A.H.; Schopfer, F.J. *J. Biol. Chem.* **2012**, 287, 41651.
14. Powell, W.S.; Hashefi, M.; Falck, J.R.; et. al. *J. Leukocyte Biol.* **1995**, 57, 257.
15. Wainwright, S.L.; Powell, W.S. *J. Biol. Chem.* **1991**, 266, 20899.
16. Naccache, P.H.; Leblanc, Y.; et. al. *Biochim Biophys Acta.* **1991**, 1133, 102.
17. Altmann, R.; Hausmann, M.; Rogler, G.; et al. *Biochem. Pharm.* **2007**, 74, 612.

18. Seeley, S.K.; Poposki, J.A.; et al. *Biochim. Biophys. Acta.* **2006**, 1760, 1064.
19. Bull, A.W.; Seeley, S.K.; Geno, J.L. *Biochim. Biophys. Acta.* **2002**, 1571, 77.
20. Podgorski, I. A.; Bull, W. *Biochim. Biophys. Acta.* **2001**, 1533, 55.
21. Singh, J.; Petter, R.C.; Baillie, T.A. *Nat. Rev. Drug Discov.* **2011**, 10, 307.
22. Cohen, M.S.; Zhang, C.; Shokat, K.M; Taunton, J. *Science*, **2005**, 308, 1318.
23. Zhang, T.; Gray, N.S.; et al. *Chem Biol*, **2012**, 19, 140.
24. Hornig, M.; Markoutsas, S.; et al. *Mol. Cell Biol. Lipids.* **2012**, 1821, 279.
25. Amagata, T.; Whitman, S.; et al. *J. Nat. Prod.* **2003**, 66, 230.
26. Holman, T.R.; Zhou, J.; Solomon, E.I. *J. Am. Chem. Soc.* **1998**, 120, 12564.
27. Martinez, Y.V.; Ohri, R.V.; et al. *Bioorg. Med. Chem.* **2007**, 15, 7408.
28. Robinson, S.J.; Hoobler, E.K.; Riener, M; et al. *J. Nat. Prod.* **2009**, 72: 1857.
29. Sloane, D.L.; et al. *Biochem. Biophys. Res. Comm.* **1990**, 173, 507.
30. Rai, G.; Kenyon, V.; Jadhav, A.; Schultz, L.; et al. *J. Med. Chem.* **2010**, 53, 7392.

Chapter 3

DISCOVERY OF THREE SMALL MOLECULE INHIBITORS TARGETING HUMAN EPITHELIAL 15-LIPOXYGENASE-2

3.1 Introduction

Lipoxygenases catalyze the peroxidation of polyunsaturated fatty acids into their corresponding hydroperoxy derivatives.¹ These fatty acids contain a bisallylic hydrogen surrounded by two cis double bonds such as linoleic acid (LA) and arachidonic acid (AA).¹ The reaction is initiated by abstraction of the doubly allylic hydrogen atom via a proton-coupled electron transfer mechanism generating a substrate radical which is oxidized two carbons away from the site of abstraction.² The enzymes are named according to their product specificity with AA as the substrate. Arachidonic acid serves as a major precursor of active lipid metabolites that are involved in a number of significant disease states.³⁻⁵

The human genome consists of six functional lipoxygenase (LOX) genes (ALOX5, ALOX12, ALOX12B, ALOX15, ALOX15B, eLOX3) encoding for six different LOX isoforms (h5-LOX, h12S-LOX, h12R-LOX, h15-LOX-1, h15-LOX-2, eLOX3).⁴ The biological role in health and disease for each LOX isozyme varies dramatically, ranging from asthma (h5-LOX) to diabetes (h12-LOX) to stroke (h15-LOX-1).³ Interestingly, the role of epidermal human 15-lipoxygenase-2 is not as clear as those of the other isozymes. However, recently epithelial h15-LOX-2 was found to be highly expressed in atherosclerotic plaques and linked to the progression of macrophages to foam cells, which are present in atherosclerotic plaques.^{3,6-10} The transformation of macrophages to foam cells is a key component in the progression of atherosclerosis. This process induces the secretion of pro-inflammatory cytokines,

attracting more macrophages and contributing to plaque inflammation and instability.³ Two key features of atherosclerosis are lipid retention and inflammation. Macrophage-derived foam cells are deposited in plaques that grow, restricting vascular blood flow or causing arteries to rupture, which results in a heart attack or stroke.¹¹ Coronary artery disease is the primary cause of deaths in both men and women in America and finding tools to better understand the key players involved in this disease, such as h15-LOX-2, is of clinical interest.¹²

The specific role of h15-LOX-2 in plaque formation is still unclear. Recent data demonstrate that silencing the ALOX15B gene in human macrophages leads to decreased cellular lipid accumulation, a major factor in foam cell formation and thus plaque accumulation.¹³⁻¹⁴ Furthermore, h15-LOX-2 mRNA levels are highly elevated in human macrophages isolated from carotid atherosclerotic lesions of symptomatic rather than asymptomatic patients.^{13,15} Human 15-LOX-2 predominantly catalyzes the formation of 15-HpETE from AA and the hydroperoxide is then reduced to hydroxides in the cell. The reduced 15-HETE product has been shown to promote formation of atherosclerotic lesions in a mouse model.¹⁶

The role of h15-LOX-2 in atherosclerosis suggests that it may be an appropriate therapeutic target for heart disease. Currently, only a few published inhibitors targeting h15-LOX-2 have been reported to date. Nordihydroguaiaretic acid (NDGA), a redox inhibitor, has a potency of 11.0 (0.7) μM while 27c, a flavanoid derivative has an $\text{IC}_{50} = 8.3$ (0.9) μM but neither molecule is selective towards h15-

LOX-2.^{17,18} However, two molecules previously discovered by our laboratory, MLS000545091 and MLS000536924, do exhibit strong potency as well as selectivity for h15-LOX-2, with K_{ic} values of 0.9 (0.4) μ M and 2.5 (0.5) μ M, respectively.¹⁹ The discovery of more inhibitors that are potent and selective against h15-LOX-2 would be advantageous in understanding its role in atherosclerosis. Herein, we report two new molecular scaffolds discovered using high throughput screening (HTS) that exhibit potency and selectivity against h15-LOX-2.

3.2 Materials and Methods

3.2.1 Materials. All commercial fatty acids were purchased from Nu Chek Prep, Inc. (MN, USA). BWb70c was purchased from Sigma/Aldrich Chemicals. The inhibitors were obtained from the NIH Molecular Libraries Small Molecule Repository (MLSMR): (<https://mli.nih.gov/mli/compound-repository/>). All other chemicals were reagent grade or better and were used without further purification.

3.2.2 Protein Expression. All the LOX isozymes used in this publication were expressed and purified as previously reported (h5-LOX²⁰, h12-LOX²¹, h15-LOX-1²¹ and h15-LOX-2²²). Human leukocyte 5-lipoxygenase was expressed as a non-tagged protein and used as a crude ammonium sulfate precipitated protein. The remaining enzymes: h15-LOX-1, h15-LOX-2 and h12-LOX were expressed as N-terminal His6-tagged proteins and purified via immobilized metal affinity chromatography (IMAC) using Ni-NTA resin. The purity of each protein was analyzed by SDS-PAGE and found to be greater than 90%.

3.2.3 Lipoygenase UV-Vis-based IC₅₀ Assay. The initial one-point inhibition percentages were determined by following the formation of the conjugated diene product at 234 nm ($\epsilon = 27,000 \text{ M}^{-1}\text{cm}^{-1}$) with a Perkin-Elmer Lambda 40 UV/Vis spectrophotometer at 25 μM inhibitor concentration. All inhibitors that showed greater than 70% inhibition were investigated further to determine their IC₅₀ values. The full IC₅₀ experiments were done with at least five different inhibitor concentrations. All reaction mixtures were 2 mL in volume and constantly stirred using a magnetic stir bar at room temperature (23°C) with the appropriate amount of LOX isozyme (h5-LOX (~ 200 nM); h12-LOX (~ 50 nM); h15-LOX-1 (~ 60 nM); h15-LOX-2 (~ 200 nM)). The protein concentrations are the total protein concentration; however, active protein concentration will be significantly less due to incomplete metallation. Reactions with h12-LOX were carried out in 25 mM HEPES (pH 8.0) 0.01% Triton X-100 and 10 μM AA. Reactions with the crude, ammonium sulfate precipitated h5-LOX were carried out in 25 mM HEPES (pH 7.3), 0.3 mM CaCl₂, 0.1 mM EDTA, 0.2 mM ATP, 0.01% Triton X100 and 10 μM AA. Reactions with h15-LOX-1 and h15-LOX-2 were carried out in 25 mM HEPES buffer (pH 7.5), 0.01% Triton X-100 and 10 μM AA. The concentration of AA was quantitated by allowing the enzymatic reaction to proceed to completion in the presence of soybean 15-LOX-1 (s15-LOX-1). IC₅₀ values were obtained by determining the percent inhibition at various inhibitor concentrations and plotting against inhibitor concentration, followed by a hyperbolic saturation curve fit. The percent inhibition was calculated by comparing the enzymatic rate of the control (DMSO) to the

enzymatic rate with the respective inhibitor present. The experiments used for generating the saturation curves were performed in duplicate or triplicate, depending on the quality of the data. All inhibitors were stored at -20°C in DMSO.

3.2.4 Steady-State Inhibition Kinetics of h15-LOX-2. The steady-state equilibrium constants of dissociation for MLS000327069, MLS000327186, MLS000327206 were determined by monitoring the formation of the conjugated product, 15-HpETE, at 234 nm ($\epsilon = 27,000 \text{ M}^{-1} \text{ cm}^{-1}$) with a Perkin Elmer Lambda 40 UV/Vis spectrophotometer. Reactions were initiated by adding h15-LOX-2 to a constantly stirring 2 mL reaction mixture containing 0.7 μM – 20 μM AA in 25 mM HEPES buffer (pH 7.5), in the presence of 0.01% Triton X-100. Kinetic data were obtained by recording initial enzymatic rates, at varied inhibitor concentrations, and subsequently fitting the data to the Henri-Michaelis-Menten equation using KaleidaGraph (Synergy) to determine V_{max} ($\mu\text{mol}/\text{min}$) and K_{M} (μM). The primary data were then plotted in Dixon format using Microsoft Excel by graphing $1/v$ vs. $[I]$ μM at the chosen substrate concentrations. From the Dixon plots, the slope at each substrate concentration was extracted and plotted against $1/[S]$ μM to produce the Dixon replots. The K_{ic} equilibrium constant of dissociation was calculated by dividing $K_{\text{M}}/V_{\text{max}}$ by the slope of the replot. To obtain K_{iu} , $1/V_{\text{max}}$ was divided by the y-intercept of the replot. K_{ic} and K_{iu} are defined as the equilibrium constant of dissociation from the catalytic and secondary sites, respectively.

3.2.5 Pseudo-peroxidase Assay. The pseudo-peroxidase activity of MLS000327069, MLS000327186 and MLS000327206 were determined with h15-LOX-2 on a Perkin-Elmer Lambda 40 UV/Vis spectrophotometer as described previously.²³ 13-HpODE was used as the oxidant and BWb70c as the positive control. The reaction was initiated by addition of 20 μ M 13-HpODE to 2 mL buffer (50 mM sodium phosphate (pH 7.4), 0.3 mM CaCl₂, 0.1 mM EDTA, 0.01% Triton X-100) containing 20 μ M MLS000327069, MLS000327186, or MLS000327206 and 200 nM h15-LOX-2. The reaction mixtures were constantly stirred at 23°C. Activity was determined by monitoring the decrease at 234 nm (product degradation) and the percent consumption of 13-HpODE was recorded. More than 25% 13-HpODE degradation indicates redox activity of that particular inhibitor. The negative controls used were: enzyme alone with product, enzyme alone with inhibitor, as well as inhibitor alone with product. These formed a baseline for the assay, reflecting non-pseudo-peroxidase dependent hydroperoxide product decomposition. To rule out the auto-inactivation of the enzyme from pseudo-peroxidase cycling, the h15-LOX-2 residual activity was determined by the addition of 20 μ M AA at the end of each reaction. The initial rates of the inhibitor and 13-HpODE were compared to initial rates of inhibitor alone because the inhibitor by itself inherently lowers the rate of oxygenation. Activity is characterized by direct measurement of the product formation with the increase of absorbance at 234 nm.

3.2.6 Cyclooxygenase Selectivity Assay. Cyclooxygenase selectivity assay was performed as previously described.²³ Approximately 3 μ g of either ovine COX-1

(COX-1) or human recombinant COX-2 (COX-2) (Cayman Chemical) were added to buffer containing 0.1 M Tris-HCl buffer (pH 8.0), 5 mM EDTA, 2 mM phenol and 1 μ M hemin at 37°C. The selected inhibitors, MLS000327069, MLS000327186, or MLS000327206, were added to the reaction cell, followed by a 5 minute incubation with either of the COX isozymes. The reaction was then initiated by adding approximately 100 μ M AA in the reaction cell, as indicated in the enzymatic protocol (Cayman Chemicals). A Hansatech DWI oxygen electrode was utilized for data collection and the consumption of oxygen was recorded. Indomethacin and the vehicle of inhibitor (DMSO) were the positive and negative controls, respectively. The percent inhibition of the enzyme was calculated by comparing the rates of O₂ consumption for experimental samples (with inhibitor) to the rates of control samples (with DMSO).

3.2.7 Determination of Substrate Activity of Inhibitors. The inhibitors MLS000327069, MLS000327186, or MLS000327206 were reacted with h15-LOX-2 to determine if they act as substrates. All buffer conditions and the determination of each rate are identical to the UV-Vis assay mentioned above (Methods section 3.2.3). 20 μ M of each inhibitor was reacted with h15-LOX-2 in 2 mL reaction mixtures in the absence of AA. Controls consisted of DMSO (vehicle), 10 μ M AA and enzyme. All reactions were conducted on a Perkin Elmer Lambda 40 UV/Vis spectrophotometer. No change of absorbance at 234 nm or at 280 nm was observed for each reaction. Each reaction mixture was subsequently extracted and analyzed via RP-HPLC using a Higgins HAsiL analytical column. Solution A was 99.9% ACN

and 0.1% acetic acid; solution B was 99.9% H₂O and 0.1% acetic acid. An isocratic elution of 55%A:45%B was used in the HPLC analysis. Retention times and absorbance spectra of each of the reactions were compared to spectra of the controls. Collectively, the data from the UV-Vis experiments as well as the HPLC analysis confirm that these inhibitors do not act as substrates to h15-LOX-2.

3.2.8 Virtual Screening of h15-LOX-2 Inhibitors. In order to determine the binding mode of the ligands MLS000327069, MLS000327186 and MLS000327206, we used virtual screening, with the Glide software (version 66013, Schrodinger Suite 2015 release 1). These studies were performed by our collaborators at the University of California, San Francisco in Dr. Matt Jacobson's laboratory. Before performing the computational screening, we subjected the h15-LOX-2 crystal structure (pdb id 4nre) to a protein preparation step (Schrodinger Inc). The protein preparation step consists of: (i) adding hydrogens, (ii) setting proper atom types for the metal ions, (iii) assigning appropriate protonation state to titratable residues such as His, Asp and Glu, (iv) optimizing Asn, Gln, Thr and Tyr residues for better hydrogen bond interaction and (v) a short minimization of the whole protein structure such that the heavy atom RMSD does not exceed 0.3 Å from the starting structure. During the protein preparation step, we retained the co-crystallized ligand, metal ion (Fe²⁺) and a water molecule that co-ordinates the metal ion. In our previously published docking studies we did not include the water and treated the iron as ferric ion. However, our recent docking calculations on h15-LOX-1 have shown that the ability to identify high affinity inhibitors (ML094 series inhibitors with IC₅₀ < 1 μM) at the top 1% of the

docking hitlist was two-fold higher when we included ferrous ion and water than ferric ion and hydroxide. Therefore, we included water and ferrous ion in the present work.

The h15-LOX-2 ligands were built using Edit/Built panel of the Maestro software (Schrodinger Inc). They were subsequently energy minimized using LigPrep software (Schrodinger Inc).

In our earlier calculation we successfully docked the h15-LOX-2 inhibitors, MLS000545091 and MLS000536924, after opening the active site by means of induced fit docking (using the software InducedFit Dock, Schrodinger Inc). Following this approach, we docked the potent inhibitor MLS000327069 using InducedFit Dock software. After the induced fit docking side chains of most of the active site residues remained unchanged. However, the side chain of Leu420 flipped to accommodate the heterocyclic ring of MLS000327069. We carried out the protein preparation step on the resulting structure and used it in the subsequent docking studies.

Docking consists of two steps. The first step is the grid preparation step. The binding pocket characteristics were identified and stored for later use during docking pose and rank (score) evaluation. The second step is the actual docking step. During the docking step we kept the protein structure rigid, only the ligand conformations were sampled in the protein active site. The low energy binding conformation was selected by means of Glide extra-precision (XP) score.²⁴ After the docking poses

were generated, we refined the poses using molecular-mechanics energy function (MM-GBSA).²⁵

3.3 Results and Discussion

3.3.1 Compound Identification and Inhibitor Potency. Previously, our laboratory reported the identity of two novel and specific h15-LOX-2 inhibitors, MLS000545091 and MLS000536924, from our High Throughput Screening (HTS) of a 107,261 compound library. Structurally, MLS000545091 contains a 1,3,4-oxadiazole heterocycle, while MLS000536924 contains a 1,2,4-triazole ring. These two inhibitors were discovered from manually screening the top 300 molecules of the HTS. We continued to manually screen the next top 600 molecules and discovered three additional inhibitors, MLS000327069, MLS000327186, and MLS000327206. The newly discovered molecules are structurally different from the two inhibitors mentioned previously in that they contain an imidazole ring, which is substituted at the one and two positions. The new HTP inhibitor “hits” were screened against h15-LOX-2 (25 μM), but only inhibitors that exhibited greater than 70% inhibition were investigated further. MLS000327069, MLS000327186, and MLS000327206 were the only compounds that exhibited greater than 70% inhibition and therefore full IC_{50} experiments on each molecule were performed with five different inhibitor concentrations (**Figure 3.1**). MLS000327069 inhibited h15-LXO-2 with an IC_{50} equaling $0.71 \pm 0.06 \mu\text{M}$, while MLS000327186 had a potency of $0.9 \pm 0.1 \mu\text{M}$ and finally MLS000327206 showed a similar potency with a value of $1.1 \pm 0.1 \mu\text{M}$.

3.3.2 Steady-State Inhibition Kinetics. The mode of inhibition which MLS000327069, MLS000327186, and MLS000327206 exhibit against h15-LOX-2 was probed utilizing steady-state inhibition kinetics. The formation of 15-HpETE was monitored as a function of substrate and inhibitor concentration in the presence of 0.01% Triton-X-100. A Dixon plot of the primary data for MLS000327186 is shown in **Figure 3.2A**, while a Dixon replot of the secondary data is shown in **Figure 3.2B**. Fitting the data yielded a K_{ic} of $0.80 \pm 0.05 \mu\text{M}$ and a K_{iu} of $4.0 \pm 2.6 \mu\text{M}$, which are defined as the equilibrium constants of inhibitor dissociation from the enzyme and enzyme substrate complex, respectively. The steady-state inhibition kinetic experiments were also performed for MLS000327069 and MLS000327186. **Table 3.1** lists the equilibrium constants of inhibitor dissociation for all three molecules, which were all determined from Dixon plots and Dixon replots. The data (**Table 3.1**) demonstrate that all three inhibitors exhibit mixed inhibition against h15-LOX-2, with the numbers being consistent with the IC_{50} values (**Figure 3.1**).

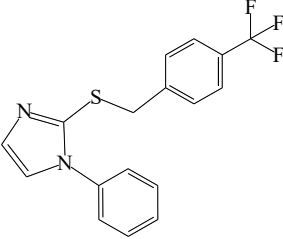
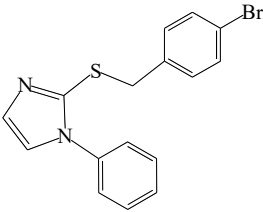
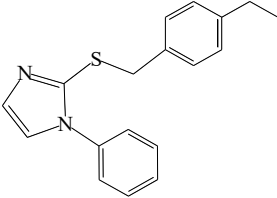
Inhibitors	Structure	IC ₅₀ (μM) (± SD)
MLS000327069		0.71 (0.06)
MLS000327186		0.9 (0.1)
MLS000327206		1.1 (0.1)

Figure 3.1. IC₅₀ values for the newly discovered inhibitors targeting h15-LOX-2 with error in parentheses. All experiments were conducted in duplicate and with 10 μM AA.

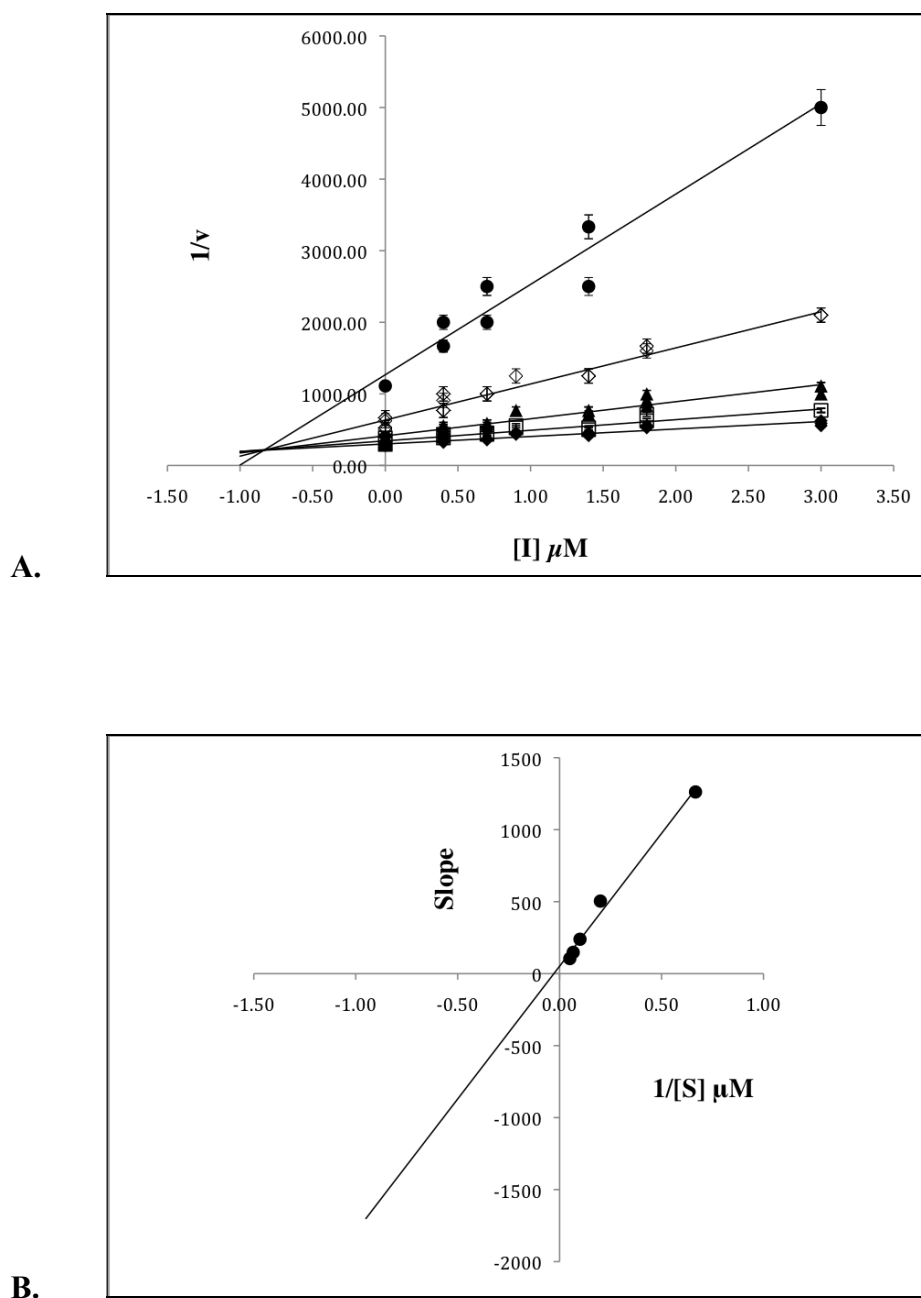
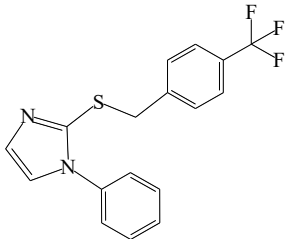
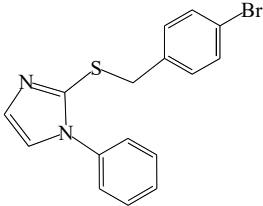
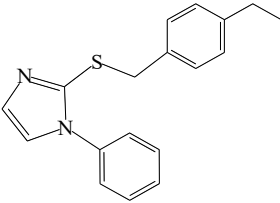
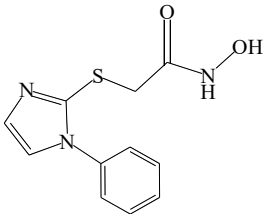
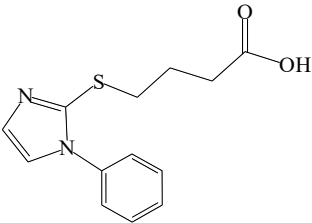


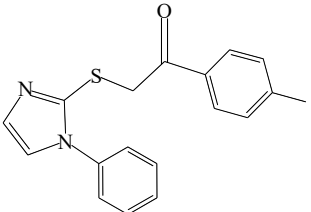
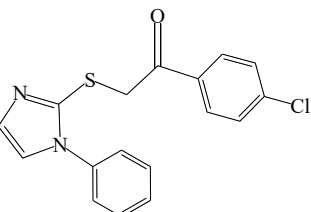
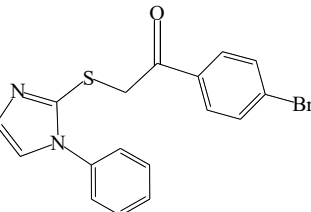
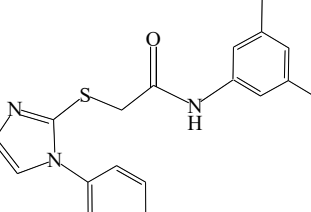
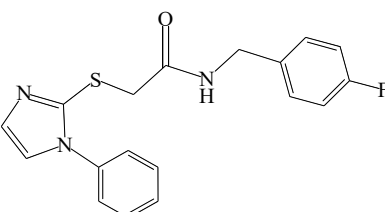
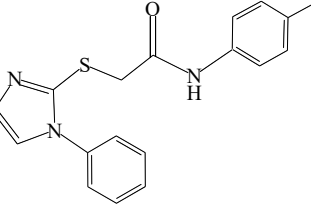
Figure 3.2. Steady-state inhibition kinetic data for the determination of K_{ic} and K_{iu} of h15-LOX-2 and MLS000327186. (A) Dixon plot of the primary data of h15-LOX-2 and MLS000327186. The substrate concentrations are 1.5 μM (closed circles), 5 μM (open diamonds), 10 μM (closed triangles), 15 μM (open squares) and 20 μM (closed diamonds). The Dixon replot of slope versus [Inhibitor] yielded a K_{ic} of 0.80 (0.05) μM and a K_{iu} of 4.0 (2.6) μM .

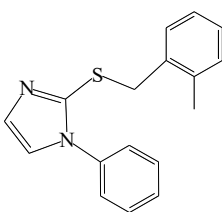
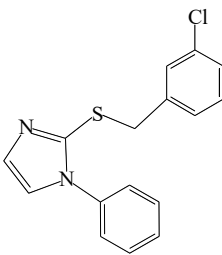
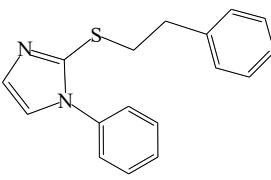
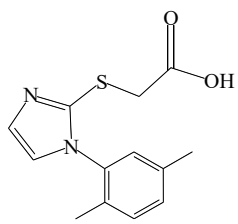
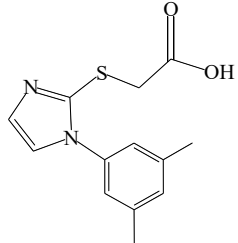
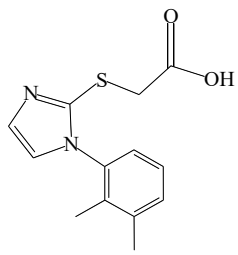
Inhibitor	K_{ic} (μM)	K_{iu} (μM)
MLS000327069	0.70 (0.07)	1.2 (0.90)
MLS000327186	0.80 (0.05)	4.0 (2.6)
MLS000327206	0.90 (0.04)	3.4 (2.4)

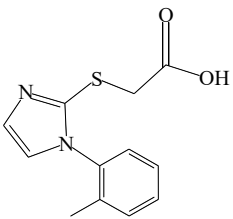
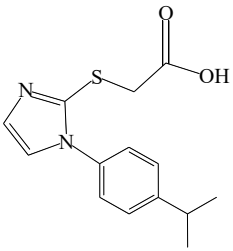
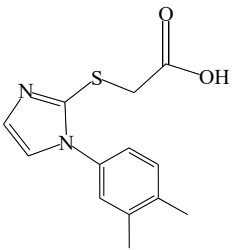
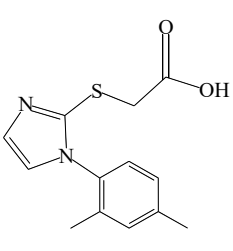
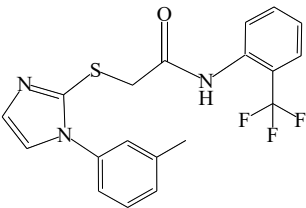
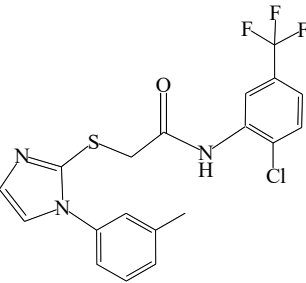
Table 3.1. The equilibrium constant of dissociation from the catalytic (K_{ic}) and secondary (K_{iu}) sites extracted from Dixon plots and Dixon replots of h15-LOX-2 and MLS000327069, MLS000327186, and MLS000327206.

3.3.3 Structure/Activity Relationship (SAR) Study. Following the discovery of the three new molecules, a limited SAR, utilizing molecules in the public domain was performed. Twenty-three molecules were screened at 20 μM inhibitor concentration (**Figure 3.3**). The three lead molecules, MLS000327069, MLS000327186, and MLS000327206 possess an imidazole ring substituted at the one and two positions. The one position of the imidazole heterocycle contains a phenyl in all three molecules. The second position of the imidazole ring is substituted with a sulfur attached to a para-substituted benzyl. The three lead compounds had various substituents at the para position of the benzyl ring, a trifluoromethyl (MLS000327069), bromo (MLS000327186) and ethyl (MLS000327206) which all demonstrated comparable potency (98-100% inhibition at 20 μM). Replacement of the para-substituted benzyl with a hydroxamic acid (A), carboxylic acid (B), or amide (F-H) completely abolishes inhibitor potency with only 0-18% inhibition (Table). When a ketone (C-E) is inserted on the benzylic carbon, 51-62% inhibition is seen. Substitutions on the ortho (I) and meta (J) position, instead of the para position, drops the inhibition to 31% and 39%, respectively. Addition of a methylene carbon in between the sulfur and benzylic carbon has a modest effect (68%) on the inhibition (K). Modifications to the substitution patterns on the phenyl ring at position one of the imidazole (L-R), while retaining the carboxylic acid replacement of benzyl substituent near the sulphur, decreases the potency (4-16%). In summary, only slight structural modifications can be tolerated with regards to maintaining the potencies of the three lead molecules.

Inhibitors	Structure	% I at 20 μ M	IC ₅₀ (μ M) (\pm SD)
MLS000 327069		100	0.71 (0.06)
MLS000 327186		100	0.9 (0.1)
MLS000 327206		98	1.1 (0.1)
Group 1			
A		4	> 100
B		8	> 100

C		56	> 25
D		62	> 25
E		51	> 25
F		0	> 100
G		8	> 100
H		18	> 50

I		31	> 50
J		39	> 50
K		68	> 25
Group 2			
L		4	> 100
M		7	> 100
N		7	> 100

O		8	> 100
P		13	> 100
Q		14	> 100
R		16	> 50
Group 3			
S		4	> 100
T		13	> 100

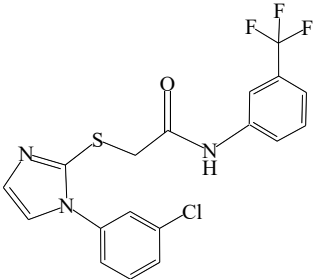
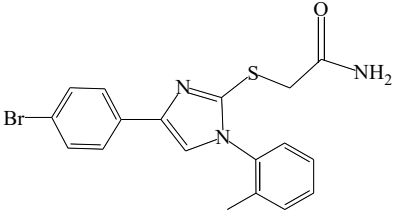
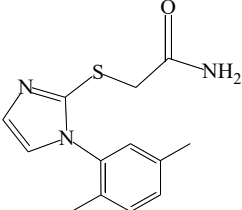
U		13	> 100
V		5	> 100
W		3	> 100

Figure 3.3. IC₅₀ values of h15-LOX-2 inhibitors selected for the structure/activity relationship study; errors when available are in brackets. Experiments were conducted in the presence of 10 μ M AA with 0.01% Triton X-100, 20 μ M inhibitor concentration and were performed in duplicate.

3.3.4 Selectivity Assays. Once the potencies of the three small molecule inhibitors against h15-LOX-2 had been determined, their selectivity against h5-LOX, h15-LOX-1, h12-LOX, COX-1 and COX-2 were investigated. All three molecules displayed extremely high selectivity for h15-LOX-2 against all enzymes tested (**Table 3.2**), with approximately 100-fold selectivity against h5-LOX, h12-LOX, COX-1 and COX-2. Against h15-LOX-1, the three molecules displayed slightly less selectivity, approximately 50-fold.

3.3.5 Pseudo-peroxidase Activity Assay. To better understand the mechanism of inhibition between MLS000327069, MLS000327186, and MLS000327206 and h15-LOX-2, the redox capability of the three molecules was investigated in a pseudo-peroxidase activity assay. Although many LOX inhibitors in the literature exhibit redox activity, they are not regarded as good therapeutics due to their tendencies for off-target redox reactions.³⁻⁶ All three inhibitors were tested using the UV-Vis pseudo-peroxidase assay. The lack of degradation of 13-HpODE at 234 nm confirmed that the inhibitors are not redox active.

Inhibitors	h15-LOX-2	h15-hLO-1	h12-LOX	h5-LOX	COX-1	COX-2	Redox
MLS000 327069	0.71 (0.06)	> 50	> 100	> 100	> 100	> 100	No
MLS000 327186	0.9 (0.1)	> 50	> 100	> 100	> 100	> 100	No
MLS000 327206	1.1 (0.1)	> 50	> 100	> 100	> 100	> 100	No

Table 3.2. Full IC₅₀ experiments were performed with h15-LOX-2, while for the other oxygenases the IC₅₀ values were estimated at 25 μ M inhibitor concentration. Inhibition that was less than 15% and less than 30% at 25 μ M are estimated to have IC₅₀ values of > 100 μ M and > 50 μ M, respectively. All experiments were done in duplicate and all assays were performed with 10 μ M AA except for the cyclooxygenases which were conducted at 100 μ M AA. The values are in units of micromolar with error displayed in the parentheses.

3.3.6 Substrate Activity of Inhibitor. To determine whether h15-LOX-2 has the capability of modifying the inhibitors, 20 μM of each inhibitor was reacted with h15-LOX-2 and the reaction monitored at 205 nm, 234 nm and 280 nm. An increase in absorbance at each wavelength was not detected indicating no chemical reaction. To confirm these results, the reactions were extracted, dried under N_2 and brought up in methanol for RP-HPLC analysis. No significant difference in spectra or retention time was observed at 212 nm (λ_{max} of inhibitor), 234 nm or 280 nm confirming that MLS000327069, MLS000327186, and MLS000327206 are not substrates to h15-LOX-2.

3.3.7 Computational Docking of h15-LOX-2 Inhibitors. The low energy binding poses predicted by the docking program for the five h15-LOX-2 specific inhibitors are shown in **Figure 3.1**. The inhibitors bind in the U-shaped active site, similar to the co-crystallized ligand. The heterocyclic ring occupies the pocket near the metal ion and both aromatic rings fill the hydrophobic pockets on either side of the heterocycle. A nitrogen atom on the ligand is approximately 2.8 Å away from a hydrogen atom of the water molecule, indicating a water-mediated interaction between the metal ion and the inhibitor. The binding affinities predicted by the docking score (Glide XP) and the relative molecular-mechanics energy function based refinement energy (MM-GBSA) are given in **Table 3.3**. Although the Glide XP score does not correlate well with the experimental IC_{50} values, the molecular-mechanics energy function based MM-GBSA score correlates well with the experimental IC_{50} values for the five h15-LOX-2 inhibitors. For comparison, specific

platelet h12-LOX and reticulocyte h15-LOX-1 inhibitors were docked. The h15-LOX-1 inhibitor, ML094, ranks higher than the h15-LOX-2 inhibitors, even though its binding affinity is $>100 \mu\text{M}$. Both Glide XP and MM-GBSA scores tend to predict high score for this inhibitor. The binding pose of ML094 shows that its ester group makes a hydrogen bonding interaction with the water. Both scoring functions seem to favor this type of electrostatic interaction, which we believe is the reason for this anomalous value. The h12-LOX inhibitor ML355 and h15-LOX-1 inhibitor ML351 have poor affinities by the MM-GBSA calculations, correlating well with their high IC_{50} values. Critical energy terms, such as desolvation, entropy change and electrostatics, are either ignored or approximated in both scoring functions and therefore, the ranking does not agree with the experimental values.

3.4 Conclusion. In summary, we have discovered three potent inhibitors MLS000327069, MLS000327186, and MLS000327206 that are highly selective for h15-LOX-2 over other oxygenases. These inhibitors along with the two we previously published, MLS000545091 and MLS000536924, add to our tools that can be utilized in gaining a better understanding of this enzyme's role and activity in plaque formation. All five inhibitors have similar binding poses according to the computational docking data. These results along with the tight SAR data suggest that these inhibitors contain the structural determinants that make up a potent pharmacophore for inhibition of h15-LOX-2. We are currently testing the cellular activity of these inhibitors in human macrophages and eventually in an atherosclerotic mouse model.

Compound (Target LOX)	Docking Score (Glide XP)	Relative MM-GBSA Binding Score (kcal/mol)	h15-LOX-2 IC ₅₀ (μM)
ML094 (h15-LOX-1)	-10.39	-36.28	>100
MLS000327069 (h15-LOX-2)	-8.72	-36.12	0.71
MLS000327186 (h15-LOX-2)	-8.59	-32.77	0.90
MLS000327206 (h15-LOX-2)	-8.68	-30.07	1.10
MLS000545091 (h15-LOX-2)	-6.77	-23.52	2.60
MLS000536924 (h15-LOX-2)	-7.67	-22.68	3.10
ML351 (h15-LOX-1)	-6.53	-12.84	>100
ML355 (h12-LOX)	-4.55	31.99	>100

Table 3.3. Docking scores and relative binding energies of h15-LOX-2 ligands docked to the h15-LOX-2 crystal structure (pdb id 4nre).

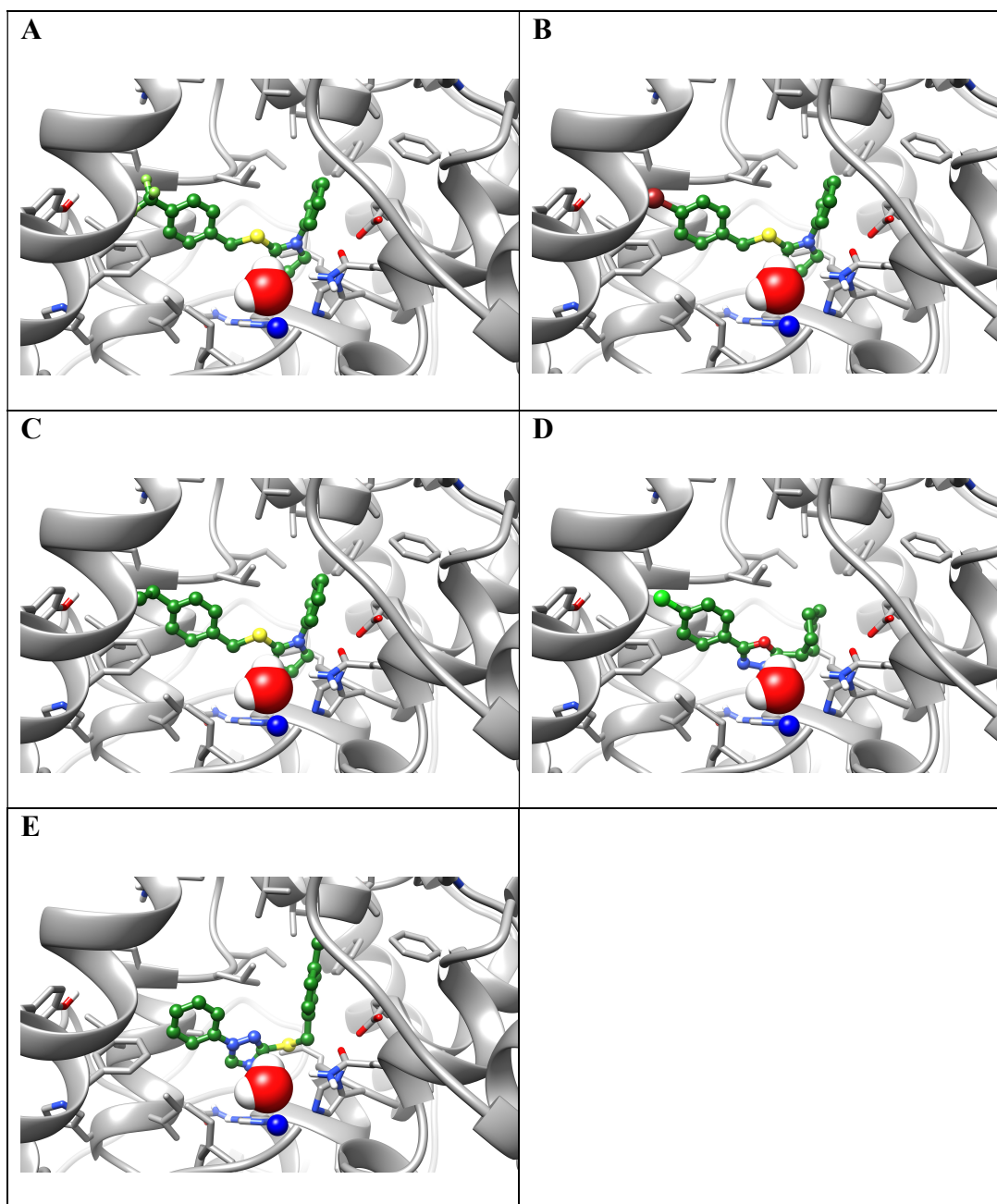


Figure 3.4. The docking pose of ligands bound to h15-LOX-2 (A) MLS000327069, (B) MLS000327186, (C) MLS000327206, (D) MLS000545091, and (E) MLS000536924. Carbon atoms of the ligands are shown in green color and the protein are shown in grey color. Nitrogen, oxygen and hydrogen atoms are shown in blue, red and white colors respectively and the metal ion is shown in blue color.

3.5 References

1. Brash, A.R. *J. Biol. Chem.* **1999**, 274, 23679.
2. Klinman, J.P. *Acc. Chem. Res.* **2007**, 40, 325.
3. Dobriana, A.C.; et. al. *Prog. Lipid Res.* **2011**, 50, 115.
4. Funk, C.D.; et. al. *Prostaglandins Other Lipid Mediat.* **2002**, 68, 303.
5. Funk, C.D. *Thromb. Vasc. Biol.* **2006**, 26, 1204.
6. Kobe, M.J.; et. al. *J. Biol. Chem.* **2014**, 289, 8562.
7. Danielsson, K.N.; et. al. *Atherosclerosis.* **2008**, 199, 34.
8. Rydberg, E.K.; et al. *Arterioscler. Thromb. Vasc. Biol.* **2004**, 24, 2040.
9. Hersberger, M. *Clin. Chem. Lab. Med.* **2010**, 48, 1063e73.
10. Hultén, L.; et. al. *Eur. J. Clin. Invest.* **2010**, 40, 11.
11. Kuhn, H; et. al. *J. Cardiovasc. Pharmacol.* **2007**, 50, 609.
12. *Deaths: Final data for 2013.* National Vital Statistics Report, **2015**, 64(2).
13. Gertow, K.; et. al. *Atherosclerosis.* **2011**, 215, 411.
14. Magnusson, L.U.; et. al. *PLOS One.* **2012**, 7, e43142.
15. Wuest, S.J.; et. al. *Atherosclerosis.* **2012**, 225, 121.
16. Kotla, S.; et. al. *Science Signaling.* **2013**, 6, ra83.

17. Schweizer, S.; et. al. *J. Nat. Prod.* **2000**, 63, 1058.
18. Martinez, Y.; et. al. *Bioorg. Med. Chem.* **2007**, 15, 7408.
19. Jameson, B.; et. al. *PLOS One.* **2014**, 9, e104094.
20. Robinson, S.J.; et. al. *J. Nat. Prod.* **2009**, 72, 1857.
21. Amagata, T.W.; et. al. *J. Nat. Prod.* **2003**, 66, 230.
22. Vasquez-Martinez, Y.; et. al. *Bioorg. Med. Chem.* **2007**, 15, 7408.
23. Rai, G.; et. al. *J. Med. Chem.* **2010**, 53, 7392.
24. Friesner, R.; et. al. *J. Med. Chem.* **2006**, 49, 6177.
25. Kalyanaraman, C.; et. al. *Biochemistry.* **2005**, 44, 2059.

Chapter 4

A POTENT AND SELECTIVE INHIBITOR TARGETING HUMAN AND MURINE 12/15-LOX

4.1 Introduction

Lipoxygenases are a family of non-heme iron containing enzymes that oxidize lipids, generating eicosanoids that are important mediators in inflammation and numerous diseases.^{1,2} The human genome contains six functional LOX genes (ALOX3, ALOX5, ALOX12, ALOX12B, ALOX15B, ALOX15) which encode for six distinct LOX-isoforms.³ Human reticulocyte 12/15-LOX (h12/15-LOX and/or h15-LOX-1), encoded by the ALOX15 gene, preferentially reacts with free polyunsaturated fatty acids (PUFAs) but also can directly oxidize lipid membranes containing PUFAs.^{3,4,5} These oxidized lipids within the lipid bilayer lead to the formation of hydrophilic pores, which affect the barrier function of the membrane and thus lead to cellular dysfunction, particularly in stroke.⁶

Stroke kills approximately 130,000 Americans each year and is the fifth leading cause of death in the United States.⁷ Two types of stroke can occur in the brain, ischemic and hemorrhagic.⁷ Ischemic stroke makes up approximately 85% of all strokes and is associated with thrombosis (clots), while hemorrhagic stroke results in excessive bleeding due to the bursting or leaking of the blood vessels.⁷ There is currently only one FDA approved stroke drug, tissue plasminogen activator (tPA). tPA is a protease that dissolves blood clots but, due to its propensity to initiate a hemorrhagic response, it is given to less than 5% of patients; therefore other therapeutic targets would be beneficial.⁸

A target strongly linked to stroke is h12/15-LOX. The activity of m12/15-LOX is increased in the mouse brain following ischemic induction and m12/15-LOX

co-localizes with a marker for oxidized lipids, MDA2.⁴ In addition, a similar co-localization as well as increased levels of apoptosis-inducing factor, AIF, were detected in the brain of human stroke patients.^{4,6} Finally, animal studies by van Leyen et al. demonstrated a 40% reduction of infarct size in a m12/15-LOX knockout (K/O) mouse relative to wild type (WT).⁹ These data strongly suggest that h12/15-LOX is involved in stroke and might be an attractive therapeutic target.

Discovery of potent and selective inhibitors that target h12/15-LOX for the treatment of human disorders has proved to be a challenge. Although many inhibitors have been reported targeting 12/15-LOX, most of them target the non-human species, like soybean lipoxygenase, which lack clinical significance.¹⁰⁻¹² The lack of an X-ray crystal structure of h12/15-LOX and a bound inhibitor also hampers rational inhibitor design. In addition, as reflected in their inhibitor profiles, the murine ortholog of 12/15-LOX (m12/15-LOX), which is involved in mouse stroke, exhibits 12-lipoxygenating activity, while h12/15-LOX exhibits 15-lipoxygenating activity.¹³⁻¹⁵ This is problematic because mice are effective/inexpensive models for stroke, making an inhibitor that targets both h12/15-LOX and m12/15-LOX critical for developing a stroke therapeutic.

Recently, Pelcman *et al.* identified BLX-2477 (N-(2-chloro-4-fluorophenyl)triazole-4-carboxamide) (**Figure 4.1**) as a potential therapeutic due to its potency ($IC_{50} = 99$ nM) and selectivity for h12/15-LOX, but unfortunately it had adverse off-target effects in mini-pigs and did not exhibit potency against the dog or rat orthologs.^{16,17} Bristol-Myers Squibb synthesized a series of sulfonamide

derivatives, which inhibited rabbit reticulocyte 12/15-LOX *in vitro* ($IC_{50} = 19$ nM) and were later tested in a Chinese hamster ovary (CHO) cell-based assay that over-expressed human recombinant 12/15-LOX.¹⁸ However, these analogs exhibited poor pharmacokinetics in rodent models and were deemed not suitable for further evaluation.¹⁸ Parke-Davis/Warner-Lambert (Pfizer) discovered an indole-based inhibitor, PD-146176 ($IC_{50} = 810$ nM), which had *in vivo* activity against rabbit reticulocyte 12/15-LOX for atherosclerosis.¹⁹ Eleftheriadis *et. al.* published a novel class of 6-benzyloxysalicylates inhibitors that selectively target h15-LOX-1 (N206, $IC_{50} = 7100$ nM).²⁰ Our collaborative team has discovered two different families of inhibitors, ML094 (4-(5-(Naphthalen-1-yl)-1,3,4-oxadiazol-2-ylthio)but-2-ynylthiophene-2-carboxylate) and ML351 (5-(methylamino)-2-(naphthalene-1-yl)oxazole-4-carbonitrile) (**Figure 4.1**). ML094 has low nanomolar potency against recombinant h12/15-LOX *in vitro* ($IC_{50} = < 10$ nM) but lacks activity in cell-based assays, possibly due to the hydrolyzable nature of the ester moiety.²¹ In comparison, ML351 has sub-micromolar potency ($IC_{50} = 200$ nM) and exhibits *in vivo* activity in mice.¹³ In the current work, we expand on our initial h12/15-LOX screen and present another unique chemical scaffold for h12/15-LOX inhibition. Utilizing high throughput screening (HTS), cellular screening, SAR, and kinetic studies, we report a new family of inhibitors that are both selective and potent against h12/15-LOX, as well as being active in mouse neuronal cells.

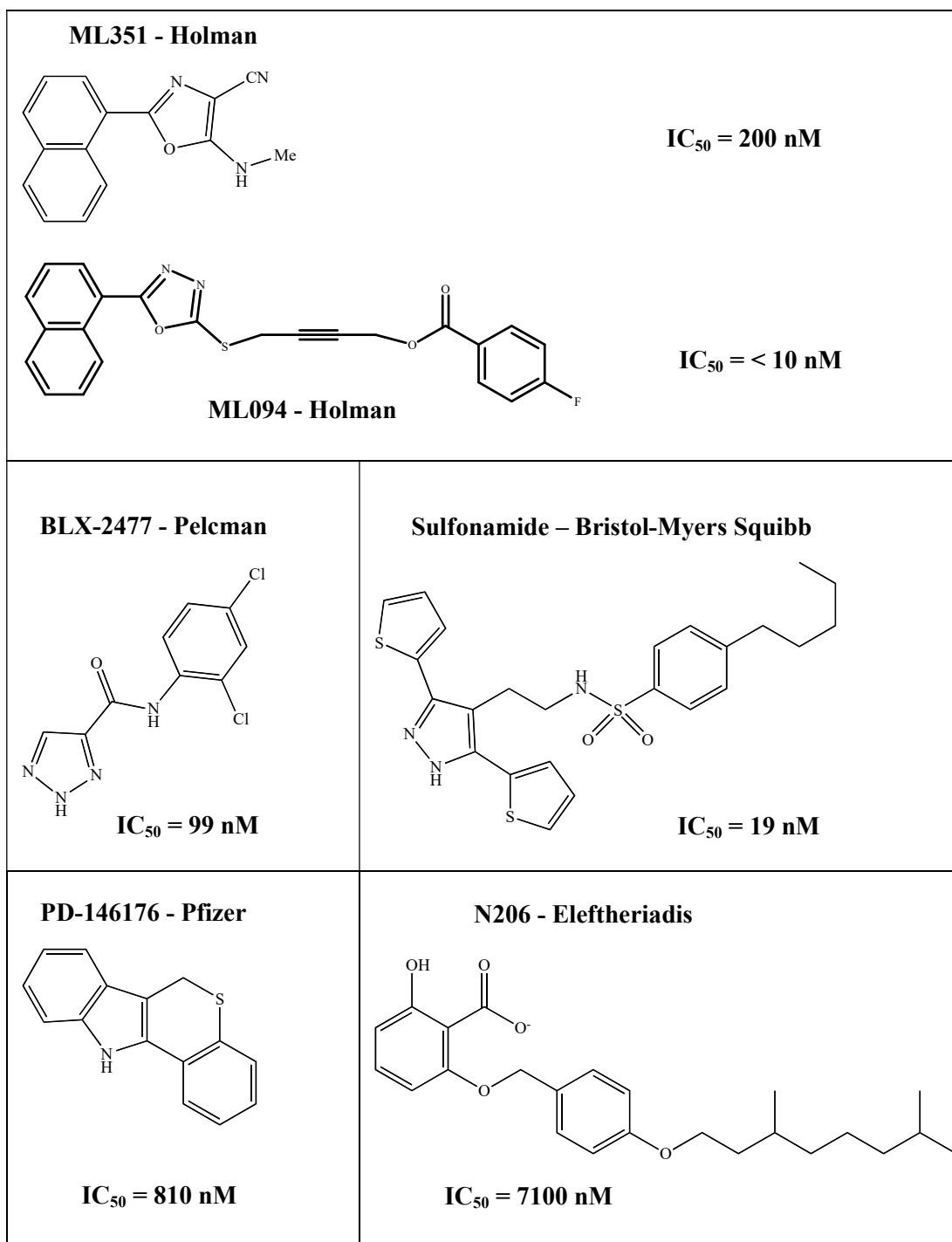


Figure 4.1. Relevant h12/15-LOX inhibitors.

4.2 Materials and Methods

4.2.1 Materials. All commercial fatty acids were purchased from Nu Chek Prep, Inc. (MN, USA). BWb70c was purchased from Sigma/Aldrich Chemicals. The inhibitors were obtained from the NIH Molecular Libraries Small Molecule Repository (MLSMR): (<https://mli.nih.gov/mli/compound-repository/>). All other chemicals were reagent grade or better and were used without further purification.

4.2.2 Protein Expression. All the LOX isozymes used in this publication were expressed and purified as previously published (h5-LOX²², h12-LOX²³, h12/15-LOX²³ and h15-LOX-2²⁴). Human leukocyte 5-lipoxygenase was expressed as a non-tagged protein and used as a crude ammonium sulfate precipitated protein. The remaining enzymes, h12/15-LOX, h15-LOX-2 and h12-LOX, were expressed as N-terminal His6-tagged proteins and purified via immobilized metal affinity chromatography (IMAC) using Ni-NTA resin. The purity of each protein was analyzed by SDS-PAGE and found to be greater than 90% purity, except for h5-LOX. The iron content of each protein, except for h5-LOX, were determined with a Thermo Element XR inductively coupled plasma mass spectrometer (ICP-MS), using cobalt (EDTA) as an internal standard. Iron concentrations were compared to standard iron solutions. The protein concentrations were determined using the Bradford assay, with bovine serum albumin (BSA) as the protein standard. The iron loading was found to range from 20 – 50% for all proteins except h5-LOX.

4.2.3 Lipoxygenase UV-Vis-based IC₅₀ Assay. One-point inhibition percentages of approximately 100 derivatives of MLS000099089 (**99089**), the parent

compound, were determined by following the formation of the conjugated diene product at 234 nm ($\epsilon = 27,000 \text{ M}^{-1}\text{cm}^{-1}$) with a Perkin-Elmer Lambda 40 UV/Vis spectrophotometer at 20 μM inhibitor concentration. Twenty-nine selective derivatives were investigated further to determine their IC_{50} values. The full IC_{50} experiments were done with at least four different inhibitor concentrations. All reactions mixtures were 2 mL in volume and constantly stirred using a magnetic stir bar at room temperature (23°C) with the appropriate amount of LOX isozyme h12/15-LOX (~ 30 nM). Reactions were carried out in 25 mM HEPES buffer (pH 7.5), 0.01% Triton X-100 and 10 μM AA. The concentration of AA was quantitated by allowing the enzymatic reaction to proceed to completion in the presence of s12/15-LOX. IC_{50} values were obtained by determining the enzymatic rate at various inhibitor concentrations and plotted against inhibitor concentration, followed by a hyperbolic saturation curve fit. The experiments used for the saturation curves were performed in duplicate or triplicate, depending on the quality of the data. All inhibitors were stored at -20°C in DMSO.

4.2.4 HT-22 Cellular Assay. Oxidative stress leading to 12/15-LOX dependent cell death was induced in HT-22 cells by glutamate treatment as previously described.^{13,25,26} Briefly, HT-22 cells were cultured in DMEM containing 10% fetal bovine serum and penicillin / streptomycin (all media from Invitrogen). For initial screening of compounds, cells were seeded at 1×10^4 cells/well in 96-well plates (Corning) and treated 18h later when the cells were approximately 50-70% confluent. Treatment consisted of exchanging the medium with 100 μL fresh culturing medium

and adding 5 mM glutamate (stock solution 0.5 M in PBS) in the presence or absence of DMSO (maximum 0.1% final concentration) as control or 5, 10, or 20 μM concentration of the indicated compound. Titration of **99089** over a broader concentration range was then carried out in the same way in 24-well plates, with the cells seeded at 5×10^4 cells/well. In all cases, lactate dehydrogenase (LDH) content was determined separately for the cell extracts and corresponding media using a Cytotoxicity Detection Kit (Roche), and the percentage of LDH released to the medium calculated after subtracting the corresponding background value. The Z' values for the 96-well plate format are typically in the range of 0.6-0.9, indicating an excellent assay.²⁷

4.2.5 Selectivity Assay. **99089** was screened to determine its selectivity towards h12/15-LOX. Reactions with h12-LOX were carried out in 25 mM HEPES (pH 8.0) 0.01% Triton X-100 and 10 μM AA. Reactions with the crude, ammonium sulfate-precipitated h5-LOX were carried out in 25 mM HEPES (pH 7.3), 0.3 mM CaCl_2 , 0.1 mM EDTA, 0.2 mM ATP, 0.01% Triton X-100 and 10 μM AA. Reactions with h15-LOX-2 were carried out in 25 mM HEPES buffer (pH 7.5), 0.01% Triton X-100 and 10 μM AA. Human 12-LOX and h15-LOX-2 were tested with 20 μM , 25 μM , and 35 μM inhibitor concentration and all reactions were performed in duplicate. Concentrations above 35 μM for **99089** were not possible due to solubility problems with the inhibitor. Human 5-LOX and COX-2 were screened only at 20 μM inhibitor concentration of **99089** due to their low inhibition. Zileuton (20 μM) was utilized as a positive control with h5-LOX and shown to produce 97% inhibition.

4.2.6 Steady-State Inhibition Kinetics. The steady-state equilibrium constants of inhibition for **99089** and h12/15-LOX rates were determined the same way as the UV-Vis-Based Assay (Section 4.2.3). Reactions were initiated by adding h12/15-LOX to a constantly stirring 2 mL reaction mixture containing 2 μM – 14 μM AA in 25 mM HEPES buffer (pH 7.5) in the presence of 0.01% Triton X-100. Kinetic data were obtained by recording initial enzymatic rates at varied inhibitor concentrations and subsequently fitting the data to the Henri-Michaelis-Menten equation, using KaleidaGraph (Synergy) to determine the microscopic rate constants, V_{max} ($\mu\text{mol}/\text{min}/\text{mg}$) and $V_{\text{max}}/K_{\text{M}}$ ($\mu\text{mol}/\text{min}/\text{mg}/\mu\text{M}$). These rate constants were subsequently replotted as $1/V_{\text{max}}$ or $K_{\text{M}}/V_{\text{max}}$ versus inhibitor concentration to yield K_{iu} and K_{ic} , respectively, which are defined as the equilibrium constants of dissociation from the secondary and catalytic sites. The primary data were also plotted in the Dixon format, graphing $1/v$ vs. $[\text{I}]$ μM at chosen substrate concentrations. From the Dixon plots, the slope at each substrate concentration was extracted and plotted against $1/[\text{S}]$ μM to produce the Dixon parameters, K_{ic} and K_{iu} .

4.2.7 Pseudoperoxidase Assay. The pseudo-peroxidase activity of **99089** was determined on a Perkin-Elmer Lambda 40 UV/Vis spectrophotometer as previously described previously with h12/15-LOX enzyme utilizing 13-HpODE as the oxidant and BWb70c as the positive control.²⁸ The reaction was initiated by addition of 20 μM 13-HpODE to 2 mL buffer (50 mM Sodium Phosphate (pH 7.4), 0.3 mM CaCl_2 , 0.1 mM EDTA, 0.01% Triton X-100) containing 20 μM **99089** and 60 nM h12/15-LOX. The reaction mixtures were constantly mixed with a stir bar at 23°C. Activity

was determined by monitoring the decrease at 234 nm (13-HpODE consumption). More than 25% 13-HpODE degradation indicates redox activity of that particular inhibitor. The negative controls used were: enzyme alone with product, enzyme alone with inhibitor, and inhibitor alone with product. These formed a baseline for the assay, reflecting non-pseudo-peroxidase dependent hydroperoxide product decomposition. To rule out auto-inactivation of the enzyme from pseudo-peroxidase cycling, the h12/15-LOX residual activity was observed after the addition of 20 μ M AA at the end of each reaction. In addition, initial rates of inhibitor and 13-HpODE were compared to initial rates of inhibitor alone because the inhibitor by itself inherently lowers the rate of oxygenation. Activity is characterized by direct measurement of the product formation with the increase of absorbance at 234 nm.

4.2.8 Computational Modeling. A homology model of human reticulocyte 12/15-lipoxygenase protein (Uniprot ID P16050) was built using the software PRIME Version 3.9 (Schrodinger Inc)²⁹ from the rabbit reticulocyte 15-Lipoxygenase-1 crystal structure (PDB ID 2p0m, chain B). The two LOX isozymes have 90% similarity and 81% identity between the two. Both the co-crystallized ligand and the metal ion were retained during the homology modeling. After the model was built, it was subjected to a protein preparation step using Protein Preparation Wizard (Schrodinger Inc). During this step hydrogen atoms were added, proper bond-orders and atom-types were set and the protein structure was minimized such that heavy-atoms were not allowed to move beyond 0.3Å. Iron was treated as ferric ion (Fe^{3+}). The **99089** inhibitor structure was built using Maestro's Edit/Build panel. We

minimized the structure using LigPrep software (Schrodinger Inc) and enumerated plausible protonation states of the inhibitor by applying the empirical pK_a prediction software Epik (Schrodinger Inc). We docked the inhibitor to h12/15-LOX active site using Glide software with the standard-precision docking scoring function (Schrodinger Inc).

4.3 Results and Discussion

4.3.1 HTS Discovery. A HTS of approximately 74,000 compounds was performed with h12/15-LOX as previously reported,²¹ and the top 1000 compounds were manually screened using the UV-Vis assay with h12/15-LOX. All molecules were screened at 20 μM inhibitor concentration, with **99089** inhibiting h12/15-LOX greater than 90% at this concentration. A full IC_{50} was performed on h12/15-LOX with five different **99089** concentrations and an IC_{50} of $3.4 \pm 0.5 \mu\text{M}$ was determined (Figure 4.2).

Compound	Structure	IC ₅₀ (μM) (± SD (μM))
<p style="text-align: center;">99089 (MLS000099089)</p>		<p style="text-align: center;">3.4 (0.5)</p>

Figure 4.2. Structure and potency of the novel h12/15-LOX inhibitor.

4.3.2 HT-22 Cellular Assay. As mentioned above, in order for an h12/15-LOX inhibitor to be developed into a therapeutic, it needs to be effective in the mouse stroke model. Therefore, we modified our workflow such that as soon as a potent h12/15-LOX inhibitor was discovered, it was tested against m12/15-LOX in a mouse neuronal cell line, HT-22, with 10 μ M ML351 used as reference standard. In this cell line, glutathione depletion is induced by adding exogenous glutamate. This leads to oxidative stress and subsequent cell death, termed oxytosis or oxidative glutamate toxicity, which is dependent on 12/15-LOX activity and thus reversed by inhibition of 12/15-LOX.^{13,25} In the current work, we screened **99089** against HT-22 and found it to be potent, with an approximate cellular EC₅₀ of 10 μ M (**Figure 4.3**).

4.3.3 Compound Selectivity. After determining that **99089** was active against both h12/15-LOX and m12/15-LOX, we sought to establish whether our new inhibitor scaffold is selective to h12/15-LOX over other human LOX isozymes. Therefore, **99089** was screened against human lipoxygenases for its selectivity towards h12/15-LOX utilizing the UV-Vis assay (**Figure 4.4**). **99089** exhibited approximately 15-fold selectivity over h12-LOX and h15-LOX-2 and greater than 30-fold selectivity over h5-LOX. The potency of **99089** was also investigated against COX-2, with no inhibitor potency being observed (extrapolated IC₅₀ > 100 μ M).

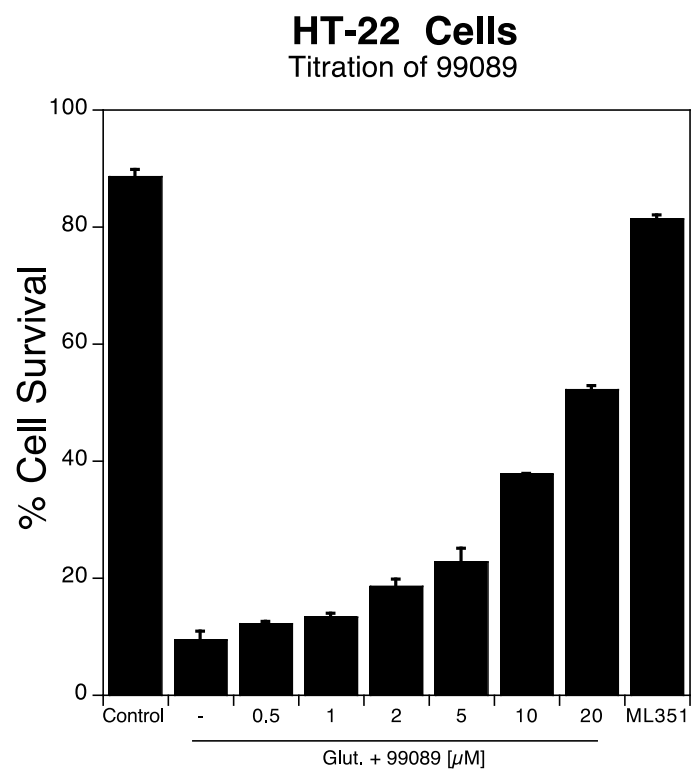


Figure 4.3. Titration of **99089** in HT-22 cells, with increasing cell survival. ML351 was used as a positive control at 10 μM .

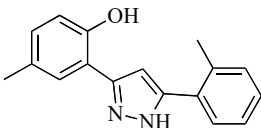
Compound	Structure	h12-LOX	h15-LOX-2	h5-LOX	COX-2
99089		>50	> 50	> 100	> 100

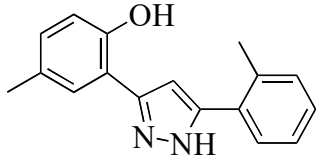
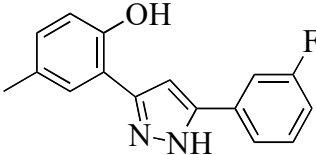
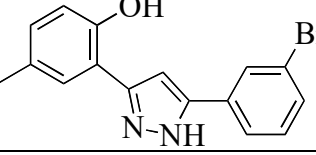
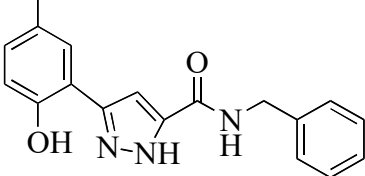
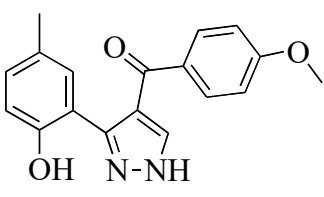
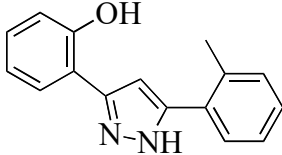
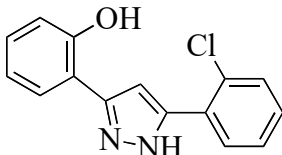
Figure 4.4. Selectivity potency (μM) against h12-LOX, h15-LOX-2 and 5-LOX with **99089**. Three inhibitor concentrations ($20\ \mu\text{M}$, $25\ \mu\text{M}$, $35\ \mu\text{M}$) were screened against h12-LOX and h15-LOX-2, and the IC_{50} value averaged. For h5-LOX and COX-2 we only screened at $20\ \mu\text{M}$, due to their low potency and the solubility problems of **99089** above $35\ \mu\text{M}$.

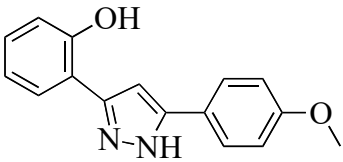
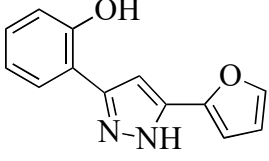
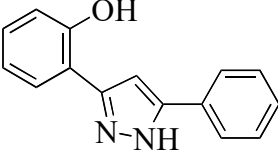
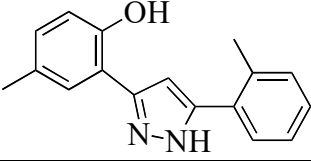
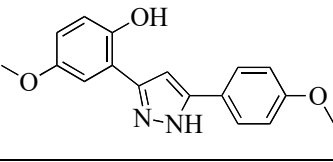
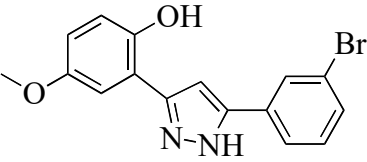
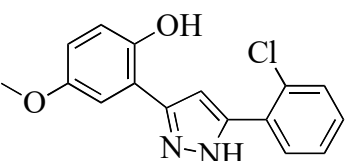
4.3.4 Structure-Activity Relationship (SAR) Study. After the identification of the parent analogue, 28 derivatives were screened to investigate structure-activity relationships (**Table 4.1-4.3**). The compounds were subjected to IC₅₀ determination, using four or more inhibitor concentrations (ranging from 0.5 μ M to 30 μ M), depending on the potency of the molecule.

Structurally the parent molecule, **99089**, contains a pyrazole ring with phenyl substituents at C-3 and C-5. The 3-position of the pyrazole is substituted with a 2-OH, 5-Me-phenyl group, while the 5-position is substituted with a 2-Me-phenyl group (**Figure 4.2**). As observed in **Table 4.1**, modification of the 5-position with either a 3-F-phenyl or 3-Br-phenyl had little effect on the observed inhibition (**1** and **2**, respectively). However, replacing the 5-phenyl group with an N-benzylcarboxamide (**3**) or a 4-methoxyphenylmethanone (**4**) lowered activity over 10-fold, suggesting larger substituents on this side of the molecule are not well tolerated. It was also observed that removing the 5-Me on the 3-phenyl group of the parent molecule (**5**) had little effect on its potency. Subsequent changes to the 5-phenyl group of compound **5** had minor effects on potency, such as replacement of the 2-Me with a 2-Cl (**6**) or a 4-OMe (**7**), or complete replacement of the 5-phenyl moiety with a furan (**8**). Interestingly, removal of the 2-Me decreased the potency approximately 6-fold (**9**). Replacement of the 5-Me on the other phenyl group (C-3) with a 5-OMe also had minimal effect on potency (**10-13**) as shown in **Table 4.2**. Moreover, repositioning of the 5-Me on the 3-phenyl to the 4-position (**14**) also had no effect. The additional change of the 2-Me on the 5-phenyl group to a halogen had varied effects (**15-17**), but

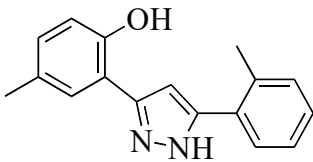
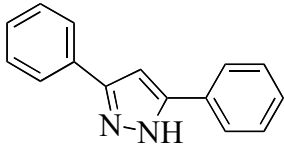
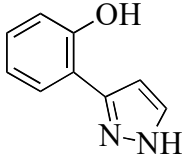
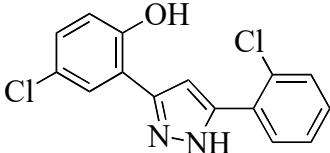
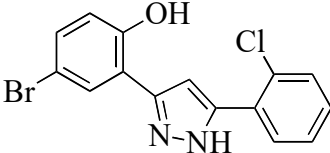
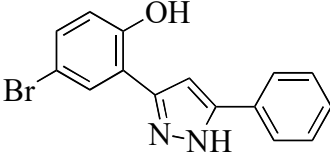
in general did not affect potency dramatically. However, converting the 2-Me to a 4-Me (**18**) lowered the potency greater than 15-fold, suggesting that adding steric bulk on opposite ends of the molecule induces steric clashes with active site residues. This hypothesis is supported by the lack of potency of **19**, which has a 4-OMe on the 3-phenyl group and a 4-Me on the 5-phenyl. As seen in **Table 4.3**, the most sensitive moiety of the parent molecule was the 2-OH on the 3-phenyl group, whose removal abolishes all potency (**20**), as compared to compound **9**. Potency was not regained if the 2-OH group was restored to a minimal structure (**21**). These data suggest that the 2-OH moiety binds directly to the active-site iron. This is a reasonable hypothesis since phenols are known to be strong ligands to ferric ions. However, the fact that compound **21** did not inhibit h12/15-LOX indicates that there are other structural interactions besides metal ligation that contribute to inhibitor potency. This hypothesis of metal ligation is supported by the fact that electron-withdrawing groups opposite the 2-OH group eliminated all potency (**22**, **23** & **24**). The electron-withdrawing substituents lower the phenolate's ability to bind the ferric iron because the electrons are not readily available to ligate the metal. It should be noted that although we propose that these inhibitors ligate the iron center, preventing the catalytically essential ferric-hydroxyl moiety being formed, these inhibitors do not exhibit redox activity (*vide infra*), indicating a mismatch in their reduction potentials. In summary, the collective data indicates that bulky substituents on both the phenyl substituents of the pyrazole can have deleterious effects, as does lowering the ability of the molecule to ligate the active site iron.

As mentioned above, the mouse stroke model is essential for developing a human stroke therapeutic; however, the mouse analogue to the human LOX (m12/15-LOX) preferentially generates 12-HpETE, suggesting a difference in their active sites. This hypothesis is supported by our HT-22 mouse neuronal cell assay, which models the stress induced by stroke. Effective 12/15-LOX inhibitors increase the survival percentage of the HT-22 cells by lowering the activity of the enzyme. As seen in **Tables 4.1-4.3**, there is a poor correlation between h12/15-LOX and HT-22 potency, indicating a difference in the active sites of h12/15-LOX and m12/15-LOX. For example, compounds **7** and **10** have comparable potency against h12/15-LOX, but exhibit dramatically different potency against m12/15-LOX. It should be noted that the HT-22 assay is a cellular assay and thus other factors could be at play, such as cell permeability, which was not investigated in the current work.

Table 4.1				
Compound	Structure	% I (20 μM)	IC₅₀ (\pmSD) (μM)	HT-22 Survival % (5 μM)
99089		94	3.4 (0.5)	20
1 MLS000 068545		80	10 (1)	49
2 MLS000 856489		75	9.1 (2)	18
3 MLS000 551826		0	>50	
4 MLS000 1163892		15	>50	
5 MLS000 066802		92	7.0 (0.4)	76
6 MLS000 060847		74	4.0 (0.4)	

7 MLS000 551030		75	10 (1)	7
8 MLS000 122998		66	7.0 (2)	34
9 MLS002 473404		59	20 (4)	
Table 4.2				
Compound	Structure	% I (20 μM)	IC₅₀ (\pmSD) (μM)	HT-22 Survival % (5 μM)
99089		94	3.4 (0.5)	20
10 MLS000 068611		82	6.0 (0.5)	96
11 MLS000 108293		78	7.0 (1)	70
12 MLS001 204578		82	6.6 (0.4)	83

13 MLS001 163964		74	11 (2)	78
14 MLS000 547497		66	10 (1)	71
15 MLS000 106958		79	17 (2)	77
16 MLS001 207693		69	11 (1)	25
17 MLS000 066801		65	18 (2)	66
18 MLS00 1209799		32	> 50	
19 MLS000 1197234		24	>50	
Table 4.3				
Compound	Structure	% I (20 μM)	IC₅₀ (\pmSD) (μM)	HT-22 Survival % (5 μM)

99089		94	3.4 (0.5)	20
20 MLS000 1194968		14	>50	
21 MLS000 2473395		4	>50	
22 MLS000 035498		29	> 50	
23 MLS000 547918		32	>50	
24 MLS000 547918		35	>50	

Tables 4.1-4.3. IC₅₀ values of h12/15-LOX inhibitors selected for the structure-activity relationship study; errors are in parentheses when available. Experiments were conducted in the presence of 10 μ M AA and 0.01% Triton X-100. Each experiment was performed in duplicate with at least four different inhibitor concentrations.

4.3.5 Steady-State Inhibition Kinetics. The mode of inhibition of h12/15-LOX by **99089** was investigated utilizing steady-state inhibition kinetics. The formation of hydroperoxide product was monitored in a UV-Vis assay as a function of substrate and inhibitor concentration in the presence of 0.01% Triton X-100. The reaction was performed with substrate concentration ranging from 2 μM to 14 μM and three inhibitor concentrations of 2.5 μM , 5 μM and 10 μM . A Dixon plot of the primary data for **99089** is shown in **Figure 4.5A**, while a Dixon replot of the secondary data is shown in **Figure 4.5B**. Fitting the data yielded a K_{ic} of 1.0 ± 0.08 μM and a K_{iu} of 6.0 ± 3.3 μM , which are defined as the equilibrium constants of dissociation from the enzyme and enzyme substrate complex, respectively. These numbers are slightly lower than the IC_{50} values and are indicative of a mixed-type inhibitor, which is a common trait among LOX inhibitors.

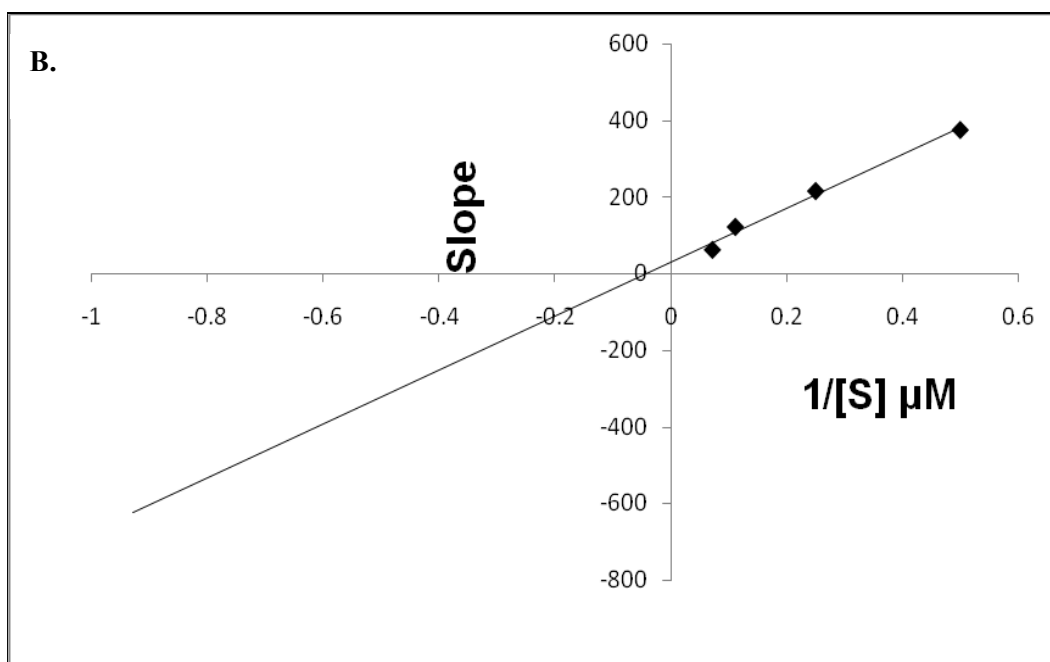
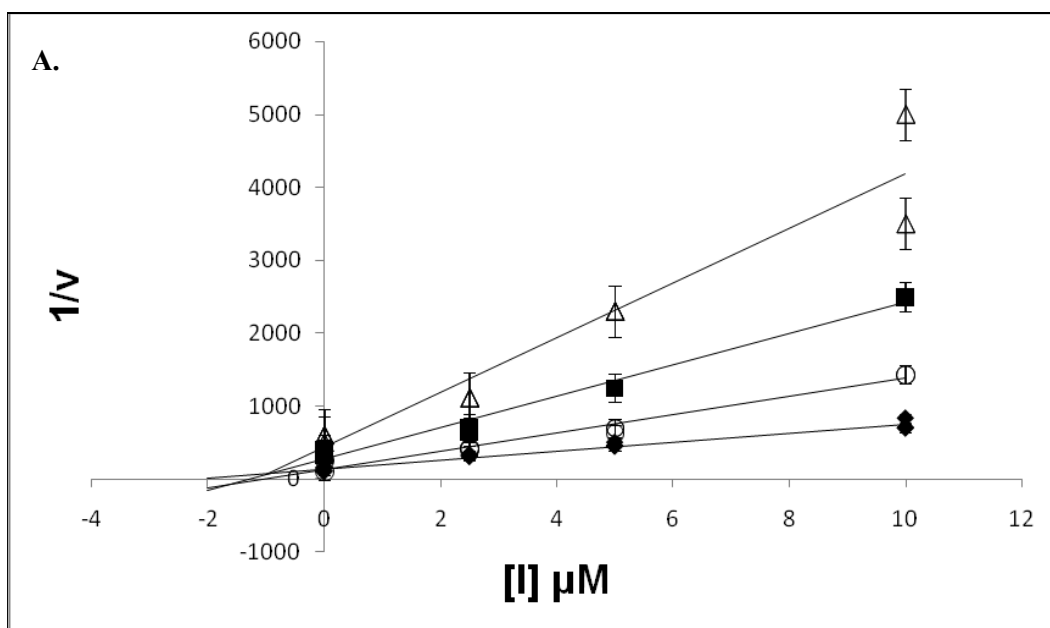


Figure 4.5. Steady-state inhibition kinetics for the determination of K_{ic} and K_{iu} of h12/15-LOX and **99089**. (A) Dixon plot of the primary data of h12/15-LOX and **99089**. The substrate concentrations are 2 μM (open triangles), 4 μM (closed squares), 9 μM (open circles), 15 μM (closed diamonds). (B) The Dixon replot of slope versus [Inhibitor] in μM yielded a K_{ic} of 1.0 (0.08) μM and a K_{iu} of 6.0 (3) μM .

4.3.6 Pseudoperoxidase Activity Assay. Some LOX inhibitors in the literature inactivate these enzymes by reduction of the iron center.^{24,30-32} Because redox inhibitors can cause off-target reactions in the cell, the mechanism of action of a particular inhibitor is important.^{32,33} A UV-Vis pseudoperoxidase assay was utilized to determine the mechanism of inhibition of **99089**.²⁸ In the pseudoperoxidase assay, the only fatty acid present is 13-HpODE, which oxidizes the inactive Fe²⁺ enzyme to an active Fe³⁺ enzyme. If the inhibitor (**99089**) were a redox inhibitor, consumption of 13-HpODE would be seen as the degradation of the 234 nm signal on the UV-Vis spectrophotometer. The degradation of the hydroperoxide product, 13-HpODE, was not observed, demonstrating that **99089** does not inhibit h12/15-LOX via a redox mechanism.

4.3.7 Computational Modeling. **99089** was docked to a homology model of h12/15-LOX model, and the standard-precision Glide score for the docked pose is -7.77 kcal/mol (**Figure 4.6**). In this pose, the inhibitor directly interacts with the metal ion and hydrogen bonds with the side chain of Glu356. The predicted pose in which the phenolate anion directly interacts with the metal ion may explain why removing the 2-OH group of 3-phenyl ring (as in **20**) abolishes all potency. In addition, the ortho-methyl 5-phenyl ring nicely packs into the hydrophobic pocket created by Phe352, Phe414 and Met418 and appears to have a π - π stacking interaction with Phe414. The close proximity (3.5-4.5 Å) of the 5-phenyl ring to these hydrophobic residues may further explain why larger substitution to the 5-phenyl ring is not well tolerated. Thus, the docking results are consistent with the key aspects of the SAR.

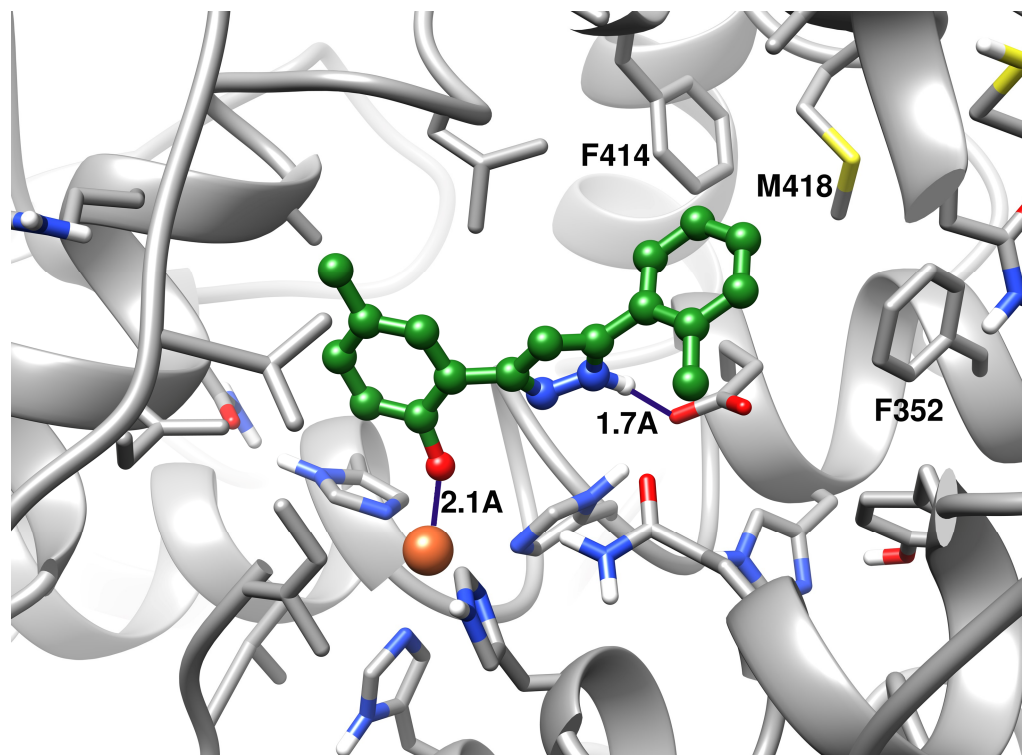


Figure 4.6. 99089 docking pose in the active site of h12/15-LOX. Carbon atoms of the protein and ligand are shown in grey and green, respectively. Nitrogen, oxygen, hydrogen atoms are blue, red and white, respectively. The ferric ion is shown as an orange sphere. 99089 is shown in ball-and-stick representation.

4.4 Conclusion. In summary, we have identified a novel chemical scaffold that selectively inhibits h12/15-LOX over other human LOX isozymes, but still inhibits m12/15-LOX. This property is critical for development of an anti-stroke therapeutic, which will require the use of a mouse animal model. The SAR studies indicate that this class of inhibitors ligate the metal center and are constrained by sterics on either end of the molecule. We are currently investigating its potency and efficacy in our MCAO mouse stroke model.

4.5 References

1. Brash, A. R. *J. Biol. Chem.* **1999**, *274*, 23679.
2. Funk, C. D. *Arterioscle. Thromb. Vasc. Biol.* **2006**, *26*, 1204.
3. Kuhn, H. et. al. *Biochim. Biophys. Acta.* **2014** *4C*, 1
4. van Leyen, K. *CNS Neurol. Disord. Drug Targets* **2013**, *12*, 191.
5. van Leyen, K.; Holman, T.R.; Maloney, D.J. *Future Med. Chem.* **2014**, *6*, 1853.
6. Kuhn, H.; Banthiya, S.; van Leyen, K. *Biochim. Biophys. Acta* **2015**, *1851*, 308.
7. Mozaffarian, D. Benjamin, E.J.; Go, A.S.; et. al. *Circulation* **2015**, e29.
8. Marler, J. R. *N. Engl. J. Med.* **1995**, *333*, 1581.
9. van Leyen, K.; Kim, H.Y.; Lee, S.R.; et. al. *Stroke* **2006**, *37*, 3014.
10. Mahdavi, M.; et. al. *Eur. J. Med. Chem.* **2014**, *82*, 308.
11. Tehrani, M. B.; et. al. *Eur. J. Med. Chem.* **2014**, *87*, 759.
12. Iranshahi, M.; et. al. *Eur. J. Med. Chem.* **2012**, *57*, 134.
13. Rai, G.; et. al. *Probe Reports from the NIH Molecular Libraries Program* **2010**.
14. Rai, G.; Joshi, N.; et. al. *J. Med. Chem.* **2014**, *57*, 4035.
15. Haeggstrom, J. Z.; Funk, C.D. *Chem. Rev.* **2011**, *111*, 5866.
16. Pelcman, B., Sanin, A.; et al. *Bioorg. Med. Chem. Lett.* **2015**, *25*, 3024.
17. Pelcman, B.; Sanin, A.; et al. *Bioorg. Med. Chem. Lett.* **2015**, *25*, 3017.
18. Weinstein, D. S.; Liu, W.; Gu, Z.; et al. *Bioorg. Med. Chem. Lett.* **2005**, *15*, 1435.
19. Nair, D. G.; Funk, C.D. *Prostaglandins Other Lipid Mediat.* **2009**, *90*, 98.
20. Eleftheriadis, N. et. al. *Eur. J. Med. Chem.* **2015**, *94*, 265.
21. Rai, G.; Kenyon, V.; et. al. *J. Med. Chem.* **2010**, *53*, 7392.

22. Robinson, S.J.; et. al. *J. Nat. Prod.* **2009**, *72*, 1857.
23. Amagata, T.; Whitman, S.; et. al. *J. Nat. Prod.* **2003**, *66*, 230.
24. Vasquez-Martinez, Y.; et. al. *Bioorg. Med. Chem.* **2007**, *15*, 7408.
25. Li, Y.; Maher, P.; Schubert, D. *Neuron* **1997**, *19*, 453.
26. van Leyen, K.; Arai, K.; et. al. *J. Neurosci. Res.* **2008**, *86*, 904.
27. Zhang, J. H.; Chung, T.D.; Oldenburg, K.R. *J. Biomol. Screen.* **1999**, *4*, 67.
28. Hoobler, E. K.; Holz, C.; Holman, T.R. *Bioorg. Med. Chem.* **2013**, *21*, 3894.
29. Prime, version 3.9., Glide, version 6.6, LigPrep, version 3.3., Maestro, version 10.1. New York, NY: Schrodinger, LLC. **2015**.
30. Carter, G. W.; Young, P.R.; et. al. *J. Pharmacol. Exp. Ther.* **1991**, *256*, 929.
31. Cichewicz, R. H.; et. al. *J. Am. Chem. Soc.* **2004**, *126*, 14910.
32. Pergola, C.; Werz, O. *Expert Opin. Ther. Pat.* **2010**, *20*, 355.
33. McMillan, R. M.; Walker, E.R. *Trends Pharmacol. Sci.* **1992**, *13*, 323.

4.5 Credit to Coauthors

The following experiments were performed by or under the supervision of the following people and not by Michelle M. Armstrong.

1) HT-22 Cellular Assay

Joo Eun Jung, Yi Zheng, Klaus van Leyen
Neuroprotection Research Laboratory, Department of Radiology, Massachusetts
General Hospital, Harvard Medical School, Charlestown, Massachusetts 02129

2) Molecular Modeling

Chakrapani Kalyanaraman, Matthew P. Jacobson
Department of Pharmaceutical Chemistry, School of Pharmacy, University of
California San Francisco, San Francisco, CA 94143

3) Synthesis of Inhibitors

Anton Simeonov, David J. Maloney, Ajit Jadhav
National Center for Advancing Translational Sciences, National Institutes of Health,
9800 Medical Center Drive, MSC 3370, Bethesda, Maryland 20892

Chapter 5

HUMAN 15-LOX-1 ACTIVE SITE MUTATIONS ALTER INHIBITOR BINDING AND DECREASE POTENCY

5.1 Introduction

Human reticulocyte 15-lipoxygenase-1 (h15-LOX-1 or h12/15-LOX) has been linked to inflammation, cardiovascular disease, carcinogenesis/metastasis, and metabolic disorders/neurological disorders¹⁻¹³. One disorder in which h15-LOX-1 has been strongly associated with is stroke¹³⁻¹⁵. Stroke is the fifth leading cause of death and the leading cause of disability in the United States, but the only FDA approved drug currently available on the market is tissue plasminogen activator (tPA). Therefore, finding inhibitors that target h15-LOX-1 with low nano-molar potency, as well as cellular activity could be an excellent alternative for treatment of stroke.

h15-LOX-1 catalyzes the dioxygenation of various polyunsaturated fatty acids (PUFAs), both as the free fatty acid and as the phospholipid linked fatty acid. Over the years, a variety of inhibitors have been discovered which target h15-LOX-1. Bristol-Myers Squibb's tryptamine sulfonamide exhibited a potency of 21 nM¹⁶. A family of pyrazole-based sulfonamides and sulfamides were reported to have potencies of about 1 nM, while a class of imidazole-based derivatives had potencies around 75 nM^{17,18}. Pelcman et. al. identified BLX-2477 (N-(2-chloro-4-fluorophenyl)triazole-4-carboxamide) with a potency of 99 nM but the inhibitor exhibited adverse off-target effects in mini-pigs and was not potent against the dog or rat LOX orthologs^{19,20}. Eleftheriadis et. al. published a novel family of 6-benzyloxysalicylate inhibitors with only modest potency (7100 nM) against h15-LOX-1²¹. We have previously discovered two series of inhibitors that target h15-LOX-1, based on **ML094** (4-(5-(Naphthalen-1-yl)-1,3,4-oxadiazol-2-ylthio)but-2-

nylthiophene-2-carboxylate, and **ML351** (5-(methylamino)-2-(naphthalene-1-yl)oxazole-4-carbonitrile)^{22,23}. The structure of **ML094** is similar to **ML351** in that they both contain a naphthalene moiety attached to a 5-member heterocycle, but **ML094** differs in that it has a longer hydrophobic arm, opposite the naphthalene group. **ML094** exhibits low nano-molar potency *in vitro* but has no activity *in vivo*, possibly due to the cellular lability of the ester moiety. On the other hand, **ML351** has sub-micromolar potency and exhibits *in vivo* activity in mice²⁴. Due to their similar structures, we have assumed both **ML094** and **ML351** bind to similar sites on h15-LOX-1, however, the lack of a co-crystal structure of either inhibitor with h15-LOX-1 has made the improvement of these two inhibitor series challenging.

The structure of the rabbit homologue of h15-LOX-1 (r15-LOX) has been solved with an inhibitor bound to the active site (**Figure 5.1**)^{25,26}. The inhibitor, RS75091, weakly coordinates to the active site iron and interacts with the deep pocket of the active site. Specifically, the phenyl ring of RS75091 points toward the Phe415/Phe353 (Phe414/Phe352 in h15-LOX-1) and its carboxylic acid and alkyl chain pointing back into the cavity. It is also important to note that the unit cell contains two proteins, a closed and an open structure. The closed structure has the inhibitor bound, while the open does not. This difference in structure due to inhibitor binding suggests plasticity in the active site and presents challenges for structure-based design.

Previous studies have investigated specific amino acids in the active site of h15-LOX-1 through mutagenesis to better understand the residues involved in

substrate binding. Gan et. al. investigated three active site residues, R402, F414 and L407²⁷. They mutated R402 to a leucine, which led to a change in positional specificity²⁷, and supports the idea that the fatty acid substrate penetrates the active site with the methyl terminus end first, allowing the carboxyl end of the fatty acid to interact with R402 at the entrance of the substrate channel. Mutation of F414, an aromatic residue that resides near the catalytic iron, also affected proper alignment of substrate in the active site. This residue is proposed to participate in a π - π interaction with the Δ^{11} -double bond of arachidonic acid and Δ^9 -double bond of linoleic acid²⁷. L407, thought to control the entrance of the narrow pocket of the methyl-end binding region of the substrate, did not affect substrate binding significantly. However, L407 is conserved in all of the lipoxygenases and the homologous residue in soybean lipoxygenase is L546. Klinman et. al. mutated this residue to A546 and found that relative to WT s15-LOX-1, the A546 mutant made 10% more 9R-HpODE, a product resulting from oxygen attacking on the same face as H-atom abstraction²⁸. This data suggests that this residue controls the regiochemistry of oxygenation and participates in guiding oxygen to its proper location²⁸. Two catalytic residues, I417 and F352, which reside at the end of the narrow methyl-end binding region²⁷⁻³⁰, restrict the penetration of the fatty acid methyl tail, and thus 15-HpETE is the primary product, with a 9:1 ratio relative to 12-HpETE²⁷. The I417A or F352L mutants allow AA to bind deeper into the active site, resulting in the C10 hydrogen atom to be abstracted by the iron, and an increase in 12-HpETE formation (15:1 ratio relative to 15-HpETE)³¹. Finally, E356 and Q547 (E357 and Q548 in the rabbit 15-lipoxygenase

(r15-LOX)) participate in a hydrogen-bonding network in the active site of r15-LOX, which may provide a structural link between substrate binding and iron coordination²⁵.

In the current work, we mutate 8 active site residues (**Figure 5.2**), based on the above observations and molecular modeling of inhibitor binding, and determine their effects on the IC_{50} and steady state inhibition parameters of an **ML094 derivative** and/or **ML351**.

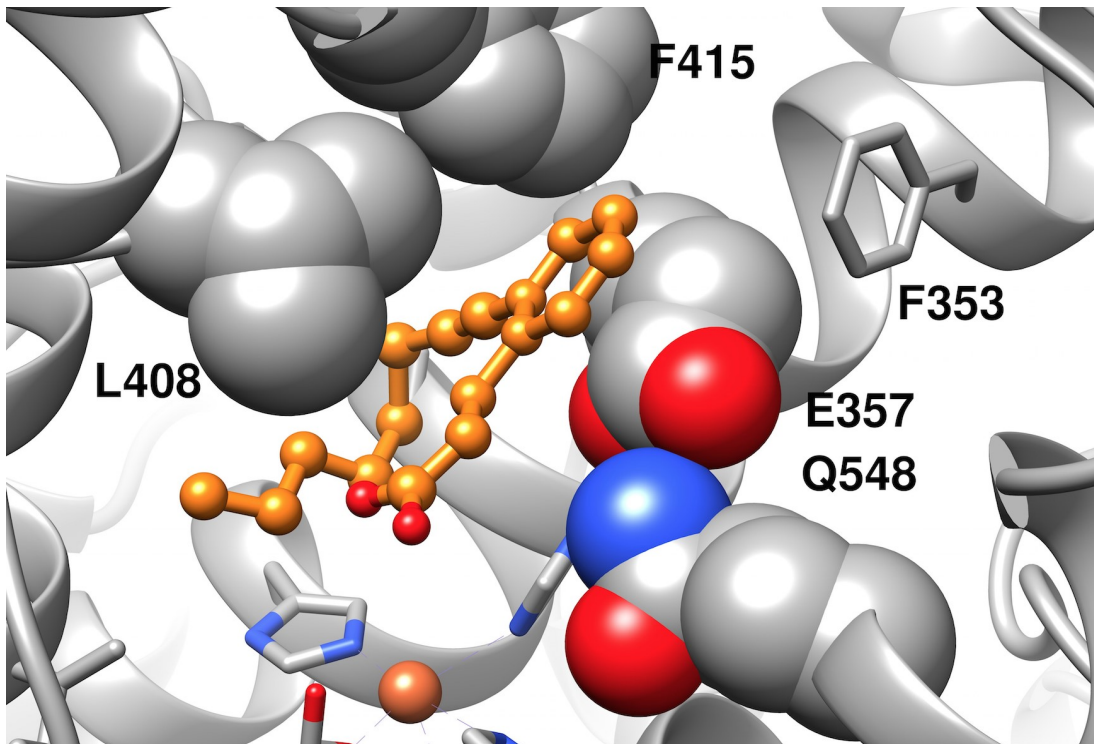


Figure 5.1. Rabbit 15-LOX and RS75091 inhibitor.

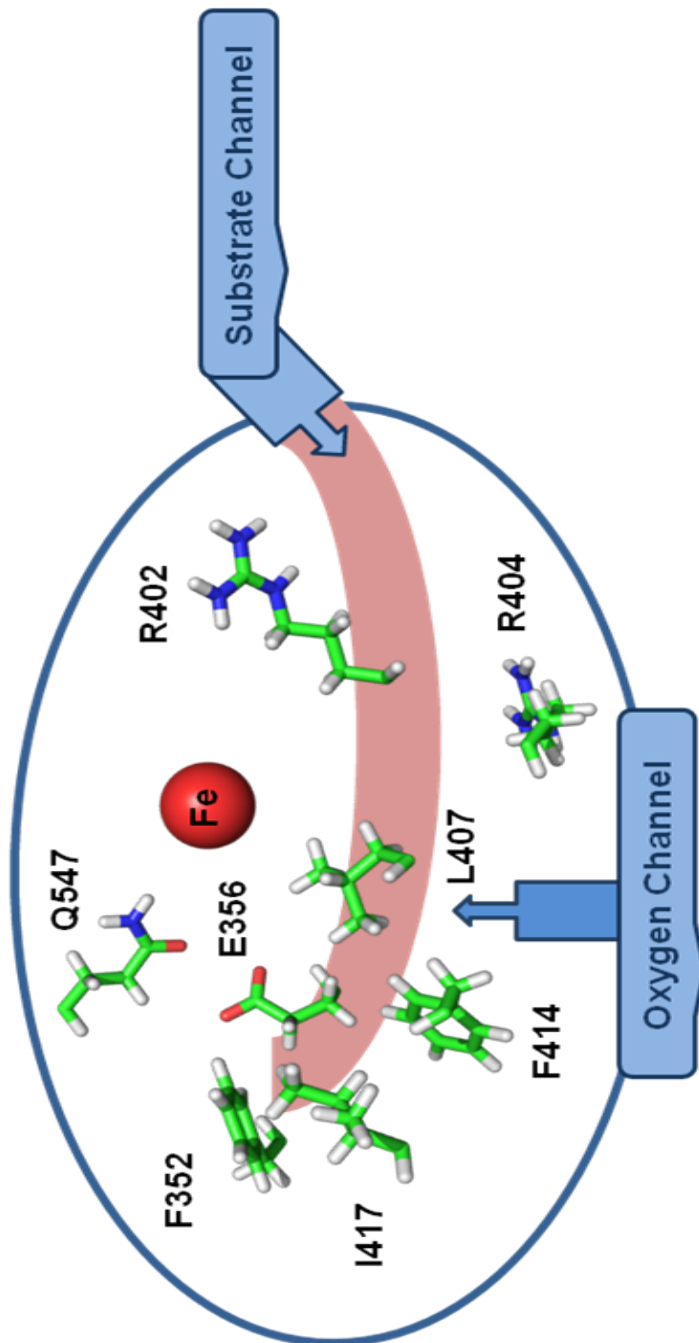


Figure 5.2. Active site residues mutated in h15-LOX-1.

5.2 Materials and Methods

5.2.1 Chemicals. All commercial fatty acids were purchased from Nu Chek Prep, Inc. (MN, USA). All other chemicals were reagent grade or better and were used without further purification.

5.2.2 Site-directed Mutagenesis. All mutations of the human 15-LOX-1 enzyme (R402L, R404L, E356Q, Q547L, F414I, F414W, L407A, I417A, F352L) were performed using the QuikChange® II XL site-directed mutagenesis kit from Agilent Technologies (CA, USA), following the instructions of the manufacturer's protocol. The mutation was confirmed by sequencing the LOX insert in the pFastBac1 shuttle vector (Operon, gene with Operon (KY, USA)).

5.2.3 Protein Expression. The h15-LOX-1 enzyme used in this publication were expressed and purified as previously published³². All mutants, (R402L, R404L, F414I, F414W, E356Q, Q547L, I417A, L407A), were expressed as N-terminal His6-tagged proteins and were purified via cation exchange affinity chromatography using Bio-Rad Macro-Prep High S cation exchange resins or with an IMAC column, depending on the mutation. The protein purity was evaluated by SDS-PAGE analysis and was found to be greater than 90%.

5.2.4 Determination of Iron Content using ICP-MS. The iron content of the mutants were determined relative to WT h15-LOX-1 using a Thermo Element XR inductively coupled plasma mass spectrometer (ICP-MS), using cobalt (EDTA) as an internal standard. Iron concentrations were compared to standard iron solutions. All kinetic data were normalized to the iron content. The protein concentration was

determined using the Bradford assay, with bovine serum albumin (BSA) as the protein standard.

5.2.5 Lipoxygenase UV-Vis-based IC₅₀ Assay. The three-point inhibition percentages were determined by following the formation of the conjugated diene products 15-HpETE ($\epsilon = 27,000 \text{ M}^{-1}\text{cm}^{-1}$) or 13-HpODE ($\epsilon = 23,000 \text{ M}^{-1}\text{cm}^{-1}$) at 234 nm with a Perkin-Elmer Lambda 40 UV/Vis spectrophotometer at three inhibitor concentrations. All reaction mixtures were 2 mL in volume and constantly stirred using a magnetic stir bar at room temperature (23°C) with the appropriate amount of LOX isozyme h15-LOX-1 (~ 30 nM); F414I (~ 150 nM); F414W (~ 67 nM); E356Q (~ 100 nM); Q547L (~ 80 nM); R402L (~ 112 nM); R404L (~ 130 nM); I417A (~ 60 nM); L407A (~ 100 nM). All reactions were carried out in 25 mM HEPES buffer (pH 7.5), 0.01% Triton X-100 and 10 μM AA or LA. The concentration of AA or LA was quantitated by enzymatic reaction with soybean 15-lipoxygenase-1 (s15-LOX-1) and allowing the reaction to go to completion. IC₅₀ values were obtained by determining the enzymatic rate at various inhibitor concentrations and plotted against inhibitor concentration, followed by a hyperbolic saturation curve fit. The data used for the saturation curves were performed in duplicate or triplicate, depending on the quality of the data.

5.2.6 Steady-State Kinetics. The h15-LOX-1 and mutant rates were determined the same way as the UV-Vis-Based Assay. Reactions were initiated by adding the LOX enzyme to a constantly stirring 2 mL reaction mixture containing 1 μM – 20 μM AA or LA in 25 mM HEPES buffer (pH 7.5), in the presence of 0.01%

Triton X-100. Kinetic data were obtained by recording initial enzymatic rates at each substrate concentration and subsequently fitted to the Henri-Michaelis-Menten equation, using KaleidaGraph (Synergy) to determine k_{cat} and k_{cat}/K_M values.

5.2.7 Steady-State Inhibition Kinetics. h15-LOX-1 and mutant rates were determined the same way as the UV-Vis-Based Assay. Reactions were initiated by adding the LOX isozyme to a constantly stirring 2 mL reaction mixture containing 1 μM – 20 μM AA or LA in 25 mM HEPES buffer (pH 7.5), 0.01% Triton X-100. Kinetic data were obtained by recording initial enzymatic rates, at varied inhibitor concentrations, and subsequently fitted to the Henri-Michaelis-Menten equation, using KaleidaGraph (Synergy) to determine the microscopic rate constants, V_{max} ($\mu\text{mol}/\text{min}/\text{mg}$) and V_{max}/K_M ($\mu\text{mol}/\text{min}/\text{mg}/\mu\text{M}$). These rate constants were subsequently replotted as $1/V_{\text{max}}$ or K_M/V_{max} versus inhibitor concentration, to yield K_{iu} and K_{ic} , respectively, which are defined as the equilibrium constant of dissociation from the secondary and catalytic sites. The primary data was also plotted in the Dixon format, graphing $1/v$ vs. $[I]$ μM at the chosen substrate concentrations. From the Dixon plots, the slope at each substrate concentration was extracted and plotted against $1/[S]$ μM to produce the Dixon parameters, K_{iu} and K_{ic} .

5.2.8 Computer Methods. A homology model of human 15-Lipoxygenase-1 (h15-LOX-1) sequence (UniProt accession P16050) was built from the closed inhibitor bound structure of rabbit reticulocyte 15-LOX (pdb id 2p0m, chain B, sequence identity 81%), using the software PRIME (Schrodinger Inc). Both metal ion (Fe^{2+}) and co-crystallized inhibitor were included during homology modeling. In

addition, we have also copied a water molecule that coordinates to the metal ion in the h15-LOX-2 structure (pdb id 4nre). The model was energy minimized using Protein Preparation Wizard (Schrodinger Inc). After energy minimization the inhibitor was separated, leaving the protein, Fe²⁺ ion and a water molecule as a separate entry in the Maestro project table (Maestro v97012, Schrodinger Inc). We copied this protein model into multiple entries and in each entry we made one specific mutation (viz. E356Q, F414I, F414W, L407A, and Q547L) using Maestro's Edit/Build panel (Schrodinger Inc). After making the virtual mutation, the side chain of the mutated residue was optimized using PRIME side chain prediction module (Schrodinger Inc). Once a low energy side chain conformation was found, the resulting structure was used in our subsequent docking studies. We used the previously separated inhibitor coordinates to define the binding site for docking the WT and mutant LOX enzymes. Inhibitor **18**, of the **ML094** series, and **ML351** were manually built using Maestro's Edit/Build panel and energy minimized using LigPrep software (LigPrep v36017, Schrodinger Inc). In addition to adding hydrogens, LigPrep also expands protonation states and chiralities of the inhibitors. For both inhibitors only one final structure was obtained after LigPrep energy minimization. Docking software Glide (Glide v58515, Schrodinger Inc) was used for flexible-ligand rigid-receptor docking. Glide extra precision scoring function (Glide-XP) was used to obtain docking pose and score for each inhibitor. We performed the docking calculation for both WT and mutant LOX enzymes.

5.3 Results and Discussion

5.3.1 Molecular Modeling Predictions of ML351 and Compound 18

Binding Modes. To develop hypotheses concerning their binding modes, inhibitors **ML351** and compound **18** were computationally docked to a model of WT h15-LOX-1, using Glide XP. The docking scores are presented in **Table 5.1**, and the predicted binding poses in **Figure 5.3**.

Compound **18** is pseudosymmetrical and binds in a U-shape binding mode (**Figure 5.3b**), similar to the ligand binding mode observed in porcine leukocyte 12-LOX and human epithelial 15-LOX-2 co-crystal structures^{30,31}. The acetylene group in the linker region is in the vicinity of the metal ion and the water molecule, which makes a hydrogen bond donor interaction with the ester oxygen of the inhibitor (2.3 Å).

ML351 is much smaller than **18** but the naphthalene rings of both inhibitors bind deeply in the hydrophobic pocket created by F352 and F414 (**Figure 5.3d**), in a very similar manner to the aromatic group in RS75091 in its co-crystal structure with the rabbit homolog (pdb id 2p0m, chain B), suggesting a common aromatic binding site (**Figure 5.3c**). The oxazole ring in **ML351** is a bioisostere of the ester group and its hydrogen bond acceptor nitrogen is 2.8 Å from the hydrogen atom of the water molecule. However, unlike the ester group in **18**, the oxazole ring in **ML351** is geometrically constrained due to substitutions at all 3 carbons.

To assess the predicted binding modes, with the ultimate goal of further optimizing the inhibitors, we identified side chains in the active site that are predicted

to form key interactions with the inhibitors; some of the resulting mutations have been examined in other contexts previously, as described in the Introduction. Phe414 was predicted to form key hydrophobic contacts with both inhibitors, suggesting that mutations to it would perturb binding of both ligands. Two mutations were chosen, F414I, which removes the aromatic character, and F414W, which retains the aromatic character but would be expected to reduce the size of the hydrophobic pocket. We created models of these mutants of h15-LOX-1 and re-docked both inhibitors (**Table 5.1** and **Figure 5.4**). Interestingly, only F414I was predicted to negatively impact binding of **ML351** (based on worse docking score), whereas F414W was predicted to more negatively impact the binding of compound **18**. The difference in the predicted behavior appears to be due to the size of the inhibitors; while the smaller **ML351** can, in some cases, reorient itself to find other (predicted) favorable binding modes, the larger compound **18** is much more restricted.

Mutation of Leu407, specifically L407A, was likewise predicted to have differing impacts on **ML351** and compound **18**. In the U-shaped binding mode of compound **18** (**Figure 5.3b**), Leu407 is predicted to play a particularly central role, binding in the middle of the “U” and forming favorable interactions with both aromatic groups. As such, L407A is predicted to negatively impact binding affinity of compound **18**, which then docks in a completely different manner than with WT.

Another key region of the binding site involves the side chains of Glu356 and Gln547, which form a hydrogen bond with each other, but were not predicted to form hydrogen bonds with either inhibitor. The mutation E356Q was meant to test the

impact of neutralizing the negative charge of the Glu side chain, and Q547L to test the impact of making this portion of the binding site more hydrophobic. Neither mutation, however, was predicted to negatively impact inhibitor binding; the docking pose of compound **18** was different for E356Q, but in a pseudo-symmetrical manner in which the 2 aromatic groups switched positions, with the binding mode otherwise quite similar, and with a docking score even more favorable than with WT.

5.3.2 Determination of Steady-State Substrate Kinetics. The steady-state substrate kinetic experiments for F414W, E356Q, Q547L, R402L, R404L and L407A were executed using AA as the substrate, while LA was required for F414I kinetics, due to rapid product degradation of AA relative to WT. Gratifyingly, the steady-state substrate kinetic parameters for all the mutants (V_{\max} , K_M and V_{\max}/K_M) agreed well with those seen in the literature and were within 50% of the WT values²⁴ (**Table 5.2**). The data confirms the hypothesis that these active site mutations do not alter the WT kinetics significantly and represent relatively minor perturbations to the active site.

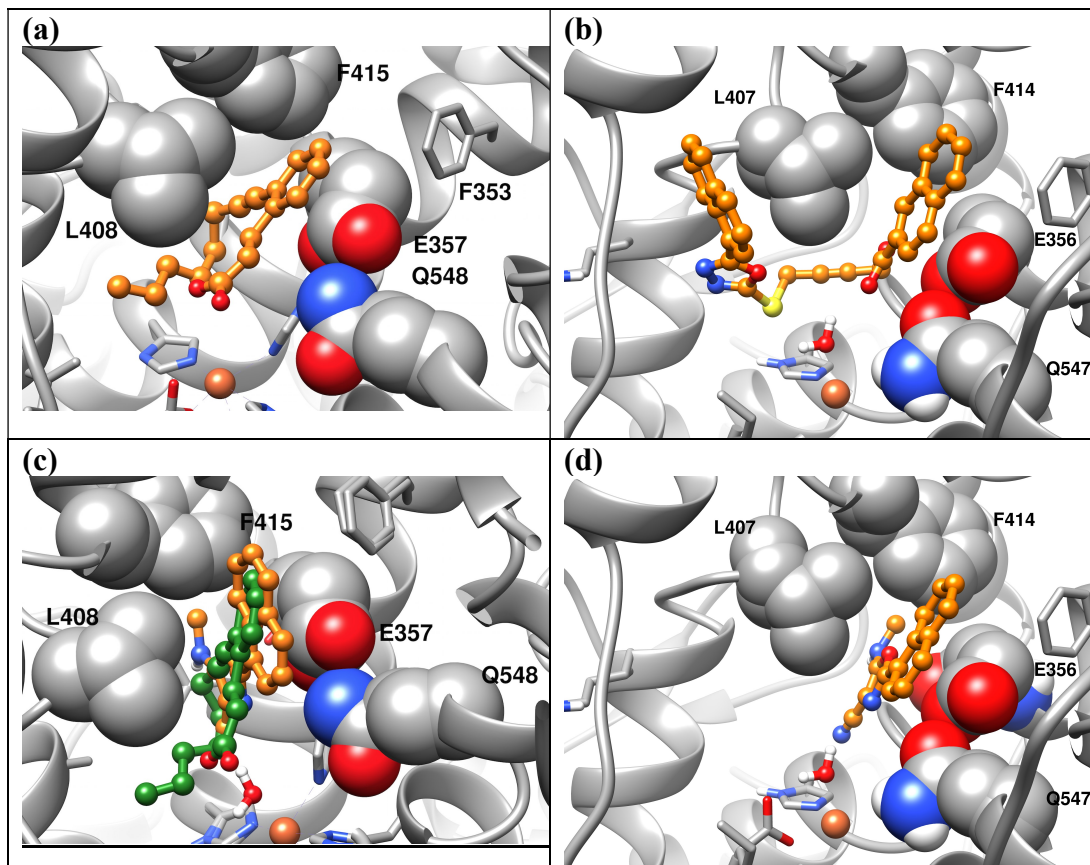


Figure 5.3. (a) Rabbit 15-LOX and RS75091 inhibitor from the crystal structure (pdb id: 2p0m, chain B), (b) docking pose of compound **18** docked to Human 15-LOX model, (c) docking pose of human 15-LOX model with **ML351** superimposed to rabbit 15-LOX structure, and (d) docking pose of **ML351** docked to Human 15-LOX. The inhibitor is shown in ball-and-stick representation and Fe^{2+} ion is shown in sphere representation. Carbon atoms of the inhibitor are shown in orange color, oxygen atoms are shown in red color. Fe^{2+} ion is shown in orange color. Protein residues mutated in this study are shown in sphere representation. Carbon, nitrogen and oxygen atoms of the protein are shown in gray, blue and red colors respectively.

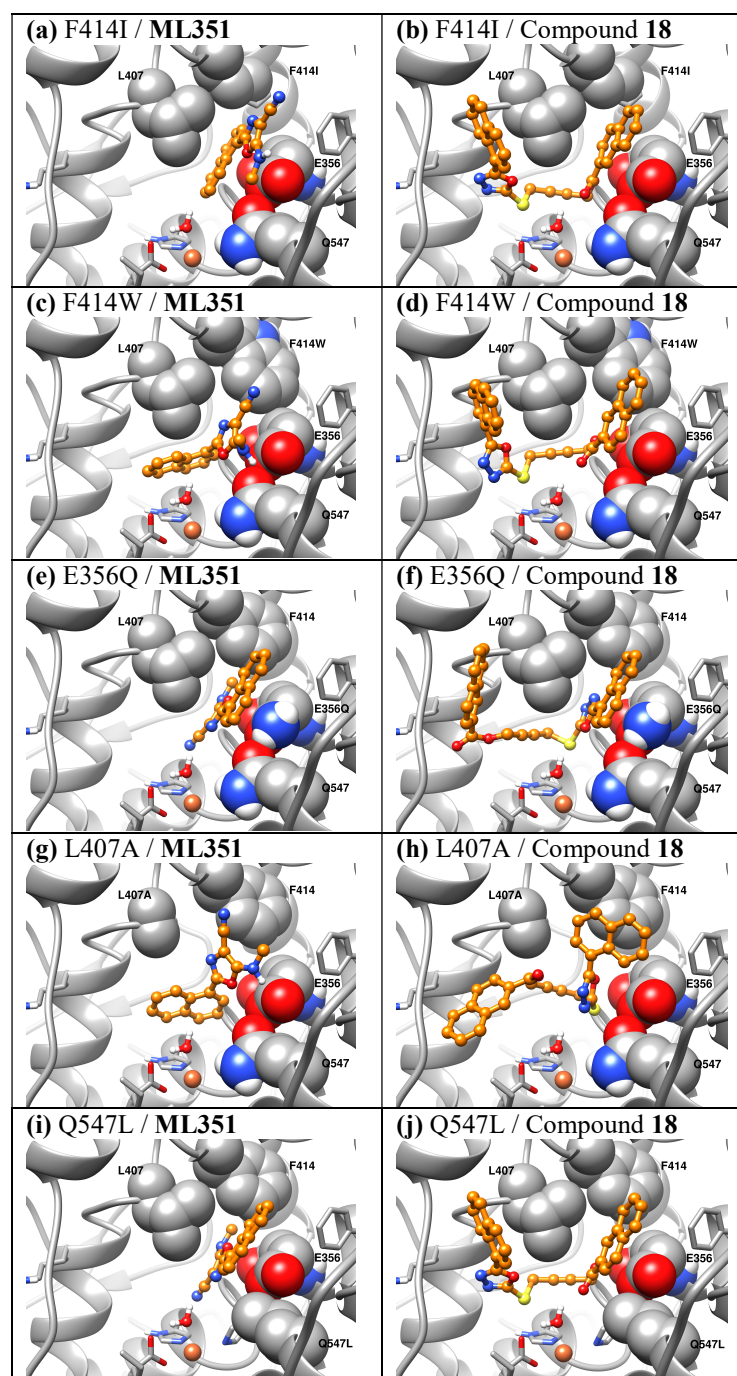


Figure 5.4. Docking pose of inhibitors, **ML351** and **compound 18**, Active site residues subjected to mutation are shown in sphere representations, inhibitors are shown in ball-and-stick representation (carbon, nitrogen, oxygen and sulfur atoms are shown in orange, blue, red and yellow color). Fe^{2+} ion is shown orange color and the water molecule is shown in ball-and-stick representation.

Protein	ML351		18	
	XP Docking	Heavy atom RMSD (Å)	XP Docking	Heavy atom RMSD (Å)
WT	-5.2	-	-10.2	-
F414I	-4.7	6.6	-9.4	1.4
F414W	-6.9	6.7	-8.7	1.9
L407A	-5.7	6.5	-8.4	8.3
E356Q	-7.3	0.2	-11.1	8.1
Q547L	-5.2	0.2	-10.3	0.3

Table 5.1. Glide-XP docking scores and heavy atom root-mean-square distance (RMSD) between the docked poses of inhibitors **18** and **ML351** docked against WT h15-LOX-1 and mutants.

		K_M	k_{cat}	k_{cat}/K_M	% Metallation
AA	WT	8.8 (0.8)	11 (0.5)	1.3 (0.06)	50
	Q547L	11 (1)	2.9 (0.1)	0.3 (0.01)	59
	E356Q	4.1 (0.4)	3.0 (0.1)	0.7 (0.04)	42
	F414W	6.5 (0.6)	2.8 (0.08)	0.4 (0.02)	52
	F414I	11 (0.7)	1.8 (0.05)	0.2 (0.006)	57
	L407A	5.5 (1)	2.5 (0.2)	0.45 (0.01)	75
LA	WT	7.7 (0.8)	11 (0.4)	1.5 (0.09)	50
	F414I	6.1 (0.2)	1.6 (0.03)	0.3 (0.007)	57

Table 5.2. Steady-state kinetic parameters of mutants that exhibited the greatest change in potency relative to WT h15-LOX-1. The substrate used is indicated on the left and the error in parentheses.

5.3.3 Determination of Mutation Effects on Inhibitor Potency. To determine the effect of a specific mutation on inhibitor potency, **ML351** and compound **18**, an **ML094** derivative^{22,24} (**Table 5.3**), were screened against active site mutants (R402L, R404L, F414I, F414W, E356Q, Q547L, L407A and I417A) in a 3-pt IC₅₀ assay. The results were related to WT h15-LOX-1, which will subsequently be referred to as WT. As is observed in **Table 5.4**, **ML351** had an IC₅₀ of 0.33 ± 0.02 μM against WT, with F414I being the only mutant manifesting a change in potency. F414I displayed an IC₅₀ of 4.1 ± 1 μM (**Table 5.4**), which was 12-fold less potent than WT, while F414W and E356Q showed little change in potency (IC₅₀ values of 0.77 ± 0.1 and 0.87 ± 0.2 μM , respectively), in qualitative agreement with the docking results. Q547L, R404L, R402L, L407A and I417A exhibited similar potency as WT, indicating minimal or no interaction with **ML351** (**Table 5.4**).

The second inhibitor screened, compound **18**, (4-(5-(Naphthalen-1-yl)-1,3,4-oxadiazol-2-ylthio)but-2-ynyl-4-naphthalene²²) is a derivative of **ML094**. This molecule was chosen due to its lower potency than **ML094**, which did not require the Morrison equation for IC₅₀ determination and thus simplified data interpretation. Analysis of compound **18** data (**Table 5.4**) indicated that L407A had the largest effect on inhibition, with a greater than 1000-fold decrease in potency (IC₅₀ > 50 μM). E356Q had a modest effect on the potency of compound **18** relative to WT (IC₅₀ = 0.14 ± 0.04 μM and 0.05 ± 0.001 μM , respectively), while Q547L exhibited no effect on potency (0.040 ± 0.01 μM). F414W also had a large change in potency relative to WT (IC₅₀ = 0.20 ± 0.04 μM), however F414I had little effect (IC₅₀ = 0.078 ± 0.03

μM) (**Table 5.4**). R404L, R402L and I417A had little or no effect on the potency of compound **18** ($\text{IC}_{50} = 0.060 \pm 0.02 \mu\text{M}$, $0.050 \pm 0.001 \mu\text{M}$ and $0.060 \pm 0.01 \mu\text{M}$, respectively).

5.3.4 Steady-State Inhibition Kinetics. Given the changes in IC_{50} value of these active site mutants, it was important to confirm these effects with steady-state enzyme inhibitor kinetics with the mutants that exhibited the greatest effect on the IC_{50} value (F414I, F414W, E356Q and L407A). Arachidonic acid was used as substrate with F414W, E356Q and L407A, while linoleic acid was used with F414I, for reasons that were previously discussed. The formation of 15-HpETE or 13-HpODE was monitored as a function of substrate and inhibitor concentration in the presence of 0.01% Triton X-100. Replots of K_M/V_{max} and $1/V_{\text{max}}$ against inhibitor concentration produced linear plots from which K_{ic} (equilibrium constant of dissociation from the enzyme) and K_{iu} (equilibrium constant of dissociation from the enzyme substrate complex) were extracted (see relative values to WT, **Table 5.5**). The data was consistent with mixed inhibition, which is typical of LOX inhibitors²⁴. All data were also plotted in the Dixon format (not shown), which confirmed the K_{ic} and K_{iu} for each mutant.

According to the data, the K_{ic} of **ML351** for F414W ($K_{\text{ic}} = 0.30 \pm 0.12 \mu\text{M}$) was similar to WT ($K_{\text{ic}} = 0.3 \pm 0.03 \mu\text{M}$), but the K_{ic} for F414I ($K_{\text{ic}} = 1.0 \pm 0.03 \mu\text{M}$) was 25-fold greater than WT ($K_{\text{ic}} = 0.04 \pm 0.016 \mu\text{M}$). Note, the WT K_{ic} varies depending on the substrate used (AA vs. LA), possibly due to the allosteric site. These data suggest that F414 interacts directly with **ML351**, possibly in a manner

analogous to the interaction between F414 and the substrate²⁷, but only the aromatic to aliphatic substitution significantly disrupts binding.

With regards to the **ML094** derivative, compound **18**, which contains a similar naphthalene moiety, but a longer hydrophobic arm than **ML351**, mutations at F414 also affected binding of the inhibitor to the enzyme but in a different way. In this case, F414I did not have an effect on the K_{ic} of compound **18** ($K_{ic} = 0.16 \pm 0.02 \mu\text{M}$) relative to WT ($K_{ic} = 0.10 \pm 0.01 \mu\text{M}$), exhibiting only a 1.6-fold decrease in potency (**Table 5.5**). However, F414W ($K_{ic} = 0.17 \pm 0.01 \mu\text{M}$) had a larger effect on K_{ic} relative to WT ($K_{ic} = 0.02 \pm 0.003 \mu\text{M}$), decreasing the potency 8.5-. Note, the WT K_{ic} varies depending on the substrate used (LA vs. AA), This result suggests that changing F414 to the larger W414 impacts the binding of compound **18** but not **ML351**, which is much smaller. On the other hand, F414I only decreased the potency slightly, supporting the hypothesis that sterics is more important than aromaticity for compound **18**.

With respect to E356Q, the K_{ic} of **ML351** increases less than 3-fold ($K_{ic} = 0.70 \pm 0.06 \mu\text{M}$) suggesting minimal inhibitor interactions, consistent with the predicted docking pose. However, a 20-fold decrease in potency was observed for E356Q with compound **18** (**Table 5.5**) relative to WT ($K_{ic} = 0.4 \pm 0.036 \mu\text{M}$ and $0.02 \pm 0.003 \mu\text{M}$, respectively). This result was not predicted by the docking calculations, although compound **18** was predicted to bind in a “flipped” orientation in E356Q. E356 is involved in the second coordination sphere of the active site iron, as seen in the soybean and rabbit 15-LOX-1 structures, therefore converting the Glu to a Gln

could either affect a direct interaction with compound **18**, or the configuration of the second coordination sphere^{25,35}.

The mutation L407A has little effect on the potency of **ML351** ($K_{ic} = 0.2 \pm 0.002 \mu\text{M}$), but greater than 1000-fold decrease in potency for compound **18** ($\text{IC}_{50} > 50 \mu\text{M}$). Qualitatively, this result was expected based on the docking predictions, although the magnitude of the decrease in potency for compound **18** is dramatic, emphasizing the critical role of the Leu407 side chain in binding the U-shaped compound **18**. It should be noted that steady-state inhibition kinetics could not be performed with L407A due to the dramatic drop in potency (greater than 1000-fold) and hence our inability to reach high enough inhibitor concentrations due to solubility constraints.

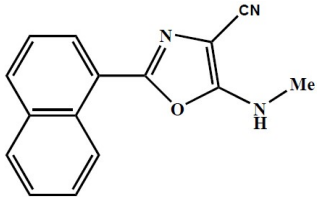
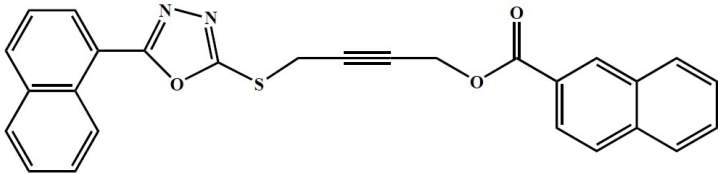
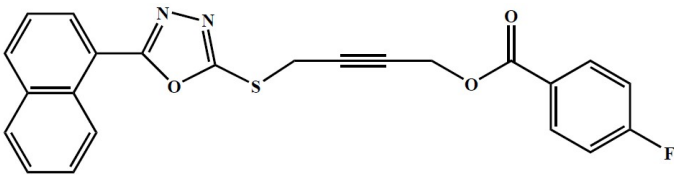
INHIBITOR STRUCTURE	INHIBITOR ID#
	<p style="text-align: center;">ML351</p>
	<p style="text-align: center;">Compound 18</p>
	<p style="text-align: center;">ML094</p>

Table 5.3. Chemical structures and identification numbers of inhibitors.

Enzyme	ML351	18
WT	0.33 ± 0.02	0.050 ± 0.001
F414I	4.1 ± 1	0.078 ± 0.03
F414W	0.77 ± 0.1	0.20 ± 0.04
E356Q	0.87 ± 0.2	0.14 ± 0.04
Q547L	0.30 ± 0.06	0.040 ± 0.01
R404L	0.30 ± 0.09	0.060 ± 0.02
R402L	0.12 ± 0.001	0.050 ± 0.001
L407A	0.39 ± 0.11	> 50
I417A	0.20 ± 0.08	0.06 ± 0.01

Table 5.4. 3-Pt IC₅₀ values (μM) of WT h15-LOX-1 and mutants against **ML351** and compound **18**.

	ML351	18
WT	1	1
F414I	25	1.6
F414W	1	8.5
E356Q	2	20
L407A	1	> 1000

Table 5.5. Inhibitor constant (K_{ic}) increase of **ML351** and compound **18** with the LOX mutants, relative to WT h15-LOX-1.

5.4 Conclusion. Overall, the results support the models shown in **Figure 5.3**, in which both **ML351** and compound **18** bind with the naphthalene group in a deep hydrophobic pocket, with F414 lying at the end of the pocket. The mutations F414I and F414W, as well as L407A, have differing impacts on the two inhibitors due to compound **18** being approximately twice the size of **ML351**, which presents greater constraints on its possible binding modes. Q547L was predicted and confirmed to have little impact on binding of either inhibitor, consistent with the Gln side chain not being predicted to form hydrogen bonds with either inhibitor. The results with E356Q are more difficult to interpret; this charge-changing mutation had little impact on **ML351** but a significant negative effect on the K_{ic} of compound **18** (although the impact on the IC_{50} measurement was more modest).

These results have differing implications for improving the binding affinity of compounds in the **ML351** and **ML094** series (compound **18** being a member of the latter). Compound **18** and other members of the **ML094** series are predicted to nearly completely fill the binding pocket, from the narrow constriction created by the side chain of Leu407 through the hydrophobic pocket terminating in Phe414. There may be modest opportunities to improve binding interactions in these regions, given these constraints, although the impact of E356Q may suggest opportunities to optimize electrostatic complementarity. By contrast, the much smaller **ML351** presents potentially significant opportunities for further optimization, although in practice this has proven to be challenging²⁴. The views of the predicted binding mode in **Figure 5.5**, in which molecular surfaces emphasize key steric constraints, suggest that the

challenge is to identify ways of extending the molecule into the narrow constriction formed by Leu407, while maintaining the hydrogen-bond of the oxazole to the ferric-water moiety. Our initial SAR investigation^{23,24} increased the length of the methylamine, which improved potency slightly (compounds **21**, **22** and **23**); however, too long of an alkyl chain or a branched chain decreased potency (compounds **24** and **26** respectively). This data is consistent with our model where the alkyl chain would extend into the active site toward the exit^{23,24}. We also observed that modifying the oxazole ring or the cyano moiety lowered potency dramatically (compounds **33-40**), possibly due to disruption of the oxazole hydrogen-bond to the ferric-water moiety. Based on the model presented here, we are currently designing new inhibitors, which maintain the hydrogen-bond interaction with the Fe²⁺-H₂O, while efficiently filling the open cavity off the alkyl amine to gain binding affinity. One possible modification to achieve this could be to design an alkyl moiety onto the oxazole, rather than the amine.

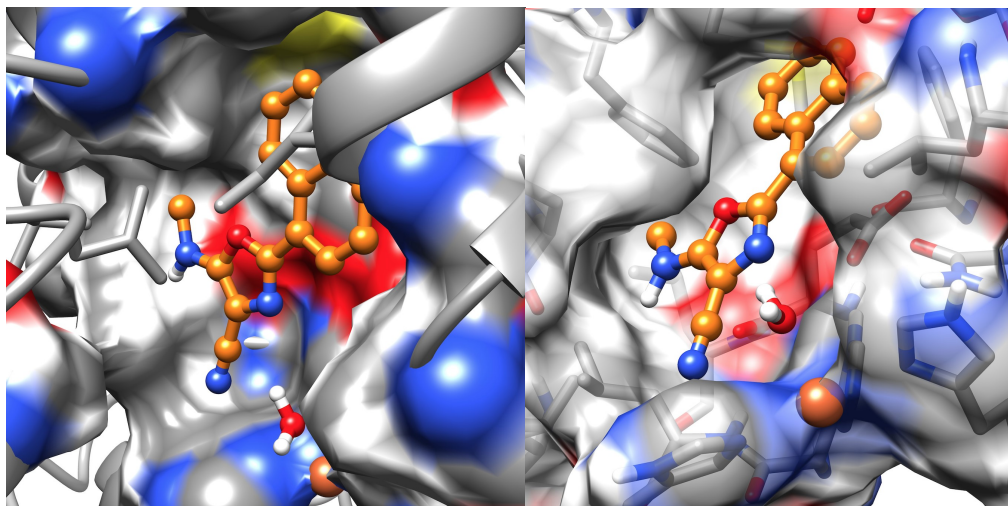


Figure 5.5. Docking pose of **ML351** to the human 15-LOX-1 model, with electrostatic van der Waals boundaries in the active site. **ML351** is shown in ball-and-stick representation. Carbon and oxygen atoms of **ML351** are shown as orange and red colors, respectively. Carbon, nitrogen and oxygen atoms of the protein residues are shown in gray, blue and red colors, respectively.

5.5 References

1. Kuhn, H.; O'Donnell, V.B. *Prog. Lipid Res.* **2006**, *45*, 334.
2. Nasjletti, A.; et. al. *Hypertension.* **1998**, *31*, 194-200.
3. Chawengsub, Y.G.; et. al. *Am. J. Physiol. Heart Circ. Physiol.* **2009**, *297*, H495.
4. Zhu, D.; Ran, Y. *Physiol. Sci.* **2012**, *62*, 163.
5. Belkner, J. S.; Kuhn, H.; et. al. *J. Biol. Chem.* **1998**, *273*, 23225.
6. Pirillo, A.; Uboldi, P.; Kuhn, H.; et. al. *Biochim. Biophys. Acta.* **2006**, *1761*, 292.
7. Folcik, V. A.; Nivar-Aristy; et. al. *J. Clin. Invest.* **1995**, *96*, 504.
8. Pidgeon, G. P.; Lysaght, J.; et. al. *Cancer Metastasis Rev.* **2007**, *26*, 503.
9. Klil-Drori, A. J.; Ariel, A. *Prostag. Other Lipid Mediat.* **2013**, *106*, 16.
10. Laybutt, D. R.; Sharma, A.; et. al. *J. Biol.Chem.* **2002**, *277*, 10912.
11. Sears, D.; Miles, P.D.; et. al. *PLoS One.* **2009**, *4*, e7250.
12. Dobrian, A.; Ma, Q.; et. al. *Biochem. Biophys. Res. Commun.* **2010**, *403*, 485.
13. van Leyen, K. *CNS Neurol. Disord. Drug Targets.* **2013**, *12*, 191.
14. van Leyen, K.; Kim, H.Y.; et. al. *Stroke.* **2006**, *37*, 3014.
15. van Leyen, K.; Arai, K.; *J. Neurosci. Res.* **2008**, *86*, 904.
16. Weinstein, D. S.; Gu, Z.; et. al. *Bioorg. Med. Chem. Lett.* **2005**, *15*, 1435.
17. Ngu, K. W.; Liu, W.; et. al. *Bioorg. Med. Chem. Lett.* **2011**, *21*, 4141.
18. Weinstein, D. S.; Ngu, K.; et. al. *Bioorg. Med. Chem. Lett.* **2007**, *17*, 5115.
19. Pelcman, B.; Sanin, A; et. al. *Bioorg. Med. Chem. Lett.* **2015**, *25*, 3017.
20. Pelcman, B.; Sanin, A; et. al. *Bioorg. Med. Chem. Lett.* **2015**, *25*, 3024.
21. Eleftheriadis, N.; Thee, S.; et. al. *Eur. J. Med. Chem.* **2015**, *94*, 265.

22. Rai, G.; Kenyon, V.; Jadhav, A.; et. al. *J. Med. Chem.* **2010**, *53*, 7392.
23. Rai, G.; et. al. *Probe Reports from the NIH Molecular Libraries Program.* **2010**.
24. Rai, G.; Joshi, N.; et. al. *J. Med. Chem.* **2014**, *57*, 4035.
25. Gillmor, S.A.; Villasenor, A.; et. al. *Nat. Struct. Biol.* **1997**, *4*, 1003.
26. Choi, J.; Chon, J.K.; et. al. *Proteins.* **2008**, *70*, 1023.
27. Gan, Q.; Sloane, D.L.; Sigal, E. *J. Biol. Chem.* **1996**, *271*, 25412.
28. Klinman, J. P. *Acc. Chem. Res.* **2007**, *40*, 325.
29. Borngraber, S.; Anton, M.; Kuhn, H. *J. Mol. Biol.* **1996**, *264*, 1145.
30. Sloane, D.L.; Barnett, J.; Sigal, C. S. *Protein Eng.* **1995**, *8*, 275.
31. Sloane D.L.; Craik C.S.; Sigal, E. *Nature.* **1991**, *354*, 149.
32. Amagata, T.; Johnson, T. A.; et. al. *J Nat. Prod.* **2003**, *66*, 230.
33. Xu, S.; Mueser, T.C.; Marnett, L.J.; Funk, M.O. *Structure.* **2012**, *20*, 1490.
34. Kobe, M.J.; Mitchell, C.E.; et. al. *J. Biol. Chem.* **2014**, *289*, 8562.
35. Tomchick, D.R.; Cymborowski, M.; *Biochemistry.* **2001**, *40*, 7509.

5.6 Credit to Coauthors

The following experiments were performed by or under the supervision of the following people and not by Michelle M. Armstrong.

- 1) Molecular Modeling

Chakrapani Kalyanaraman, Matthew P. Jacobson

Department of Pharmaceutical Chemistry, School of Pharmacy, University of California San Francisco, San Francisco, CA 94143

Chapter 6

KINETIC AND MECHANISTIC INVESTIGATION OF THE REACTION BETWEEN 15S-HPETE WITH WT h15-LOX-1 AND AN ACTIVE SITE MUTANT, F414I.

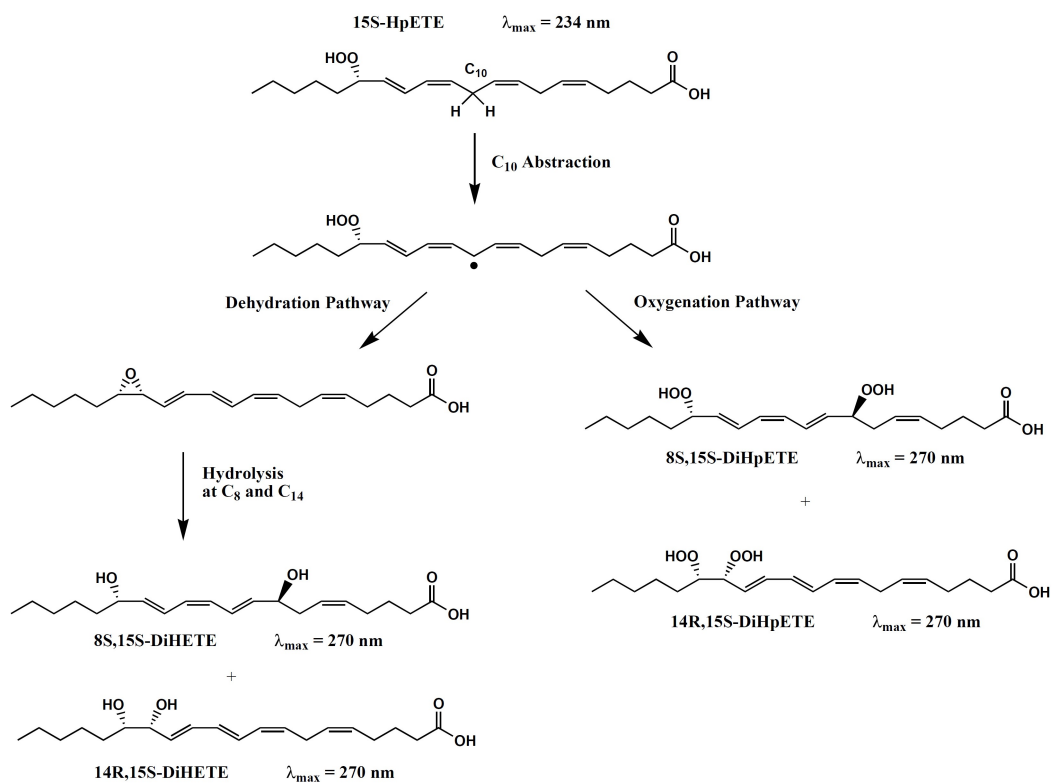
6.1 Introduction

Lipoxygenases (LOX) are non-heme iron-containing enzymes that transform polyunsaturated fatty acids to conjugated hydroperoxides and hydroxides.^{1,2,3} There are six LOX-isoforms in the human genome, which exhibit different enzymatic properties and can be categorized as 5, 12, and 15-LOXs.⁴ The LOX nomenclature is based on an isoform's positional specificity on arachidonic acid as the model substrate. Mammalian LOXs prefer free fatty acids as substrates, which are liberated from the cellular ester lipids by cytosolic phospholipase A2, but can also directly oxidize lipid membranes resulting in the degradation of intracellular organelles.⁵ The hydroperoxy products of LOXs are later converted to a large array of bioactive lipid mediators, which include leukotrienes⁶, lipoxins⁷, hepxilins⁸, eoxins⁹, resolvins¹⁰ and protectins.¹¹

Various LOX-isoforms exhibit multiple catalytic activities, including dioxygenase and dehydrase activity, which result in hydroperoxides and epoxides, respectively.¹² The primary oxygenation products of LOXs are conjugated hydroperoxide fatty acids that absorb at 234 nm, which can then serve as substrates to generate secondary lipid products that absorb at 245 and 270 nm. Dioxygenation of exogenous or endogenous conjugated hydroperoxides is initiated by abstraction of a bisallylic hydrogen, generating a substrate radical that rearranges and reacts with molecular oxygen to form a dihydroperoxide fatty acid (**Scheme 6.1**). The dehydration reaction with conjugated hydroperoxides is also initiated by bisallylic hydrogen abstraction but is followed by a homolytic cleavage of the hydroperoxy

oxygen-oxygen bond, which results in a substrate diradical. The unstable diradical forms an allylic epoxide that, in turn, is hydrolyzed by water to form dihydroxide products (**Scheme 6.1**).

Poly-unsaturated fatty acids are extremely flexible molecules with a large number of possible conformations, making it difficult to predict which conformation they adopt when bound in the active site. Based on various experimental data, one widely accepted substrate binding model, the tail-first model, has the fatty acid substrate enter the hydrophobic substrate-binding channel with the methyl end first so that the proS-hydrogen at C13 of AA is localized in close proximity to the hydrogen acceptor (iron-bound hydroxyl).¹³ In human reticulocyte 15-LOX-1, specific active site residues have been identified that interact directly with the substrate when bound tail-first: (i) ionic interaction between R402 and the negatively charged carboxylate of the fatty acid; (ii) a π - π interaction between F414 and a double bond on AA; (iii) a hydrophobic interaction between the methyl terminus of the substrate and I417 and M418.¹⁴



Scheme 6.1. Catalytic activities of LOXs: Oxygenase and Dehydrase activities.

Although the tail-first model for AA catalysis is widely accepted in the LOX scientific community, it does not completely explain the products observed in the secondary reaction, with HpETE/HETE as substrate. The soybean enzyme converts 15S-HpETE to a mixture of 8S,15S-DiHpETE and 5S,15S-DiHpETE.¹⁵ Assuming a tail-first alignment of 15S-HpETE in the active site, 5S-lipoxygenation (5S,15S-DiHpETE formation), which involves hydrogen abstraction at C7, is difficult to explain.¹³ However, if a head-first binding is assumed, the stereochemical outcome of 15S-HpETE oxygenation is more easily rationalized.¹³ This hypothesis is supported by Kuhn et al., who found that oxygenation of free 15S-HETE by rabbit reticulocyte 15-LOX led to the formation of 14R,15S-DiHpETE as the major product.¹¹ Formation of 14R,15S-DiHpETE involves removal of the C10 hydrogen and a +4 (towards the methyl end) radical rearrangement, which assumes that 15S-HETE binds in a tail-first alignment.¹³ In contrast, when rabbit reticulocyte 15-LOX is reacted with 15S-HETE methyl ester, 5S,15S-DiHpETE was found to be the major product.¹³ The formation of 5S,15S-DiHpETE requires hydrogen abstraction at C7 and a -2 (towards the carboxyl end) radical rearrangement, which assumes that the 15S-HETE methyl ester binds in a head-first alignment.¹³ This study supports that head-first binding is as likely to occur as tail-first binding, but it depends on the LOX isoform, the nature of the substrate, and the reaction conditions.

The reaction of 15-LOX and 15S-HpETE is of importance because it is implicated in the production of eoxins⁹ and lipoxins⁷. However, the current literature lacks a detailed kinetic and structural analysis of h15-LOX-1 reacting with 15S-

HpETE/15S-HETE. The aim of this chapter is to compare the 15S-HpETE kinetics of h15-LOX-1 with r15-LOX and investigate the role of active site residues, specifically F414.

6.2 Materials and Methods

6.2.1 Materials. Arachidonic acid was purchased from Nu Chek Prep, Inc. (MN, USA). DiHETE and tri-HETE standards (5S,6R-DiHETE; 5S,15S-DiHETE; 5,12-DiHETE; 5S,15S-DiHETE, 8S,15S-DiHETE, lipoxin A4 (LXA₄) and lipoxin B4 (LXB₄) were purchased from Cayman Chemical. HPLC grade solvents were used for both semi-preparative HPLC purification and analytical LC-MS/MS analysis of LOX products. Large scale product purification was achieved by using a C18HAIsil 250 x 10 mm semi-preparative column purchased from Higgins Analytical (Mountain View, CA). A Phenomenex Synergi (4 μ M, 150 mm x 4.6 mm) C-18 analytical column was used for product separation in tandem with MS/MS analysis. All other chemicals were reagent grade or better and were used without further purification.

6.2.2 Site-directed mutagenesis. All mutations of the human 15-LOX-1 enzyme (F414I, F414W) were performed using the QuikChange® II XL site-directed mutagenesis kit from Agilent Technologies (CA, USA), following the instructions of the manufacturer's protocol. The mutation was confirmed by sequencing the LOX insert in the pFastBac1 shuttle vector (Operon, gene with Operon (KY, USA).

6.2.3 Protein Expression. The h15-LOX-1 enzyme used in this chapter was expressed and purified as previously published.¹⁷ All mutants (R402L, R404L, F414I,

F414W, E356Q, and Q547L) were expressed as N-terminal His6-tagged proteins and depending on the mutation were purified using Bio-Rad Macro-Prep High S cation-exchange resins or via immobilized metal affinity chromatography (IMAC) using Ni-NTA resin. The protein purity was evaluated by SDS-PAGE analysis and was found to be greater than 90%.

6.2.4 Determination of Iron Content using ICP-MS. The iron contents of the mutants were determined relative to WT h15-LOX-1 with a Thermo Element XR inductively coupled plasma mass spectrometer (ICP-MS), with cobalt (EDTA) as an internal standard. Iron concentrations were compared to standard iron solutions. The protein concentrations were determined using the Bradford assay, with bovine serum albumin (BSA) as the protein standard. The iron loading was found to range from 40 – 60% for all proteins.

6.2.5 Accelerated Product Degradation Screen of Mutants. All mutants (R402L, R404L, F414W, F414I, Q547L, E356Q, I417A, L407A) were screened for accelerated product degradation at 234 nm using arachidonic acid as the substrate. The recombinant human 15-LOX-1 mutants were each reacted with 30 μ M AA in 2 mL of 25 mM HEPES, pH 7.5. The formation of 15-HpETE was monitored for ten minutes at 234 nm with a Perkin Elmer Lambda 40 UV/Vis spectrophotometer.

6.2.6 Synthesis of 15S-HpETE, 15S-HETE and 14R,15S-DiHETE. 15S-HpETE and 15S-HETE were synthesized enzymatically utilizing recombinant h15-LOX-2 and 40 μ M arachidonic acid (AA) in 500 mL of 25 mM HEPES (pH 7.5). The formation of 15-HpETE was monitored at 234 nm with a Perkin Elmer Lambda 40

UV/Vis spectrophotometer. 14R,15S-DiHETE was synthesized due to the lack of a commercially available conjugated 14R,15S-DiHETE standard. Recombinant human 12S-LOX was reacted with 40 μ M 15S-HETE in 100 mL of 25 mM HEPES, pH 8.0. The formation of 14R,15S-DiHETE was monitored at 270 nm. All reactions were quenched with 1-2% acetic acid, extracted using dichloromethane (DCM) and rotovapped to dryness. In the generation of 15S-HETE, crude 15S-HpETE was reconstituted with 5 mL of DCM, transferred to a 7 mL scintillation vial, reduced using trimethylphosphite and then dried under a stream of N₂ gas. The crude products, both reduced (15S-HETE and 14R,15S-DiHETE) and unreduced (15S-HpETE) were reconstituted in 200 μ L of MeOH and purified via high performance liquid chromatography (HPLC) using a Higgins HAI_{Si}L Semi-Preparative C-18 column. Solution A was 99.9% ACN and 0.1% acetic acid; solution B was 99.9% H₂O and 0.1% acetic acid. An isocratic elution of 50% A: 50% B was used to purify each compound. Analysis was performed by liquid chromatography-mass spectrometry (LC-MS/MS) utilizing a Phenomenex Synergi (4 μ M, 150 mm x 4.6 mm) C-18 column attached to a Thermo LTQ LC-MS/MS. Solution A was 99.9% H₂O and 0.1% formic acid; solution B was 99.9% ACN and 0.1% formic acid. The elution protocol consisted of 200 μ L/min, with a two step gradient as follows: (1) initial conditions consisted of 60% solution A, 40% solution B that was ramped to 55% solution A: 45% solution B over 30 min (2) solution A and solution B were jumped to 50:50 in 0.1 min and then ramped to 25% solution A and 75% solution B over 30 min. Negative ion MS/MS was utilized (collision energy of 35 eV) to

determine the fragmentation patterns. 15S-HETE, parent $m/z = 319$, fragments $m/z = 301, 275, 257, 219, 203, 175$; 15S-HpETE, parent $m/z = 335$, fragments $m/z = 301, 275, 273, 257, 219, 205, 203, 193, 183, 175$; 14R,15S-DiHETE, parent $m/z = 335$, fragments $m/z = 317, 299, 291, 273, 255, 235, 217, 205, 191, 173, 161, 129$.

The concentrations of the purified products were quantified using a Perkin Elmer Lambda 40 UV/Vis spectrophotometer using the following molar extinction coefficients: $\epsilon_{270} = 40,000 \text{ M}^{-1}\text{cm}^{-1}$ for 14R,15S-DiHETE and $\epsilon_{234} = 27,000 \text{ M}^{-1}\text{cm}^{-1}$ for 15S-HETE/15S-HpETE.

6.2.7 Substrate Studies of WT h15-LOX-1. To determine the cause of degradation of the signal at 234 nm when reacting with AA, 30 μM of exogenous 15S-HpETE, 15S-HETE, 12S-HpETE and 12S-HETE were reacted with h15-LOX-1. All reactions were performed in 2 mL of 25 mM HEPES buffer (pH 7.5) with and without 10 μM 13-HpODE. The reactions were monitored at 234 nm, 254 nm, 270 nm and 301 nm using a Hewlett-Packard diode-array 8453 UV/Vis spectrophotometer.

6.2.8 Identification of Products and Mechanism of 15S-HpETE Reaction with WT h15-LOX-1 and F414I mutant. h15-LOX-1 and F414I were reacted with 30 μM AA or 30 μM 15S-HpETE in 2 mL reaction mixtures, constantly stirred using a magnetic stir bar at room temperature (23°C). Reactions were performed in 25 mM HEPES buffer (pH 7.5). The concentration of AA was quantitated by allowing the enzymatic reaction to proceed to completion in the presence of soybean 15-LOX-1.

All reactions were monitored on a Hewlett-Packard 8453 UV/VIS spectrophotometer at 234 nm, 254 nm, 270 nm and 300 nm. The reactions were quenched after 200 s with 2% acetic acid. Ten 2 mL reaction mixtures were combined and extracted with DCM. The combined mixtures were then split in half, one-half was reduced with trimethylphosphite while the other half remained unreduced, then evaporated under a stream of N₂ gas. The products were then reconstituted in 40 μ L MeOH and analysis was performed by liquid chromatography-mass spectrometry (LC-MS/MS) utilizing a Phenomenex Synergi (4 μ M, 150 mm x 4.6 mm) C-18 column attached to a Thermo LTQ LC-MS/MS. The elution protocol is described in section 6.2.5. Products were identified by comparing retention times, UV spectra, and MS² fragmentation patterns of experimental samples to known standards.

6.2.9 Steady-State Kinetics of h15-LOX-1 and F414I with AA and 15S-HpETE. The WT and F414I rates were determined with a Perkin Elmer Lambda 40 UV/Vis spectrophotometer. Reactions were initiated by adding the LOX enzyme to a constantly stirring 2 mL reaction mixture containing 1 μ M – 20 μ M AA or 15S-HpETE in 25 mM HEPES buffer (pH 7.5), in the presence of 0.01% Triton X-100. All reactions with AA as substrate were monitored at 234 nm (ϵ_{234} value of 27,000 M⁻¹cm⁻¹), while reactions with 15S-HpETE were monitored at 270 nm (ϵ_{270} value of 40,000 M⁻¹cm⁻¹). Kinetic data were obtained by recording initial enzymatic rates at each substrate concentration and subsequently fitted to the Henri-Michaelis-Menten equation using KaleidaGraph (Synergy) to determine k_{cat} and $k_{\text{cat}}/K_{\text{M}}$ values. All kinetic data were normalized to the iron content.

6.3 Results and Discussion

6.3.1 Accelerated Product Degradation Screen of Mutants. WT human 15-LOX-1 can catalyze oxygenation and dehydration of hydroperoxide fatty acids to generate di-hydroperoxides and di-hydro products.¹² The consumption of hydroperoxides to form secondary di-oxygenation products can be monitored with the degradation of the HpETE (234 nm) and the generation of the di-oxygenation products (270 nm). To determine whether the active site mutants affect the secondary reaction with the hydroperoxides, each mutant (R402L, R404L, F414W, F414I, Q547L, E356Q, I417A, L407A) was reacted with AA and screened for accelerated product degradation at 234 nm. Only one mutant (F414I) was observed to degrade the product and decrease the 234 nm signal significantly faster than the WT enzyme.

6.3.2 Substrate Studies of WT h15-LOX-1 and F414I. Human 15-LOX-1 generates two primary products when reacting with AA, 12S-HpETE and 15S-HpETE, that result from abstraction of a bisallylic hydrogen at C10 and C13, respectively. To determine the enzyme's capability of reacting with its primary hydroperoxide products as well as their reduced counterparts (hydroxides), WT h15-LOX-1 and F414I were reacted with exogenous 15S-HpETE, 15S-HETE, 12S-HpETE and 12S-HETE with and without 13-HpODE. The presence of 13-HpODE is to ensure the enzyme is in the active Fe³⁺ oxidation state. 12S-HpETE and 12S-HETE, which contain only a bisallylic hydrogen at C7 were not turned over by h15-LOX-1. 15S-HpETE was the only substrate turned over significantly by WT h15-LOX-1 and F414I in the presence as well as in the absence of 13-HpODE. This result

is unusual because both 15S-HpETE and 15S-HETE contain bisallylic hydrogens at C7 and C10, however, h15-LOX-1 is only capable of reacting with 15S-HpETE. In comparison, Kuhn et. al. found 15S-HETE to be a substrate for rabbit 15-LOX ($K_M = 94.9 \mu\text{M}$), but only in the presence of 13-HpODE.¹³ He proposed that the poor substrate affinity might be due to the thermodynamic energy barrier associated with burying a polar hydroxyl group in the hydrophobic pocket of the substrate binding channel.¹³ Considering that both 15S-HpETE and 15S-HETE have the polar moiety at C15, it is difficult to explain their difference in reactivity with h15-LOX-1 by this proposal. Kuhn did not examine whether 15S-HpETE was a substrate for r15-LOX.

6.3.3 Product Profile and Mechanism of the 15S-HpETE Reaction with WT and F414I. Lipoxygenases exhibit multiple catalytic activities, including dioxygenation and dehydration. Dioxygenation and dehydration of conjugated monohydroperoxides are both initiated by abstraction of a bisallylic methylene hydrogen resulting in the formation of a substrate radical. If the substrate radical reacts with dioxygen, a dihydroperoxide fatty acid is formed. For the dehydration reaction of h15-LOX-1, it is thought that the substrate radical is first formed by abstraction of the doubly allylic methylene hydrogen, and then followed by a homolytic cleavage of the hydroperoxy oxygen-oxygen bond, resulting in the formation of a biradical fatty acid. The highly reactive biradical fatty acid forms an epoxide, which is then hydrolyzed by water to generate the dihydroxy fatty acid. It is important to note that dehydration only occurs with the conjugated hydroperoxide fatty acid and not the hydroxy fatty acid. To distinguish between the oxygenation and

dehydration mechanisms for the WT/15S-HpETE and F414I/15S-HpETE reaction pairs, mass spectra of the reduced and unreduced products were compared (**Figure 6.1-6.6**). It was observed that the retention time of 8S,15S-DiHETE was identical in both the reduced and unreduced products, suggesting that it formed via a dehydration mechanism (**Figures 6.1-6.2**). However, the retention time of 14R,15S-DiHETE shifts from ~ 31 min to ~ 21 min for the unreduced and reduced reactions, respectively (**Figures 6.3-6.4**). Similarly, a shift in retention time was also observed for 5S,15S-DiHETE for the unreduced and reduced reactions (**Figures 6.5-6.6**). These are indicative of an oxygenation mechanism.

To determine how the product profile of WT h15-LOX-1 and 15S-HpETE differs from that of r15-LOX and 15S-HETE, mass spectrometry was used to analyze the products formed. To simplify the initial analysis, all reactions were reduced. Mass spectral analysis revealed the formation of three major products: 14R,15S-DiHpETE (44%), 8S,15S-DiHETE (54%) and 5S,15S-DiHpETE (3%), with a minor amount of LXB₄ produced as well. The chemical structures are shown in **Figure 6.7** and the product distributions are shown in **Table 6.1** Other 15-lipoxygenating isozymes have been shown to generate similar product profiles. Kuhn et. al. found that the reaction of soybean 15-LOX-1 with 15S-HETE in the presence of 13-HpODE generate mainly 5S,15S-DiHpETE (65%), 8S,15S-DiHpETE (34%), 14R,15S-DiHpETE (< 1%) and LXB₄ (<1%).¹³ In contrast, the reaction of r15-LOX with 15S-HETE generates primarily 14R,15S-DiHpETE (49%), 8S,15S-DiHpETE (28%), 5S,15S-DiHpETE (21%) and LXB₄ (<2%).¹³ Human 15-LOX-1 generates only a small amount of

5S,15S-DiHpETE (3%) while r15-LOX generates 21% and s15-LOX-1 produces 65%. 5S,15S-DiHpETE is thought to be produced via head-first binding of the substrate and 5S-lipoxygenating activity. The data suggest that head-first binding and/or 5S-lipoxygenation in h15-LOX-1 is not well tolerated compared to that of the s15-LOX-1 and the r15-LOX. In comparison, h15-LOX-1 and r15-LOX generate 14R,15S-DiHpETE in similar amounts, 44% and 49%, respectively, while s15-LOX-1 produces < 1%. The similarity in the active sites of the h15-LOX-1 and r15-LOX may account for the observed similarity in the amount of product obtained. The major product between h15-LOX-1 and 15S-HpETE is 8S,15S-DiHETE (54%), a hydrolysis product of the dehydration pathway. Kuhn et. al. did not observe any 8S,15S-DiHETE only 8S,15S-DiHpETE in their studies because their substrate, 15S-HETE, cannot undergo epoxide formation for reasons previously mentioned.¹³ Bryant et. al. reported that r15-LOX converts 15S-HpETE to 8,15-DiHETE isomers via the hydrolysis of 14,15-epoxide triene.¹⁷ The 8S,15S-DiHETEs observed in our study may also be hydrolysis products of the 14,15-epoxide triene.

The active site mutation, F414I, generated the same products as WT when exposed to exogenous 15S-HpETE but with varying ratios (14R,15S-DiHpETE (18%), 8S,15S-DiHETE (75%), 5S,15S-DiHpETE (8%) and a minor amount of LXB₄) (**Table 6.1**). In comparison to WT h15-LOX-1, the F414I mutant produced approximately 21% more 8S,15S-DiHETEs. It seems that this mutation may be affecting the dehydration pathway and allowing for more epoxide formation with hydrolysis occurring specifically on C8. The data also suggest that the F414I

mutation does not affect the 5S-lipoxygenating ability of the WT which can be seen in the low abundance of 5S,15S-DiHpETE detected for both the WT and mutant, 3% and 8%, respectively.

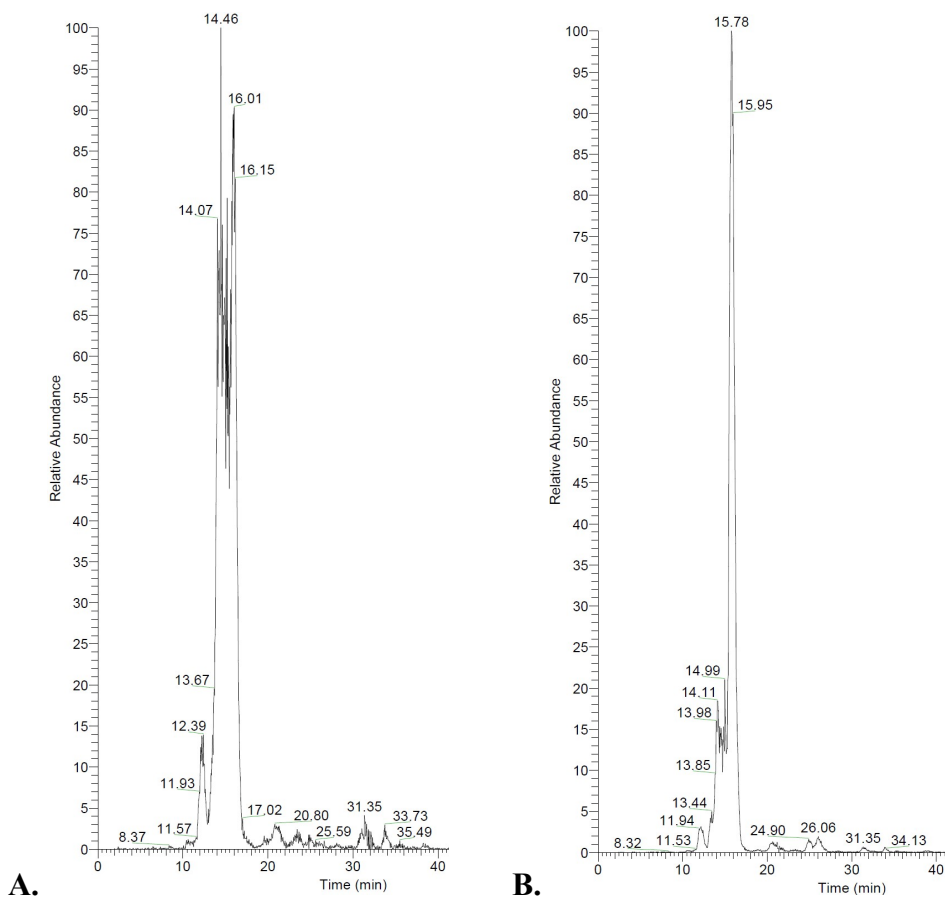


Figure 6.1. Mass spectra of 8S,15S-DiHETE ($m/z = 335$) formation between WT h15-LOX-1 and 15S-HpETE: Retention time of the unreduced form ~ 15 min (A) and retention time of the reduced form ~ 15 min (B). No shift in retention time is indicative of the hydrolyzed dehydration product.

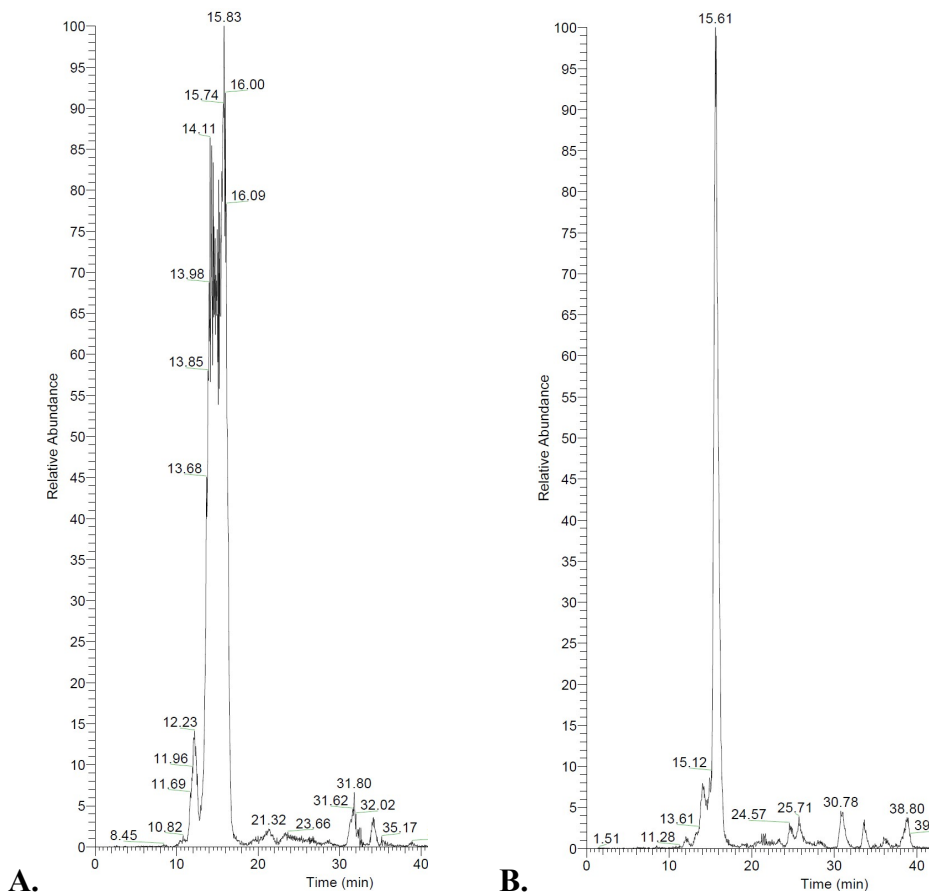


Figure 6.2. Mass spectra of 8S,15S-DiHETE ($m/z = 335$) formation between F414I and 15S-HpETE: Retention time of the unreduced form ~ 15 min (A) and retention time of the reduced form ~ 15 min (B). No shift in retention time is indicative of the hydrolyzed dehydration product.

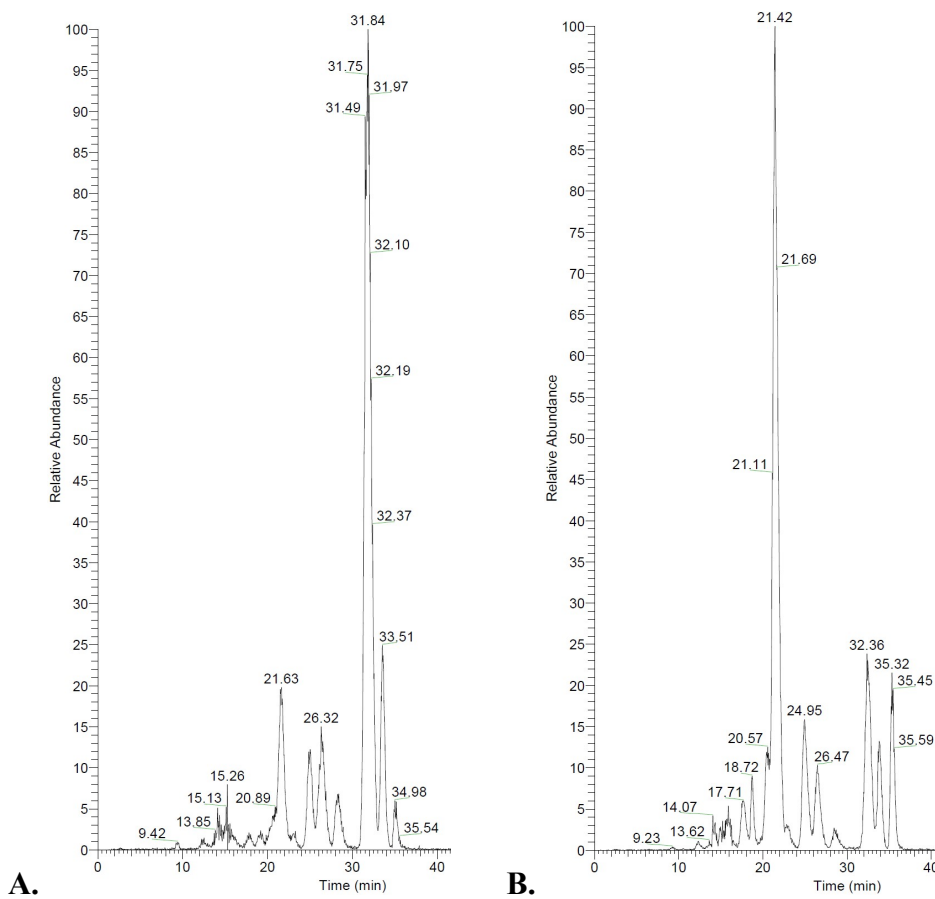


Figure 6.3. Mass spectra of 14R,15S-DiHpETE ($m/z = 335$) formation between WT h15-LOX-1 and 15S-HpETE: Retention time of the unreduced form = 31 min (A) and retention time of the reduced form = 21 min (B). Shift in retention time is indicative of a dioxygenation product.

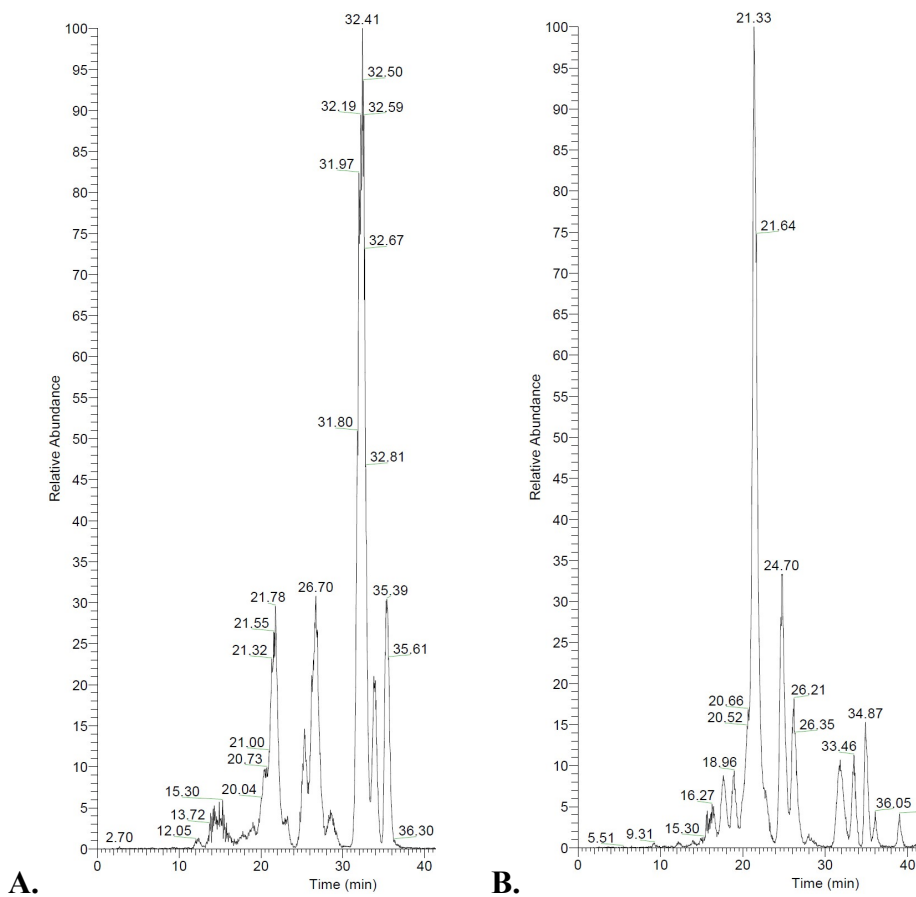


Figure 6.4. Mass spectra of 14R,15S-DiHpETE ($m/z = 335$) formation between F414I and 15S-HpETE: Retention time of the unreduced form = 31 min (A) and retention time of the reduced form = 21 min (B). Shift in retention time is indicative of a dioxygenation product.

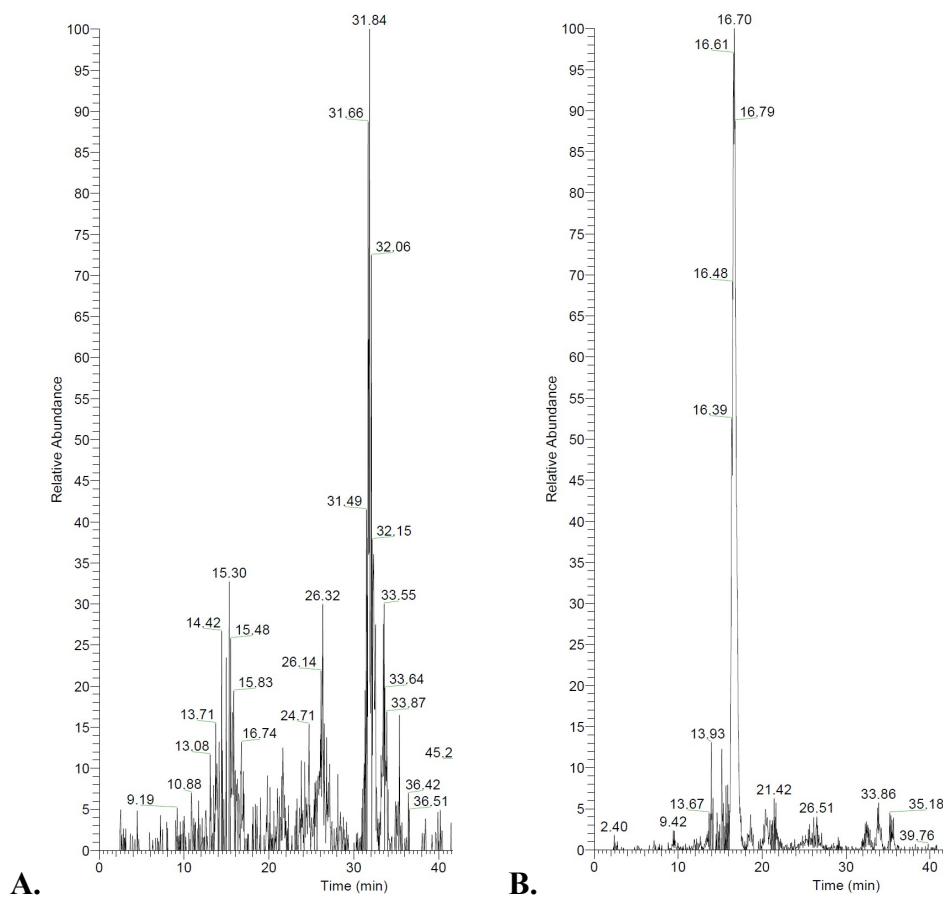


Figure 6.5. Mass spectra of 5S,15S-DiHpETE ($m/z = 335$) formation between WT h15-LOX-1 and 15S-HpETE: Retention time of the unreduced form ~ 31 min (A) and retention time of the reduced form ~ 16 min (B). Shift in retention time is indicative of a dioxygenation product.

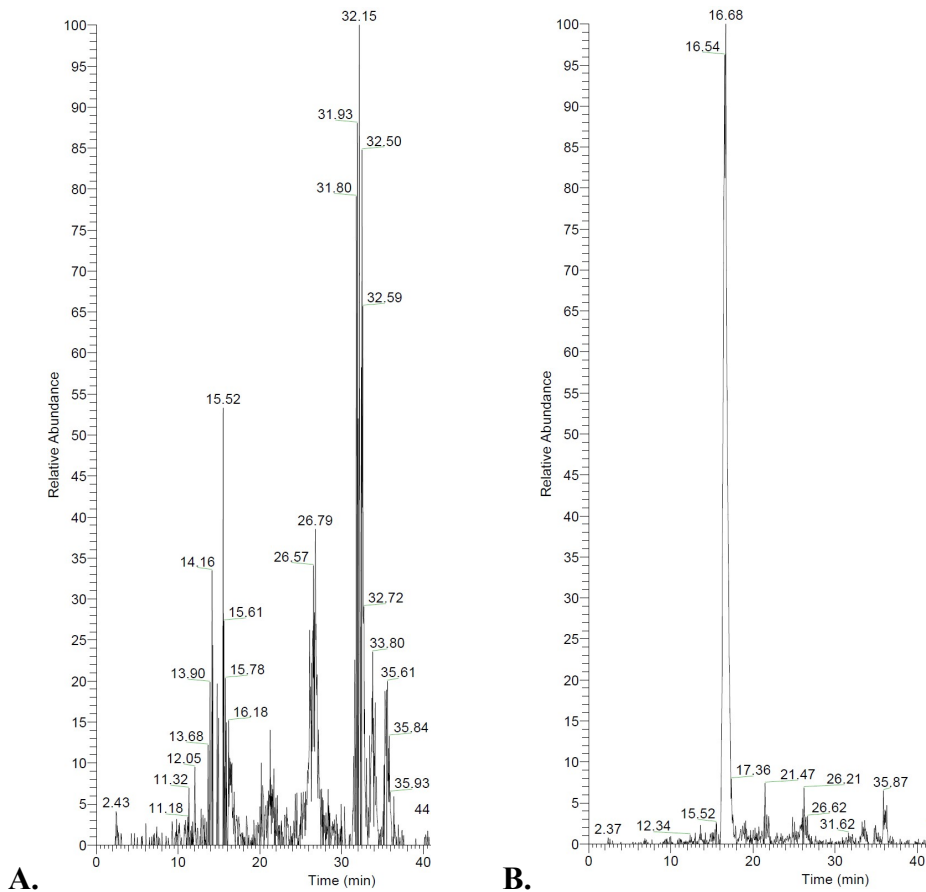


Figure 6.6. Mass spectra of 5S,15S-DiHpETE ($m/z = 335$) formation between F414I and 15S-HpETE: Retention time of the unreduced form ~ 31 min (A) and retention time of the reduced form ~ 16 min (B). Shift in retention time is indicative of a dioxygenation product.

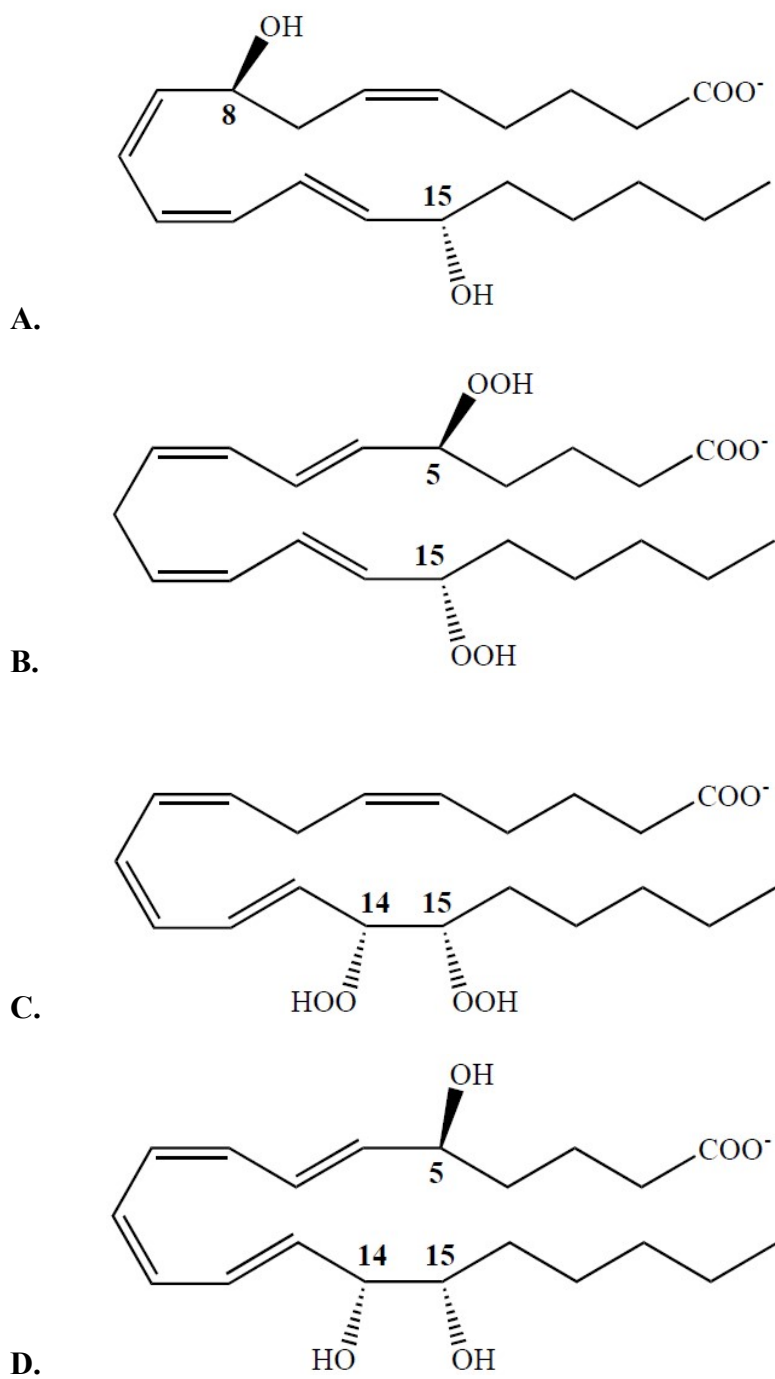


Figure 6.7. Chemical structures of A) 8S,15S-DiHETE; B) 5S,15S-DiHpETE; C) 14R,15S-DiHpETE and D) Lipoxin B4.

Reactions	% 8,15-DiHETE	% 14,15-DiHETE	% 5,15-DiHETE	%LXB4
WT + AA	74	22	4	< 1
F414I + AA	60	23	17	< 1
WT + 15-HpETE	54	44	3	< 1
F414I + 15-HpETE	75	18	8	< 1

Table 6.1. Product composition of the reaction between AA/15S-HpETE with h15-LOX-1 WT and F414I mutant.

6.3.4 Steady-State Kinetics of h15-LOX-1 WT and F414I with AA and 15S-HpETE. The fatty acid steady-state kinetics of 15S-HETE with r15-LOX ($K_M = 94.9 \mu\text{M}$, $k_{cat} = 0.4 \text{ s}^{-1}$) and s15-LOX-1 ($K_M = 440 \mu\text{M}$, $k_{cat} = 25 \text{ s}^{-1}$) have been previously published, however, the kinetics with h15-LOX-1 have not.¹³ To address this we performed steady-state kinetic experiments to obtain the kinetic parameters (**Table 6.2**) of AA and 15-HpETE by h15-LOX-1. Not surprisingly, h15-LOX-1 has four-fold lower catalytic efficiency (k_{cat} / K_M) reacting with 15S-HpETE ($k_{cat} / K_M = 0.29 \mu\text{M}^{-1}\text{s}^{-1}$) than with AA ($k_{cat} / K_M = 1.2 \mu\text{M}^{-1}\text{s}^{-1}$). WT h15-LOX-1 exhibited an AA turnover number of 10 (0.37) s^{-1} and a K_M of 8.5 (0.8) μM . In comparison, the wild-type enzyme had a 15S-HpETE turnover of 1.2 (0.04) s^{-1} (8-fold lower than AA-turnover) and a K_M of 4.2 (0.6) μM .

In contrast, F414I is less efficient than WT h15-LOX-1 when reacting with AA ($k_{cat}/K_M = 0.20 \mu\text{M}^{-1}\text{s}^{-1}$) but has comparable efficiency when reacting with 15S-HpETE ($k_{cat}/K_M = 0.17 \mu\text{M}^{-1}\text{s}^{-1}$). This relative difference is what explains the supposed “faster” secondary rate for F414I. The initial experiment which identified F414I as different from WT measured the relative rate of the primary and secondary reactions. This relative difference is now confirmed with the steady-state kinetics. The fact that the secondary rates for the wild type and F414I are similar is also confirmed by the similar products detected by LC-MS. These data therefore suggest that the binding mode for AA is distinct from that of 15S-HpETE and that the F414I mutant affects the rate of substrate capture for AA more than 15S-HpETE. Considering that F414 has been suggested to π - π stack with a double bond of AA, it is

possible that 15S-HpETE does not bind in a similar manner. The absence of F414 affects proper binding of AA in the active site, making the enzyme less efficient at reacting with AA; however, the loss of F414 does not affect 15S-HpETE catalysis. A possible explanation of this result is that 15S-HpETE binds to the active site in a distinct manner from AA, i.e. where it does not π - π stack with F414. This hypothesis is supported by the fact that the F414W mutant does not demonstrate a difference between AA and 15S-HpETE catalysis because the π - π stacking has been re-established for AA binding.

6.4 Conclusion. In the present investigation we studied the fatty acid kinetics, product profile and mechanism of product formation between WT h15-LOX-1 and 15S-HpETE and compared it to the reaction between an active site mutant, F414I, and 15S-HpETE. The substrate affinity and k_{cat} of 15S-HpETE turnover were comparable for both WT h15-LOX-1 and F414I. However, the substrate affinity and k_{cat} of AA turnover differed between WT h15-LOX-1 and F414I, with a decreased catalytic efficiency of AA turnover by F414I relative to WT h15-LOX-1. The kinetic data suggest that the active site mutant, F414I, is less efficient than WT at turning over AA but comparable at turning over 15S-HpETE. 5S,15S-DiHpETE, 8S,15S-DiHETE and 14R,15S-DiHpETE were identified as the major products in the reaction for both WT 15-LOX-1 and F414I, possibly indicating that this active site mutation does not significantly affect the binding mode of 15S-HpETE in the active site. Comparison of the mass spectra of the reduced and unreduced products of 15S-

HpETE and both enzymes revealed that 14R,15S-DiHpETE and 5S,15S-DiHpETE are dioxygenation products while 8S,15S-DiHETE is the hydrolyzed dehydration product. In contrast to rabbit 15-LOX, h15-LOX-1 does not react with 15S-DiHETE with or without 13S-HpODE. This is a surprising result and may indicate that h15-LOX-1 cannot overcome the large thermodynamic energy barrier of burying the polar hydroxyl group of 15S-HETE in its hydrophobic substrate-binding pocket.

		K_M (μM)	k_{cat} (s^{-1})	k_{cat}/K_M ($\mu\text{M}^{-1}\text{s}^{-1}$)
*AA	WT	8.5 (0.8)	10 (0.37)	1.2 (0.1)
	F414I	12.6 (2)	2.8 (0.08)	0.2 (0.02)
	F414W	6.5 (0.5)	3.0 (0.09)	0.5 (0.04)
*15-HpETE	WT	4.2 (0.6)	1.2 (0.04)	0.29 (0.02)
	F414I	4.7 (0.8)	0.82 (0.05)	0.17 (0.01)
	F414W	6.0 (0.6)	1.1 (0.04)	0.20 (0.02)

Table 6.2. Steady-state kinetic parameters for h15-LOX-1 WT, F414I and F414W. Substrate used is indicated on the left, error is listed in parentheses.

6.5 References

1. Brash, A.R. *J. Biol. Chem.* **1999**, 274, 23679.
2. Haeggstrom, J.Z.; Funk, C.D. *Chem. Rev.* **2011**, 111, 5866.
3. Kuhn, H.; Banthiya, S.; et. al. *Biochim. Biophys. Acta.* **2015**, 1851, 308.
4. Funk, C.D.; Chen, X.S.; et. al. *Prostaglandins Other Lipid Mediat.* **2002**, 68, 303.
5. Mancini, A.D.; Di Battista, J.A. *Inflamm. Res.* **2011**, 60, 1083.
6. Savari, S.; Vinnakota, K. *World J. Gastroenterol.* **2014**, 20, 968.
7. Romano, M. *Scientific World Journal.* **2010**, 10, 1048.
8. Pace-Asciak, C.R. *Br. J. Pharmacol.* **2009**, 158, 972.
9. Sachs-Olsen, C.; et. al. *J. Allergy Clin. Immunol.* **2010**, 126, 859.
10. Yoo, S.; Lim, J.Y.; Hwang, S.W. *Curr. Neuropharmacol.* **2013**, 11, 664.
11. Serhan, C.N.; Petasis, N.A. *Chem. Rev.* **2011**, 111, 5922.
12. Brash, A.R.; Yokoyama, C.; et. al. *Arch. Biochem. Biophys.* **1989**, 273, 414.
13. Schwarz, K.; Borngraber, S.; et. al. *Biochemistry.* **1998**, 37, 15327.
14. Gan, Q.; Browner, M.F.; Sloane, D.L.; Sigal, E. *J. Biol. Chem.* **1996**, 271, 25412.
15. Van Os, C.P.A.; et. al. *Biochim. Biophys. Acta.* **1981**, 663, 177.
16. Amagata, T.; Whitman, S.; et. al. *J. Nat. Prod.* **2003**, 66, 230.
17. Bryant, R.W.; et. al. *J. Biol. Chem.* **1985**, 260, 3548.